PHOSPHORITE DEPOSITS FROM THE SEA FLOOR OFF PERU AND CHILE: RADIOCHEMICAL AND GEOCHEMICAL INVESTIGATIONS CONCERNING THEIR ORIGIN

A DISSERTATION SUBMITTED TO THE GRADUATE DIVISION OF THE UNIVERSITY OF HAWAII IN PARTIAL FULFILLMENT OF THE REQUIREMENTS FOR THE DEGREE OF

DOCTOR OF PHILOSOPHY

IN GEOLOGY AND GEOPHYSICS

MAY 1974

By

William C. Burnett

Dissertation Committee:

Pow-Foong Fan, Chairman
Robert W. Buddemeier
Robert M. Garrels
Gordon A. Macdonald
Ralph Moberly
H. Herbert Veeh

ABSTRACT

Sedimentary phosphorites sampled from the sea floor off the coasts of Peru and Chile have been investigated to establish their ages and mode of formation. Uranium-series disequilibrium studies verify that phosphate deposits are currently forming in that area. The distribution of radiometric ages over the past 150,000 years implies that phosphate deposition was episodic rather than continuous during the late Pleistocene. Radiometric ages correlate well with periods of high eustatic stands of the sea. The fractionation of uranium isotopes between oxidation states (IV) and (VI) in these relatively young phosphorites is low as compared with that in older deposits. The relative amount of U(IV) contained in phosphate deposits appears to be a function of the extent of the reducing environment during deposition and how much, if any, of the uranium had been oxidized since incorporation into the apatite structure.

The bulk chemical and mineralogical compositions of the phosphate rocks reflect varying degrees of dilution of the phosphatic material, apatite, by other authigenic minerals and various allogenic components. Electron probe microanalysis shows that the composition of the phosphate rocks is complex, i.e., the rocks are derived from more than one phase, even within extremely small areas. Examination with the scanning electron microscope (SEM) of freshly fractured surfaces of phosphate rocks and small pellets from associated diatomaceous ooze suggests that the apatite was authigenic and had

formed as a direct chemical precipitate rather than by replacement. Some surfaces of siliceous biogenic materials appear to act as sites for apatite nucleation.

The model of phosphorite formation hypothesized here involves inorganic precipitation of apatite within anoxic pore waters and subsequent concentration of the apatite by physical processes. Oxidation of organic materials (mainly diatoms) during SO_4^{2-} reduction is the main source of dissolved phosphate. Apatite precipitation is favored by the high phosphate concentration in the interstitial waters, especially where the sediments have been deposited in highly oxygen-deficient waters, and by diagenetic reactions which remove interfering Mg^{2+} ions within the sediments. The common association of apatite with Mg-bearing phases (chlorite, sepiolite, dolomite) within the sediments from the Peru shelf supports the view that reactions resulting in Mg^{2+} depletion in pore waters are essential for apatite precipitation. Reactions such as dolomitization, replacement of Fe^{3+} by Mg^{2+} in clays (Drever, 1971), and the authigenic formation of Mg-silicates are proposed as the most likely controls of the Mg^{2+} content in anoxic pore waters from this region. The concentration of apatite into indurated phosphate rocks is brought about by winnowing and reworking processes, possibly in response to a change in the sedimentary environment caused by eustatic sea-level fluctuations or tectonic movements.

TABLE OF CONTENTS

LIST OF TABLES

LIST OF FIGURES

PART I: GEOGRAPHICAL LOCATIONS AND MEGASCOPIC DESCRIPTIONS

INTRODUCTION

Inorganic marine phosphate deposits occur along many of the continental margins of the world as nodules, irregular masses, sands, pellets, and oolites. In particular, phosphorites are typically found along the western margins of continents and are often associated with upwelling water and related phenomena (McKelvey, 1967; Brongersma-Sanders, 1957). An extensive phosphorite deposit located off the western coasts of Peru and Chile is the subject of this dissertation. This is the first extensive geochemical and geologic investigation of phosphorites thus far reported from this region.

The two main objectives of this study were: (1) to determine whether phosphorite formation is currently active in the region of interest; and (2) to formulate a satisfactory hypothesis for the mode of origin of the deposits. Uranium-series disequilibrium methods were selected for age determinations mainly because of the high uranium content of phosphorites (usually greater than 100 ppm U) and because the geochemistry of uranium in apatite is fairly well understood (Kolodny and Kaplan, 1970; Altschuler et al., 1958). Chemical and mineralogical analyses, petrographic examinations, and microprobe and scanning electron microscope (SEM) studies, both of the phosphatic nodules themselves and of the associated sediment, were used to ascertain how these deposits may have formed.

Besides these main objectives, it was hoped that this work would also contribute to knowledge in other fields. For example,

the geochemistry of uranium in marine apatite, with particular regard to the oxidation state of uranium in apatites formed in different environments, will form a corollary study of this work.

Sample Locations

Locations and depths of phosphorite samples used in this study are given in Table 1. Phosphorites from localities other than South America were studied to determine regional differences in chemical composition and mineralogy and to compare the results with analytical results reported for these areas by other authors. Figure 1 shows the location of the South American phosphorites used in this study. Most of the samples were collected during the Scripps Institution of Oceanography SOTOW cruise in May 1972. The remaining South American samples were collected by the Hawaii Institute of Geophysics research ship, KANA KEOKI, in 1972. A number of sediment cores also were taken on the Peru Shelf immediately adjacent to areas where phosphate rocks were recovered. The locations, depths, and other data of all sediment cores are listed in Table 2.

All phosphorites samples from the continental margins off Peru and Chile were dredged from areas shallower than 1000 meters. The phosphorites appear to be confined chiefly to two narrow bands, one at approximately 100 m depth and the other at about 400 m depth (A. Soutar, personal communication). Between these two bands lies a zone of laminated anaerobic sediments. These sediments are organic-rich diatomaceous oozes, evidence of the high organic

Table 1. Sample Identification, Location, Water Depth and Source for All Phosphate Rocks Used in This Study

Sample	Latitude	Longitude	Depth(m)	Source
		South America		
KK-71-161	5° 0.9'S	81°25.0'W	299-257	-
KK-71-96	12°22.0'S	77°27.9'W	187	-
0553	9°13.8'S	79°39.9'W	260-340	1
0546	9°48.0'S	79°23.9'W	360	1
0544	9°56.0'S	79°26.6'W	891	1
A-183	12°26.8'S	77°32.9'W	446	2
PD-12-05	12° 5.5'S	77°46.6'W	330-360	2
PD-15-13	15°13.3'S	75°22.2'W	117-123	2
PD-15-17	15°17.8'S	75°23.5'W	350-389	2
PD-18-30	18°30.0'S	70°36.5'W	346-423	2
PD-19-30	19°30.2'S	70°19.6'W	127-132	2
PD-19-33	19°33.7'S	70°23.1'W	341-370	2
PD-19-37	19°37.0'S	70°26.0'W	430	2
PD-21-24	21°23.7'S	70°18.2'W	420-450	2
PD-21-25	21°25.0'S	70°22.0'W	100	2
		California Borderland		
14415	32°52.1'N	119°23.0'S	120-130	3
14002	33°42.0'N	119°57.7'S	136	3
11876	33°43.5'N	119°18.1'S	1100-500	3
		Chatham Rise		
X-45	43°32.0'S	179°50.0'E	395	3
X-79	43°23.0'S	179°29.0'E	395	3
X-188	43°34.0'S	178°32.0'E	420	3
		Straits of Florida		
GS-4A	24°21.5'N	80°44.5'W	335	4
GS-11P	24°14.1'N	81°17.0'W	345	4
GS-25G	24°21.3'N	81°40.2'W	190	4
GS-39X	24°16.9'N	80°48.1'W	640	4
GS-41NN	24°28.4'N	80°35.3'W	295	4
G71-6B	24°40.5'N	80°33.4'W	170	4
		Other Areas		
Blake Plateau	Exact location and depth unknown			5
Necker Bank	Exact location and depth unknown			-

[1]A.P. Lisitzin, Academy of Sciences, U.S.S.R.

[2]A. Soutar, Scripps Institution of Oceanography, San Diego, Calif.

[3]D.W. Pasho, Global Marine, Inc., Los Angeles, Calif.

[4]D.N. Gomberg, University of Miami, Coral Gables, Fla.

[5]F.T. Manheim, U.S.G.S, Woods Hole, Mass.

Figure 1. Index map of the west coast of South America showing the locations of phosphate rock samples used in this study.

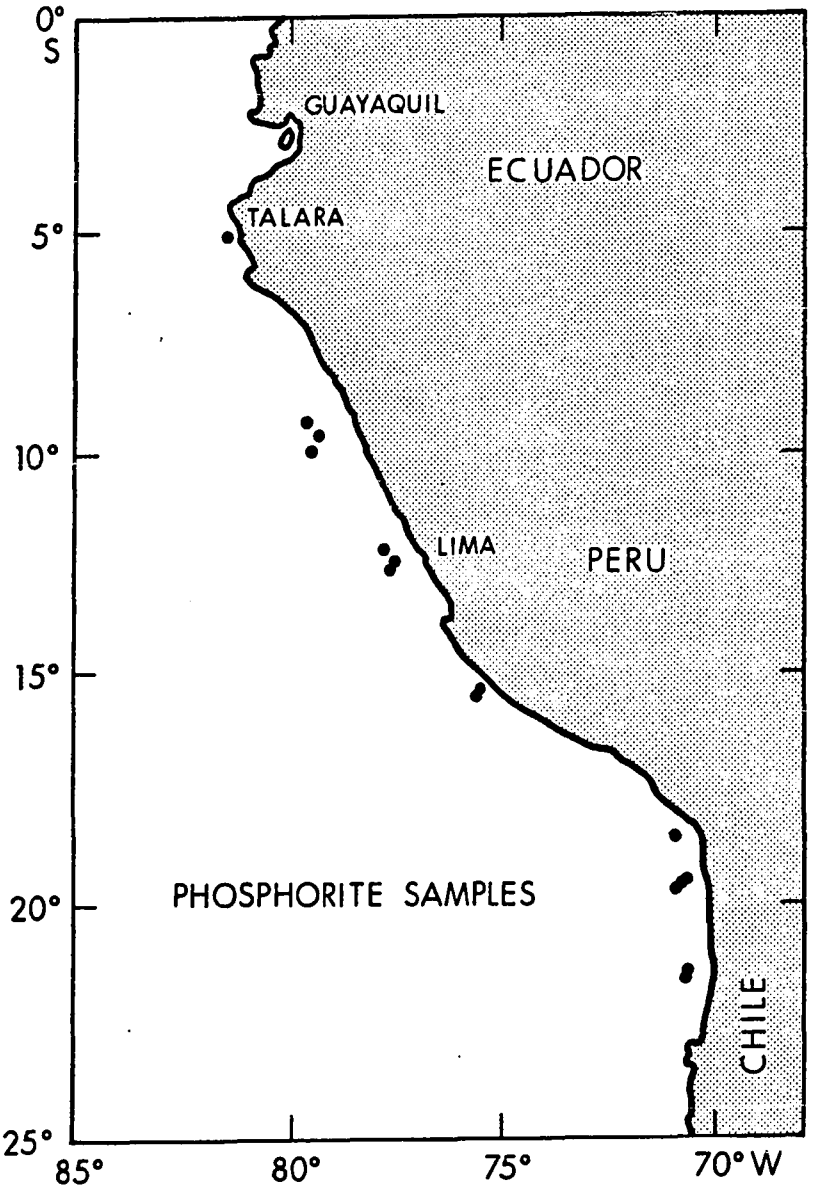
0°
S
5°
10°
15°
20°
25°
85°
80°
75°
70° W
GUAYAQUIL
ECUADOR
TALARA
LIMA
PERU
PHOSPHORITE SAMPLES
CHILE

Table 2. Sample Identification, Location, Depth, Length, and Sediment Type of Sediment Cores Used in This Study

Core No.	Latitude	Longitude	Depth (m)	Length (cm)	Type
KK-71[1]-GC[2]-01	12°26.8'S	77°33.0'W	454	76	Diatomaceous ooze
KK-71-GC-02	12°29.1'S	77°35.8'W	632	23	Diatom-foram ooze
KK-71-GC-03	12°23.4'S	77°29.3'W	363	83	Diatomaceous ooze
KK-71-GC-04	12°22.0'S	77°27.9'W	187	Surface	Phosphate rock fragments
KK-71-GC-06	12°20.1'S	77°26.7'W	224	45	Diatomaceous ooze
KK-71-FFC[3]-163	12°30.8'S	77°37.9'W	799	Surface	Glauconite sand
KK-71-RC[4]-03	9°42.6'S	79°29.0'W	379	90	Diatom-foram ooze

[1]KK-71 = KANA KEOKI, cruise began in 1971.

[2]GC = Gravity Core.

[3]FFC = Free Fall Core.

[4]RC = Rock Core.

productivity generated in this area by upwelling water. The upwelling currents are maintained by the strong eastern boundary current. The depth distribution of the phosphorites in relation to the oxygen minimum layer will be discussed in a subsequent section.

Megascopic Description

The phosphatic rocks from this area are irregular in shape, commonly with angular protuberances and pits made by burrowing organisms. They seldom display any internal zonation or structure. Many samples are flattened in one dimension, being only 1 to 2 cm thick; others are roughly equant in shape. Their color varies from light to dark gray and occasionally is pale green. The surfaces of most of the rocks are dull, in contrast to the glazed surfaces displayed by phosphate rocks from other areas, such as off California (Emery, 1960). Figures 2 and 3 show typical phosphate rock configurations. Sample PD-15-17 is a light-colored, highly mottled phosphate rock dredged off southern Peru. The two pieces of sample PD-21-25, recovered off Chile, are more compact but still show evidence of burrowing. Generally, the phosphorite nodules range in diameter from about 5 to 10 centimeters. Such a limited size range is partly a consequence of the sampling technique, of course; a much wider range of sizes is probably present. Phosphate-rich pellets of sizes varying from a few centimeters to a few millimeters also were discovered within the anaerobic green muds associated with the phosphorites.

Figure 2. Photograph of sample PD-15-17, collected from the Peru shelf. The dull surface, flattened shape and highly mottled appearance are characteristic of many of the samples from this area.

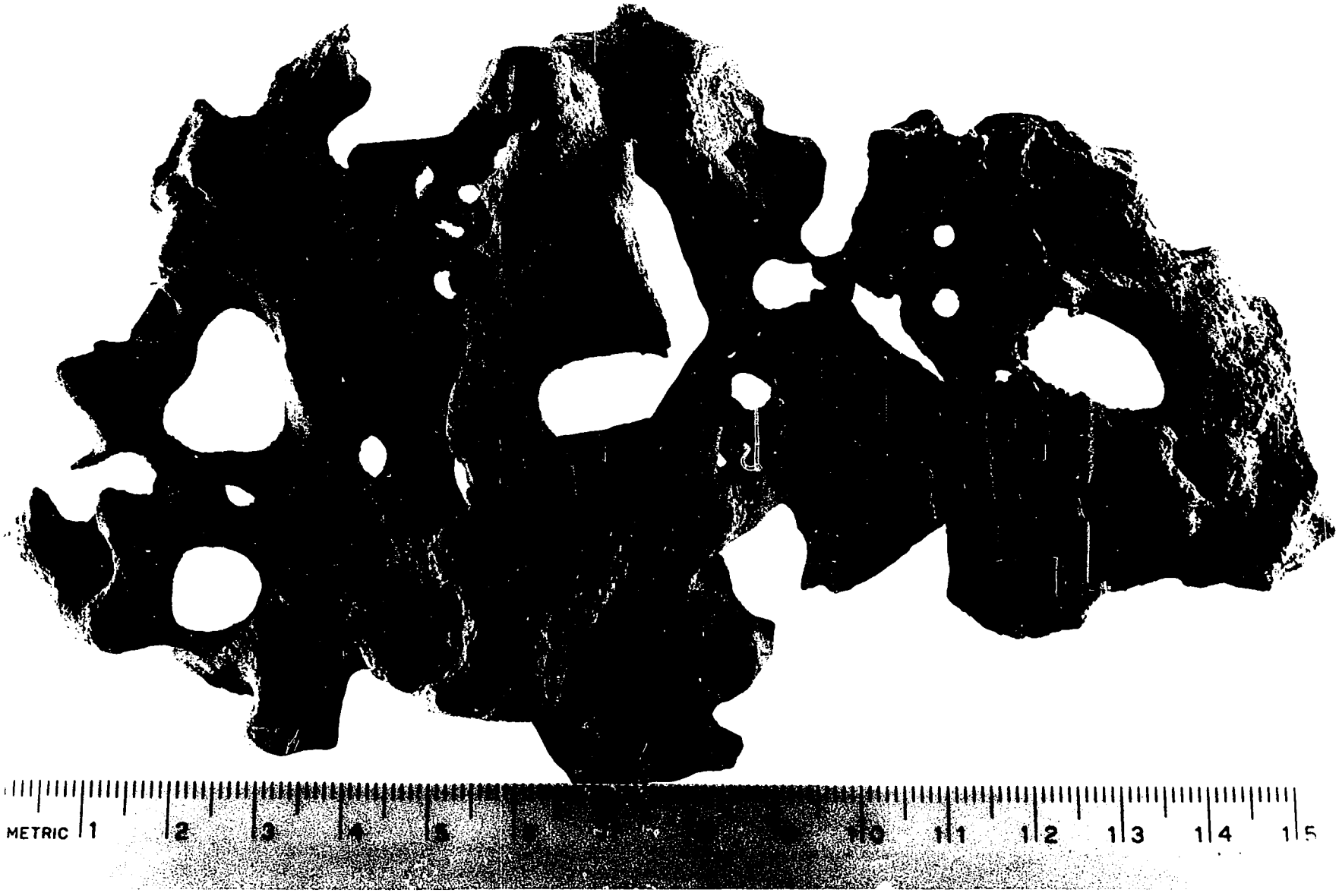
METRIC 1 2 3 4 5 10 11 12 13 14 15

Figure 3. Photograph of two portions of sample PD-21-25, collected from the Chilean shelf.

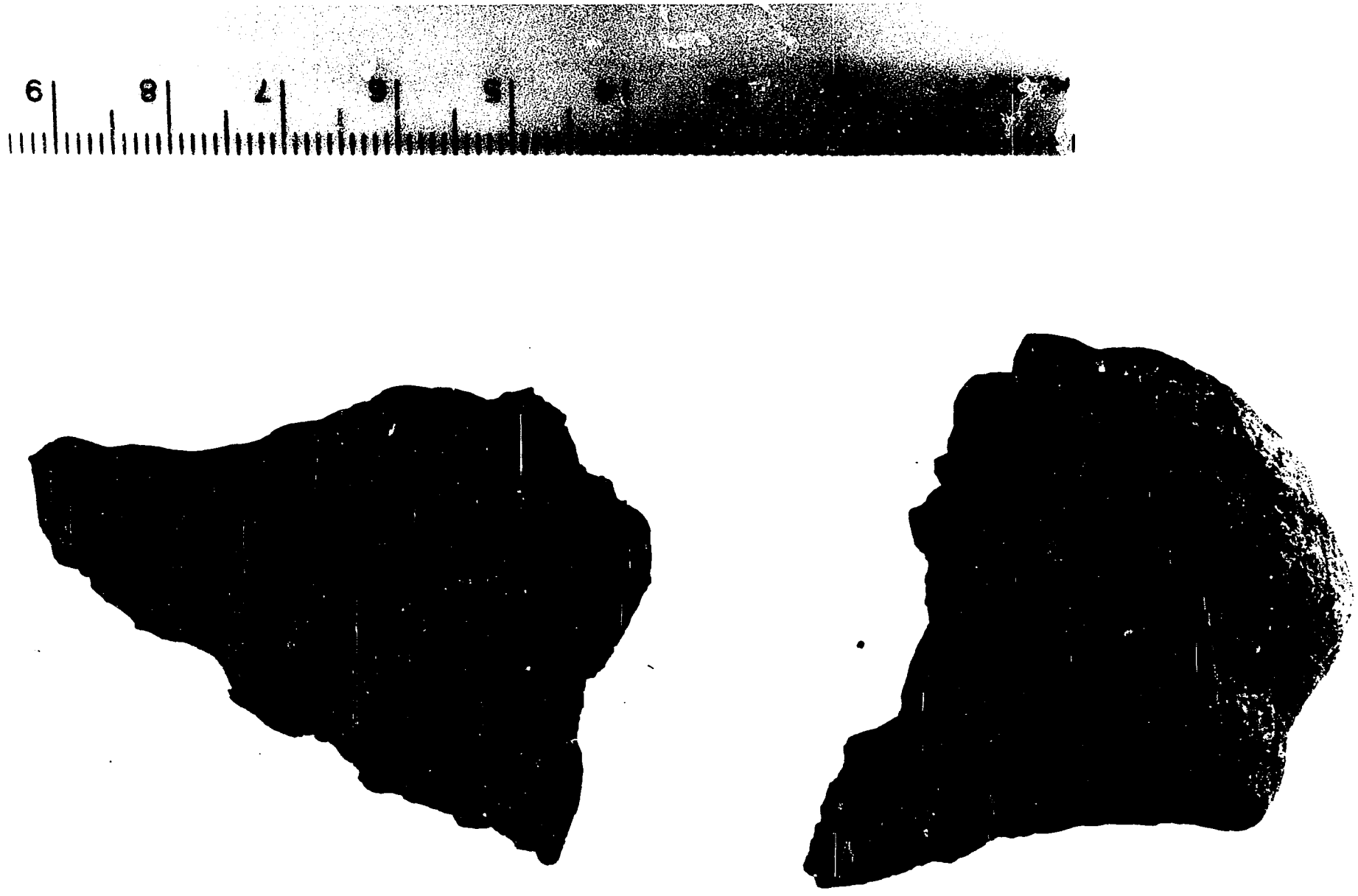

Phosphorite, as defined by Pettijohn (1957), is a sedimentary deposit composed mainly of phosphate minerals. The terms 'phosphate rock' and 'rock phosphate' are also used to describe these deposits. The main mineral component of phosphorites is a carbonate fluorapatite, also known as francolite. The term 'collophane' is also used to describe the optically isotropic, fine-grained phosphatic material observed in thin sections. The terms 'apatite' or 'marine apatite' will be used interchangeably in this report to describe the phosphate-rich component of the phosphorites.

PART II: URANIUM-SERIES DISEQUILIBRIUM STUDIES

INTRODUCTION

Marine phosphorites are composed chiefly of a fluorine-rich variety of carbonate apatite, named francolite by McConnell (1958), and are rich in uranium. Tooms et al. (1969), from data presented by Swaine (1962), reported an average concentration of 190 ppm uranium in phosphorites. This high concentration represents an almost hundredfold increase relative to uranium concentration in crustal rocks. The high concentration is favorable for radiometric age determination by uranium-series disequilibrium techniques.

The most extensive work to date on uranium isotopes in sea-floor phosphorites is that of Kolodny (1969a, 1969b) and Kolodny and Kaplan (1970). These workers determined the concentration and isotopic composition of both total and tetravalent uranium in forty phosphorite samples from several areas including the sea off California, the Chatham Rise, the Blake Plateau, and the Agulhas Bank. No significant disequilibrium of uranium-series isotopes was found to exist in these samples: Kolodny (1969b) interpreted the data to indicate that all the samples are at least as old as the dating limit of the method (approximately 800,000 years). Because the mean $^{234}U/^{238}U$ activity ratio is less than the secular equilibrium value of unity, Kolodny (1969b) has suggested that the phosphorite nodules are currently being actively leached rather than precipitating on the present-day sea floor. If we accept Kolodny's suggestion that phosphorites are probably not forming on today's sea floors, then many current ideas regarding phosphorite genesis

will have to be reassessed. Most theories of phosphorite formation are based on the observed association between phosphorite occurrences and upwelling waters. Most of the samples dated as being old by Kolodny, however, were in fact, located in areas of present-day upwelling. Kolodny (1969b) also suggested that phosphorites may be currently forming in regions of warmer waters, such as along the western coasts of Africa, Central America, and Australia.

Radiometric evidence in support of present-day formation of phosphorites has been presented by Baturin et al. (1972), who analyzed two soft phosphatic nodules from the southwest African shelf and one nodule from the Chile shelf. The $^{234}U/^{238}U$ activity ratios are all close to that of modern sea water, indicating a young age for those samples. Veeh et al. (1973) and Burnett et al. (1973) have dated phosphorites from the continental margin of Peru by uranium-series techniques. For many of the samples the isotopic results are compatible with a Holocene age. Veeh et al. (in press) have recently reported phosphorites occurring as thin, unconsolidated laminae and as lithified nodules and pellets within diatomaceous oozes on the southwest African continental shelf. Although the unconsolidated laminae were determined by isotopic means as being of Holocene age, the lithified nodules and pellets were old and presumably reworked.

This study is an extension of the work begun by Veeh et al. (1973) on the phosphate deposits off South America. Phosphorite samples from fifteen localities along the continental margins of

Peru and Chile were dated by uranium-series techniques to determine: (1) whether phosphorites are currently forming along this entire region; and (2) whether a pattern of phosphorite ages which may be related to their genesis is discernible. In addition to the radiometric age determinations, both total and tetravalent uranium concentrations and isotopic compositions were determined in the hope of revealing whether phosphate deposition occurred under oxidizing or under reducing conditions. The fractionation of uranium isotopes between oxidation states in marine phosphorites (Kolodny, 1969a) was also investigated in the samples from off South America. In addition to the data reported for these phosphate rocks, uranium isotopic measurements were made for several phosphorite samples from other areas.

Before the isotopic results are presented and discussed, the distribution of uranium within the phosphate rocks as elucidated by fission-track techniques is described, since it was necessary to know that the uranium in the phosphorites was contained primarily within the constituent apatite--a major assumption of the dating method.

The purpose of the present study was thus threefold: (1) to illustrate by fission-track techniques the distribution of uranium within rock phosphates off the South American coast; (2) to report uranium-series ages for these samples; and (3) to report the concentrations of total, tetravalent, and hexavalent uranium, and the respective $^{234}U/^{238}U$ activity ratios in each oxidation state.

METHODS

General

Phosphate rocks recovered from each dredge haul were separated into three groups: light-colored phosphorite nodules, dark-colored phosphorite nodules, and biogenic phosphates. In many cases, the material recovered was not nearly enough to allow this type of grouping. But when material was plentiful, representative pieces could be selected. Slabs for making thin sections and microprobe mounts were cut from most of the phosphate rocks. Between 10 and 20 grams of each sample selected for analysis was powdered and dried for several hours at 110°C. Unless otherwise noted, all the analytical data reported here are based on splits of this powdered material. Chemical and mineralogical analyses were also performed on this material when amounts were sufficient. Results of the analyses are presented in Part III of this report.

Uranium Distribution

Open-faced, polished thin sections of selected phosphate rock samples were prepared, covered with a Lexan plastic fission-track detector, and placed in a reactor for bombardment with thermal neutrons. The irradiation was performed in a TRIGA reactor at the Oregon State University Radiation Center at Corvallis. The phosphate samples were irradiated for one hour at a flux of 3×10^{12} n cm^{-2} sec^{-1}.

When Lexan plastic is used to register fission tracks from thermal neutron-induced fission of ^{235}U in rocks, after chemical etching a print of the rock texture is formed on the plastic surface.

Uranium-rich phases are thus more easily identified by correlation with the companion thin section, than by track registration in other materials (Kleeman and Lovering, 1967).

After irradiation, the Lexan plastic covers were removed and etched in 6N NaOH at 70°C for about ten minutes. The Lexan sheets were then rinsed with distilled water and allowed to dry. On examination under a microscope, it was discovered that the prints could easily be correlated with areas within the thin sections. By placing the Lexan print upside down alongside the polished thin section and mounting them in this fashion in the mechanical stage of a petrographic microscope, fission-track distributions could be directly related to areas within the phosphate rock thin sections. All the sections and plastic prints were photographed in this way.

Uranium Series Isotopes

Total uranium and thorium, and the activities of their isotopes, were measured by alpha spectrometry. Uranium and thorium isotopes were purified and separated by methods similar to those of Ku (1965), modified by Veeh (personal communication). After wetting with distilled water, complete sample dissolution was achieved by the addition of concentrated HCl, HNO_3, HF, and $HClO_4$ to the dried and powdered sample. After an initial evaporation, ^{232}U and ^{234}Th tracers were added for chemical-yield determinations. Two additional evaporations in the presence of HNO_3 and $HClO_4$ acids ensured both complete oxidation of all the uranium and equilibration between the radioactive tracers and the uranium and thorium in the sample.

After the final evaporation, the dissolution procedure was completed by dissolving the sample in 8N HCl. If any insoluble residue remained, it was carefully separated out by centrifuging and then fluxed with Na_2CO_3 in a platinum crucible over an open flame. After fusion, the residue was usually acid soluble. It could then be recombined with the original fraction. After dissolution, the separation procedure consisted of a series of hydroxide precipitations, ion exchanges, and solvent extraction steps. Phosphate was separated from the uranium fraction during ion exchange and from the throium fraction by precipitating the hydroxides (mainly of iron and aluminum) between a very narrow pH range, 3.0 to 3.5. Within this range, thorium is co-precipitated with other hydroxides, while phosphate remains in solution (Toribara and Koval, 1967). These steps to separate out phosphate are important because uranium may become absorbed onto $AlPO_4$, and also because formation of very insoluble $Th_3(PO_4)_4 \cdot 4\ H_2O$ may cause low thorium yields (Kolodny, 1969a). The purified uranium and thorium were ultimately electroplated onto stainless steel counting planchets for pulse-height analysis. The time required for chemical separation and purification was usually on the order of a few days to a week. Although the ion exchanges took several hours, sample dissolution was usually the more time-consuming procedure.

An artificially produced isotope of uranium was used as a yield tracer for uranium. The tracer, purchased commercially, was diluted and purified by anion exchange and then was calibrated by alpha

spectrometry against a gravimetric uranium standard (National Bureau of Standards reference material No. 950a (U_3O_8, guaranteed 99.94% pure)). The standard was ignited in a platinum crucible at 1000°C for fifteen minutes to ensure stoichiometric U_3O_8. ^{234}Th served as a yield tracer for thorium. The tracer was prepared by "milking" a uranium solution by cation exchange, a procedure similar to that described by Goldberg and Koide (1962). Because ^{234}Th has a half-life of only 24.1 days, it was necessary to use four Th tracers during the course of this investigation. After electrodeposition, ^{234}Th activities were measured on a Nuclear Chicago gas flow beta counter.

Chemical yields varied considerably. Occasionally, thorium yields as high as 70 per cent were encountered but more typically, values were closer to 30 per cent. Thorium yields were always determined before alpha counting was attempted, and samples with yields less than 10 per cent generally were discarded and prepared again. Uranium yields also were variable, commonly with values around 50 per cent.

The counting system consisted of four Ortec surface barrier detectors, each with its own bias supply, preamplifier, and low-noise amplifier/discriminator. These systems were connected to a multi-channel pulse-height analyzer (Nuclear Data Series 2200 System Analyzer) by means of a routing system. The multi-channel analyzer has a capacity of 1024 channels, 256 channels for each detection system. The accumulation of events was monitored on an oscilloscope

until teletype printout of all the events stored in the memory of the analyzer was desired.

Counting-time also varied, depending on the chemical yields and the radioactivities. Most samples were counted until the $^{234}U/^{238}U$ activity ratio could be determined within ± 0.01 (at one standard deviation). This required from about 2,500 to 5,000 minutes. Samples were not usually counted for more than 10,000 minutes (approximately one week).

After pulse-height analysis, the four detection systems were printed-out separately on a teletype for data analysis. Typical spectra, one for uranium and one for thorium, are shown in Figure 4. About sixty channels separated the channel with the most number of counts corresponding to ^{238}U from that with the most counts corresponding to ^{234}U. About sixty channels also were present between the ^{234}U peak and the ^{232}U peak. For spectrum analysis, the peaks were integrated by placing an envelope about forty channels wide around each peak so that the starting and finishing number of counts were about the same (approximately 2 per cent of the highest number). Because low-energy tails were almost always present, the envelope usually had more channels on the low-energy side of each peak than on the high-energy side. No correction was made for ^{235}U counts, which interfere slightly with ^{238}U, or for ^{232}U spillage into the ^{234}U peak area. Corrections of this kind were applied to a few samples and found to be negligible. A small but significant background, detected in the ^{234}Th tracer, was measured on each tracer used, and corrected during data analysis.

Figure 4. Alpha Spectra of Phosphorite Samples

a) Total uranium in sample PD-15-17.

b) Thorium isotopes in sample KK-71-161.

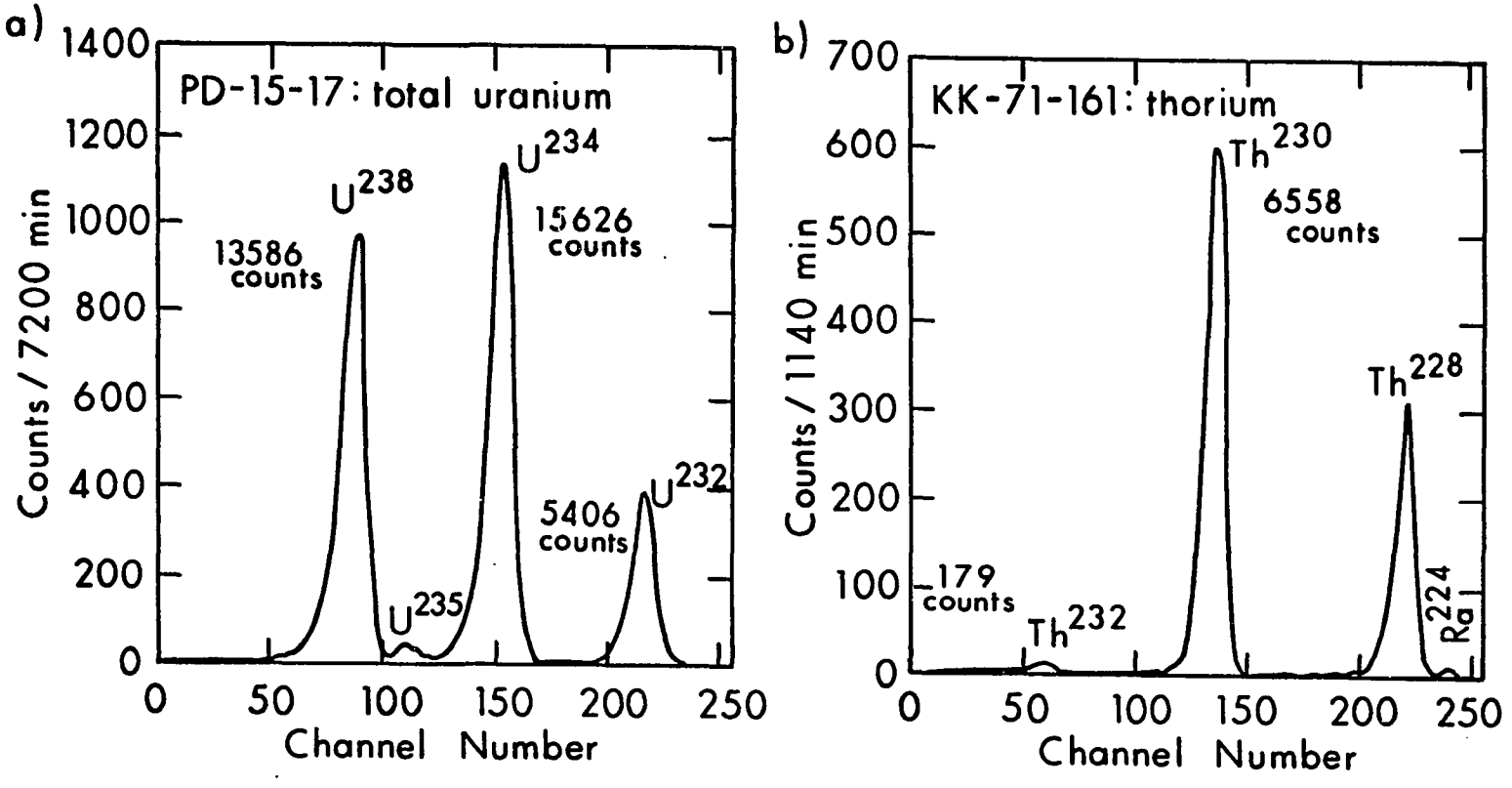
a)
PD-15-17: total uranium
Counts / 7200 min
1400
1200
1000
800
600
400
200
0
U238
U234
U235
U232
13586 counts
15626 counts
5406 counts
0
50
100
150
200
250
Channel Number
b)
KK-71-161: thorium
Counts / 1140 min
700
600
500
400
300
200
100
0
Th230
6558 counts
Th228
179 counts
Th232
Ra224
0
50
100
150
200
250
Channel Number

To test the reproducibility of the method, four separate splits of the same powder of KK-71-161 were analyzed. The precision of the results, shown in Table 3, is good except for the determination of the concentration of thorium and the $^{230}Th/^{232}Th$ activity ratio. In both cases the wide range in values is due to the low number of events for ^{232}Th, which was not very abundant. However, neither of these affect the age determinations, since only the $^{234}U/^{238}U$ and $^{230}Th/^{234}U$ activity ratios are used for calculating ages. To check for any effects due to incomplete oxidation, split number 3 of sample KK-71-161 was ignited at 800°C in a muffle furnace for two hours prior to the dissolution step. Complete oxidation of all the uranium before the anion exchange step is essential. If all the uranium is not oxidized, U(IV) may behave like Th in the exchange column, contaminating the thorium fraction. It was assumed that ignition at 800°C ensured complete oxidation. The data show no apparent difference as a result of this treatment. It therefore appears that complete oxidation was achieved during the course of the normal analysis.

Determination of the Oxidation State of Uranium

The concentration of tetravalent uranium, U(IV), and the $(^{234}U/^{238}U)_{IV}$ activity ratio were determined by alpha spectrometry after separation of U(IV) from U(VI). Separation was achieved by precipitating U(IV) as a cupferrate, as described by Clarke and Altschuler (1958) and Kolodny (1969a). Tracer was added and the U(IV) was purified, electroplated, and counted. Total uranium was

Table 3. Analytical Data on KK-71-161. Concentrations in Parts per Million (ppm); Ratios Are Activity Ratios

Sample	Uranium (ppm)	Thorium (ppm)	$\frac{^{234}U}{^{238}U}$	$\frac{^{230}Th}{^{234}U}$	$\frac{^{230}Th}{^{232}Th}$
1	103	7	1.09	0.42	27
2	103	6	1.10	0.41	36
3[1]	108	7	1.09	0.38	22
4	111	4	1.10	0.38	31
$\bar{X} \pm \sigma$	106 ± 4	6 ± 1	1.09 ± .01	0.40 ± .02	29 ± 6

[1]Ignited in furnace at 800° C for two hours.

determined from a separate split of the same sample by a slightly different dissolution procedure than was used for the age determinations; i.e., the same as that reported by Kolodny (1969a) and similar to that described in the previous section. However, after repeated treatment with hydrochloric, nitric, and perchloric acids, the solution was filtered to remove any highly insoluble materials. Several of the acid-insoluble residues were checked by X-ray diffraction procedures for complete disappearance of the apatite peak. Quartz, and possibly some mica, appeared to be the only minerals present on the filters. After dissolution, the uranium was separated and purified as described previously.

To prevent oxidation of uranium, the fraction for determination of U(IV) was dissolved in cold 1.5 M orthophosphoric acid and regulated between 4-5°C in a cold bath. The powdered sample was kept in suspension until dissolution was complete (usually about one hour for 0.5 grams of sample). After dissolution, the solution was filtered through glass-fiber filter paper into a beaker placed in the cold bath. Next, a titanium carrier was added and the U(IV) was co-precipitated with the Ti as a cupferrate by adding cold 6 per cent aqueous cupferron solution. Then the precipitate was filtered, washed, transferred to a platinum crucible, charred, and ignited over a burner. At that point, the uranium tracer was added and the ignited residue was completely dissolved in acids. The uranium in that fraction was then separated and purified as before. The uranium contained in this fraction thus represents the U(IV) contained in the sample.

To establish the precision and accuracy of this method, a phosphate rock standard prepared by the New Brunswick Laboratory (NBL) of the Atomic Energy Commission was analyzed several times. The results are shown in Table 4. The only value that the NBL had established is the total uranium content, determined by fluorometric techniques. Kolodny (1969a and personal communication) has previously reported isotopic values for this standard and they are presented in Table 4 for comparison with samples from this study. The precision is good except for the determination of tetravalent uranium. As Kolodny (1969a) pointed out, the values for U(IV) are really minimum values, since the tracer is added late in the procedure. It is encouraging, however, that the values determined in two different laboratories are similar.

DISTRIBUTION OF URANIUM

Introduction

One of the primary assumptions underlying uranium-series disequilibrium dating is that the uranium content of the sample is derived primarily from sea water. In the case of phosphorites, uranium is contained in the apatite as both tetravalent and hexavalent species (Altschuler et al., 1958). Uranium may also be present in detrital minerals or possibly as uranyl organic complexes. Most theories of phosphorite genesis propose that the apatite of phosphorites either precipitates directly out of sea water (Kazakov, 1937) or forms as a replacement of previously existing materials,

Table 4. Data on NBL Phosphate Rock Standard No. 1

Number	Total Uranium (ppm)	$(\frac{^{234}U}{^{238}U})_{total}$ [1]	Tetravalent Uranium (ppm)	$(\frac{^{234}U}{^{238}U})_{IV}$ [1]	$\%\ U_{(IV)}$
1	234	1.01	169	0.87	72
2	228	1.00	141	0.86	62
3	242	1.01	149	0.84	62
4	243	0.98	163	0.83	67
$\overline{X}$	237	1.00	155	0.85	66
NBL [2]	243	--	--	--	--
Kolodny [3]	236	1.00	169	0.86	71

[1] Activity Ratio.

[2] New Brunswick Laboratories (New Brunswick, New Jersey).

[3] Total uranium and $(\frac{^{234}U}{^{238}U})_{total}$ reported in Kolodny (1969); other values by personal communication.

such as the phosphatized limestone described by Hamilton (1956). In either case, it would follow that the uranium content of marine apatite is derived from sea water. In order to determine whether the uranium in the phosphorite samples used for dating was localized in the apatite, and therefore derived from sea water, the uranium distribution was investigated using fission-track techniques.

Results

Photomicrographs of a polished thin section of sample PD-19-30 and its matching Lexan fission track print are shown in Figure 5. All photographs were taken in plane polarized light. The area shown (Fig. 5a) is part of a coarse-grained layer and its sharp contact with finer grained material. The layer consists of detrital sand grains and biogenic debris set in a dark collophane matrix. The fission-track prints shown in Figure 5b indicate the sites of fissionable uranium, thereby providing a map of the distribution of a uranium within the area of the photomicrograph (Fig. 5a). Notice that the uranium is distributed throughout the collophane matrix and tends to be concentrated along grain boundaries. Figures 5c and 5d illustrate the same area at higher magnification. The large quartz grain in the center of the field of view displays a high concentration of uranium around its boundaries. When examined under high power, many of the detrital grains are seen to have rims of phosphatic material. These rims commonly are composed of brown collophane, but some are anisotropic, perhaps due to the presence of admixed clay

Figure 5. (a) Photomicrograph of sample PD-19-30 polished thin section.

(b) Fission-track prints of same area showing distribution of uranium.

(c) Same as (a), higher magnification.

(d) Same as (b), higher magnification.

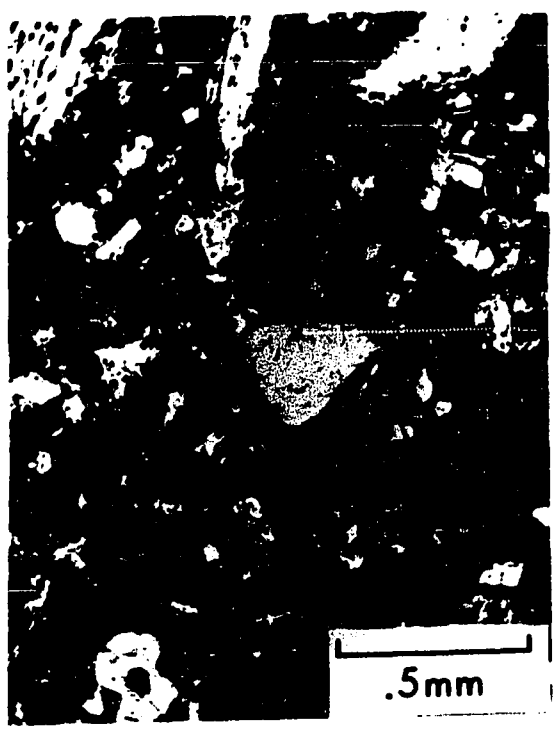

a

b

c

d

minerals. The high concentrations of uranium surrounding mineral grains are interpreted as a result of the high concentration of microcrystalline apatite in those areas. It seems reasonable that these minerals acted as nucleation sites for chemically precipitated apatite. This concept will be further developed in Part III of this report. Also present in the upper sections of Figures 5a and 5b is a fragment of fish bone which shows a very high uranium concentration, especially around its edges. This implies addition of uranium to the fish bone after deposition, since living fish contain practically no uranium (Arrhenius et al., 1958). This addition of uranium may have accompanied the diagenetic addition of fluorine to the fish-bone phosphate, i.e., transformation from dahlite to francolite (terminology of McConnell, 1958).

The distribution of fission tracks around the foraminiferal shell shown in Figures 6a and 6b closely follows the distribution of phosphatic material within this area. Notice that within the foram walls the densities of prints are very low, but both inside the chambers and surrounding the shell densities are high. This correlates very well with the distribution of cryptocrystalline apatite within these areas. Figures 6c and 6d illustrate the fission-track distribution along a contact between a sandy layer and a phosphate-rich layer. The uranium is concentrated in the fine-grained phosphatic material. A narrow band of almost pure collophane appears to have been deposited along the contact before the coarse layer was deposited. The collophane coincides with the high uranium concentra-

Figure 6. (a) Photomicrograph of foram shell in sample PD-21-24, polished thin section.

(b) Fission-track prints of same area as (a).

(c) Photomicrograph of contact between sandy layer and fine-grained, phosphate-enriched layer. Polished thin section of sample PD-21-24.

(d) Fission-track prints of same area as (c).

a

b

c

d

tion found along that boundary. The high density of tracks concentrated in one small circular phosphatic area within the sandy layer probably represents a reworked fragment of phosphorite.

The distribution of uranium in the vicinity of large glauconite grains may be seen in Figure 7. The large glauconite grain in Figure 7a is set in a matrix of buff-colored collophane. Notice that the glauconite predates the phosphatic material since the latter has filled-in the cracks and fissures within the grain. This is in contrast to reports of glauconite replacing phosphorite in some areas, such as the Chatham Rise (Pasho, 1973). The fission-track distribution in the two areas shown in Figure 7 exactly parallels the phosphate distribution.

Discussion

In all thin sections examined by this technique, the distribution of tracks can be explained in terms of the distribution of collophane within the sample. If any uranium-rich phases other than apatite are present within the phosphorites, they are very well concealed. The excellent correlations found between fission-track densities and distribution of collophane support the contention that the uranium extracted from these samples for isotopic analysis was derived primarily from apatite.

It should also be pointed out here that uranium derived from detrital phases would probably increase the uranium-series ages reported for these samples. In other words, the $^{234}U/^{238}U$ activity ratio would be lowered by an addition of detrital uranium (assuming

Figure 7. (a) Photomicrograph of glauconite grain in a phosphate matrix. Polished thin section of sample PD-19-37.

(b) Fission-track prints of same area as (a).

(c) Photomicrograph of two altered glauconite grains also contained in sample PD-19-37.

(d) Fission-track prints of same area as (c).

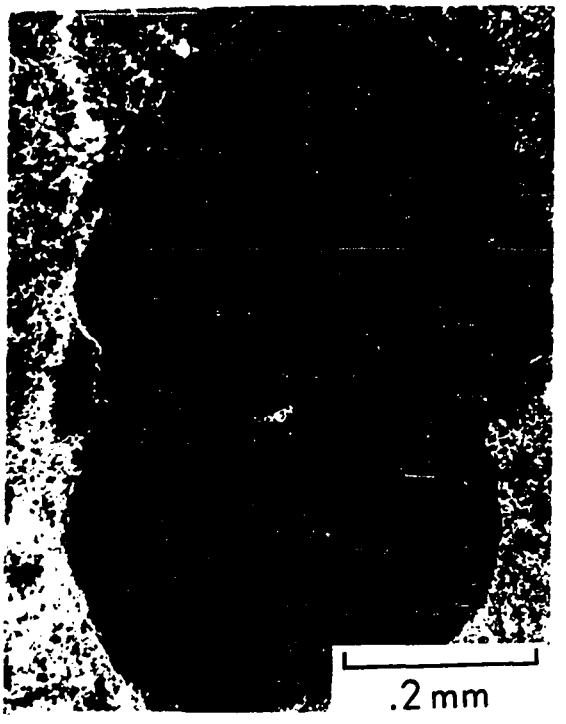

a

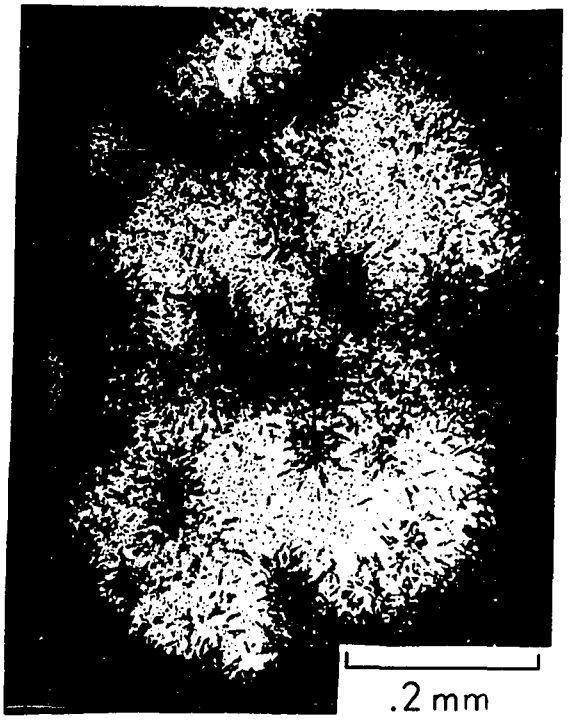

b

c

d

that uranium isotopes within detrital phases have attained equilibrium). The fact that uranium activity ratios in some of the samples have the same values as sea water further supports the contention that the uranium was contained within an authigenic phase.

RADIOMETRIC AGES

Theory

If a system contains an excess of ^{234}U relative to ^{238}U, the activity ratio $^{234}U/^{238}U$ may be useful for dating geologic events providing certain criteria are satisfied. The initial $^{234}U/^{238}U$ ratio in the sample must be known, this ratio must have changed with time only as a result of radioactive decay; and the half-lives must be known accurately. Fleming et al. (1952) have determined reliable half-lives. The initial $^{234}U/^{238}U$ activity ratio for uranium-bearing authigenic minerals on the sea floor has been established as 1.15 by Thurber (1962) and confirmed by Koide and Goldberg (1965) and Veeh (1968) for sea water and appears to be constant, even in widely separated areas of the ocean.

The $^{234}U/^{238}U$ disequilibrium in nature may be due to selective weathering of alpha recoil ^{234}U atoms present near the surface of silicate minerals. These surface atoms are leached more easily than those that are part of the lattice structure (Dooley et al., 1966). It has also been proposed (Kigoshi, 1971) that the dissolution of ^{234}Th atoms produced by the alpha decay of ^{238}U atoms located near the surface of the solid silicate particles may be one of the other mechanisms responsible for this disequilibrium.

The 15 per cent excess of ^{234}U in the oceans is inherited by minerals which extract uranium from sea water. As radioactive decay progresses, the $^{234}U/^{238}U$ activity ratio approaches the secular equilibrium value of unity. The assumption that this ratio changes only as a result of radioactive decay could be proved invalid if any degree of 'openness' of the system were to become apparent. This is an important point regarding results presented here and will be discussed in more detail later in this section.

After natural disequilibrium in sea water was recognized, several applications relating it to the dating of marine materials appeared in the literature. Corals and other carbonates were dated (Barnes et al., 1956; Sackett, 1958; Tatsumoto and Goldberg, 1959; Blanchard, 1963; Broecker, 1963; Broecker and Thurber, 1965; Thurber et al., 1965; Osmond, 1965; Kaufman and Broecker, 1965; Veeh, 1966; Broecker et al., 1968; and Kaufman, 1971). These studies showed that in general, reliable uranium-series ages could be determined in unrecrystallized corals. Ages determined in marine mollusks, however, proved unreliable, apparently because of uranium migration (Kaufman et al., 1971). Accretion rates of manganese in nodules has also been determined by uranium-series techniques (Bender et al., 1966; Ku and Broecker, 1967; and Bender et al., 1970). Uranium-series techniques have been applied to marine phosphorites by D'Anglejan (1967), Kolodny (1969a, 1969b), Kolodny and Kaplan (1970), Baturin et al. (1972), Veeh et al. (1973), and Veeh et al. (in press). Kolodny's data and results are reported here, and they indicate that uranium in

marine apatite may not behave as in a closed system (see discussion below).

The equations for calculating ages from the activity ratios $^{234}U/^{238}U$ and $^{230}Th/^{234}U$, assuming an initial 15 per cent excess of ^{234}U and no initial ^{230}Th, have been presented previously (Kolodny, 1969a). The general differential equations for describing radioactive decay when both parent and daughter atoms are radioactive are given in most standard radiochemistry texts (see for example, Friedlander and Kennedy, 1957). The equations used for age determinations are shown below. The derivations may be found in Kolodny (1969a) or Kaufman and Broecker (1965).

$$\frac{^{234}U}{^{238}U} = \frac{\lambda^{238}U}{\lambda^{234}U - \lambda^{238}U}\left[1 - e^{(\lambda^{238}U - \lambda^{234}U)t}\right] + \left(\frac{^{234}U}{^{238}U}\right)_0 e^{(\lambda^{238}U - \lambda^{234}U)t} \quad (1)$$

$$\frac{^{230}Th}{^{234}U} = \frac{^{238}U}{^{234}U}\left[1 - e^{-\lambda^{230}Th\, t}\right] + \left[1 - \frac{^{238}U}{^{234}U}\right]\left[\frac{\lambda^{230}Th}{\lambda^{230}Th - \lambda^{234}U}\right]\left[1 - e^{-(\lambda^{230}Th - \lambda^{234}U)t}\right] . \quad (2)$$

The decay constant, λ, used are those of Fleming et al. (1952). Time, t, may be determined in equation (1) using logarithms. Equation (2), however, cannot be solved explicitly for t and must be

solved by iterative convergence. To facilitate obtaining age determinations from isotopic data, graphs were prepared by plotting time as a variable against the activity ratios. Figure 8 shows a portion of the $^{234}U/^{238}U$ and the $^{230}Th/^{234}U$ decay curves.

If it is assumed that: (1) the apatite in phosphorites derived uranium from sea water; (2) the uranium was incorporated into the apatite structure when the mineral formed; (3) the uranium isotopic composition of sea water has remained the same for the last million years; and (4) apatite acts as a closed system with respect to uranium, then absolute ages may be determined simply by determining the isotopic composition and reading the age from the respective graph. While the first three assumptions are probably valid, or at least have not been challenged, Kolodny (1969a) has challenged the concept that marine apatite acts as a closed system with respect to uranium.

In the relict phosphorite samples Kolodny analyzed, he discovered that $^{234}U/^{238}U$ activity ratios in tetravalent uranium were significantly lower than unity, indicating that some ^{234}U is being transformed from U(IV) to U(VI). Of course ^{238}U atoms may also be oxidized, but an oxidation process which is not related to radioactive decay should not distinguish between ^{234}U and ^{238}U. Kolodny offered a model to describe this fractionation of activity ratios between oxidation states. He assumed that the fraction of oxidized radiogenic ^{234}U remains constant with time. The relevant equation to describe this 'semi-open system' decay is as follows:

Figure 8. Decay curves for the variation of $^{234}U/^{238}U$ and $^{230}Th/^{234}U$ with time assuming an initial $^{234}U/^{238}U$ activity ratio of 1.15.

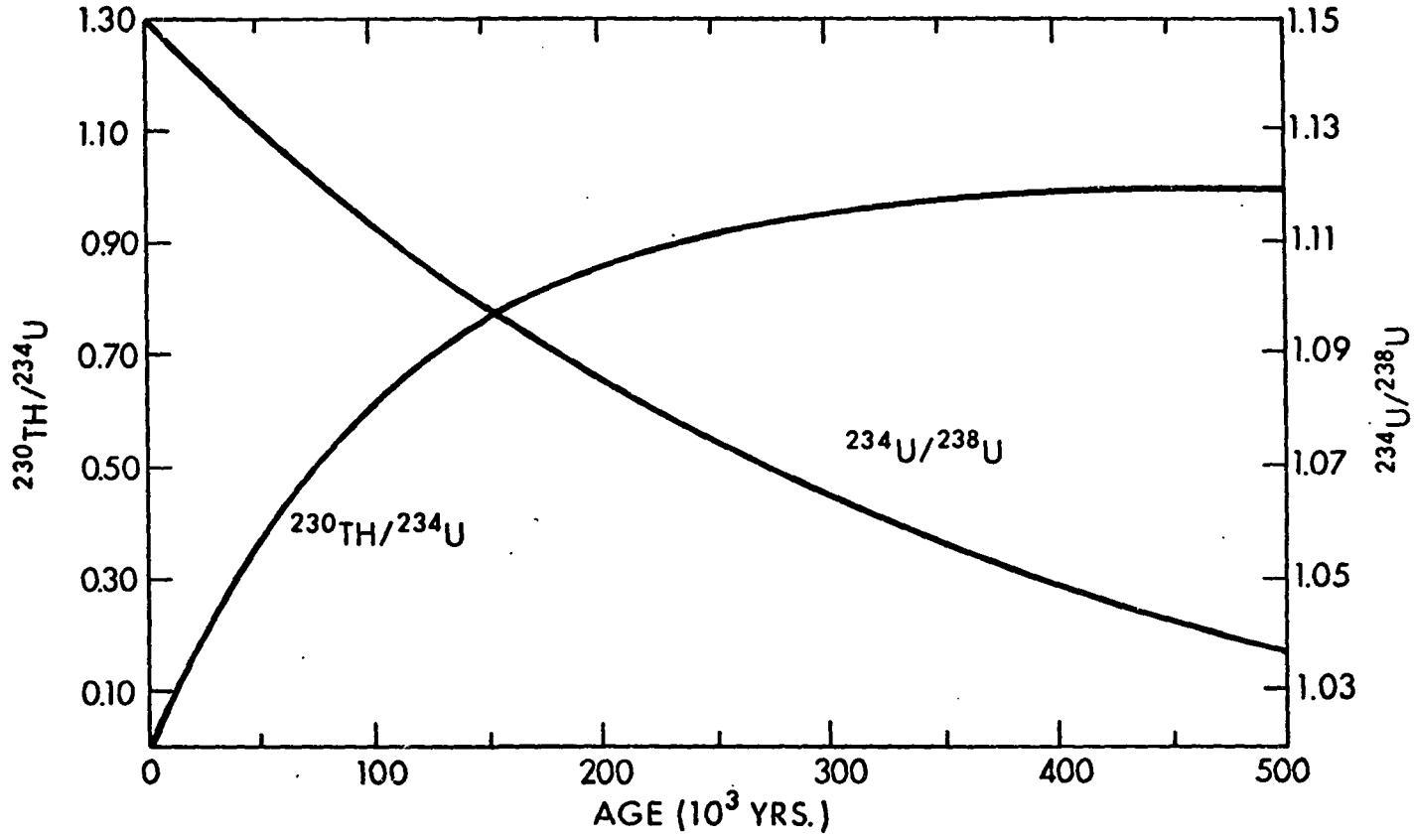
1.30
1.10
0.90
0.70
0.50
0.30
0.10
$^{230}TH/^{234}U$
1.15
1.13
1.11
1.09
1.07
1.05
1.03
$^{234}U/^{238}U$
$^{234}U/^{238}U$
$^{230}TH/^{234}U$
0
100
200
300
400
500
AGE (10^3 YRS.)

$$\left(\frac{^{234}U}{^{238}U}\right)_{IV} = (1 - R\,\frac{\lambda 238_U}{\lambda 234_U - \lambda 238_U}\left[1 - e^{(\lambda 238_U - \lambda 234_U)t}\right] \quad (3)$$

$$+\left(\frac{^{234}U}{^{238}U}\right)_{IV_o} \cdot e^{(\lambda 238_U - \lambda 234_U)t}$$

where R equals the fraction of ^{234}U that is oxidized. Note that the activity ratios given here are for tetravalent uranium. A plot of $(^{234}U/^{238}U)_{IV}$ as a function of time for two different values of R is shown in Figure 9. The initial $(^{234}U/^{238}U)_{IV}$ was again assumed to equal 1.15.

Kolodny (1969a) pointed out that at very large values of t, the right-hand side of equation (3) becomes equal to (1 - R). Therefore R can be determined if we have data for $(^{234}U/^{238}U)_{IV}$ from very old samples. The mean value of the $(^{234}U/^{238}U)_{IV}$ determinations in the relict samples analyzed by Kolodny equals 0.7, therefore R = 0.3. This agrees with Ku's (1965) model for migration of ^{234}U in pelagic sediments. Ku calculated that approximately 30 percent (or 0.3 as a fraction) of the ^{234}U has become 'mobilized', probably by oxidation and complexing of uranium atoms, making the uranium more soluble.

Results and Discussion

The uranium and thorium isotopic data and calculated ages for phosphorites from off South America as well as those from other areas

Figure 9. Variation of $(^{234}U/^{238}U)_{IV}$ with time for R = 0 (closed system) and for R = 0.3 (semi-closed system).

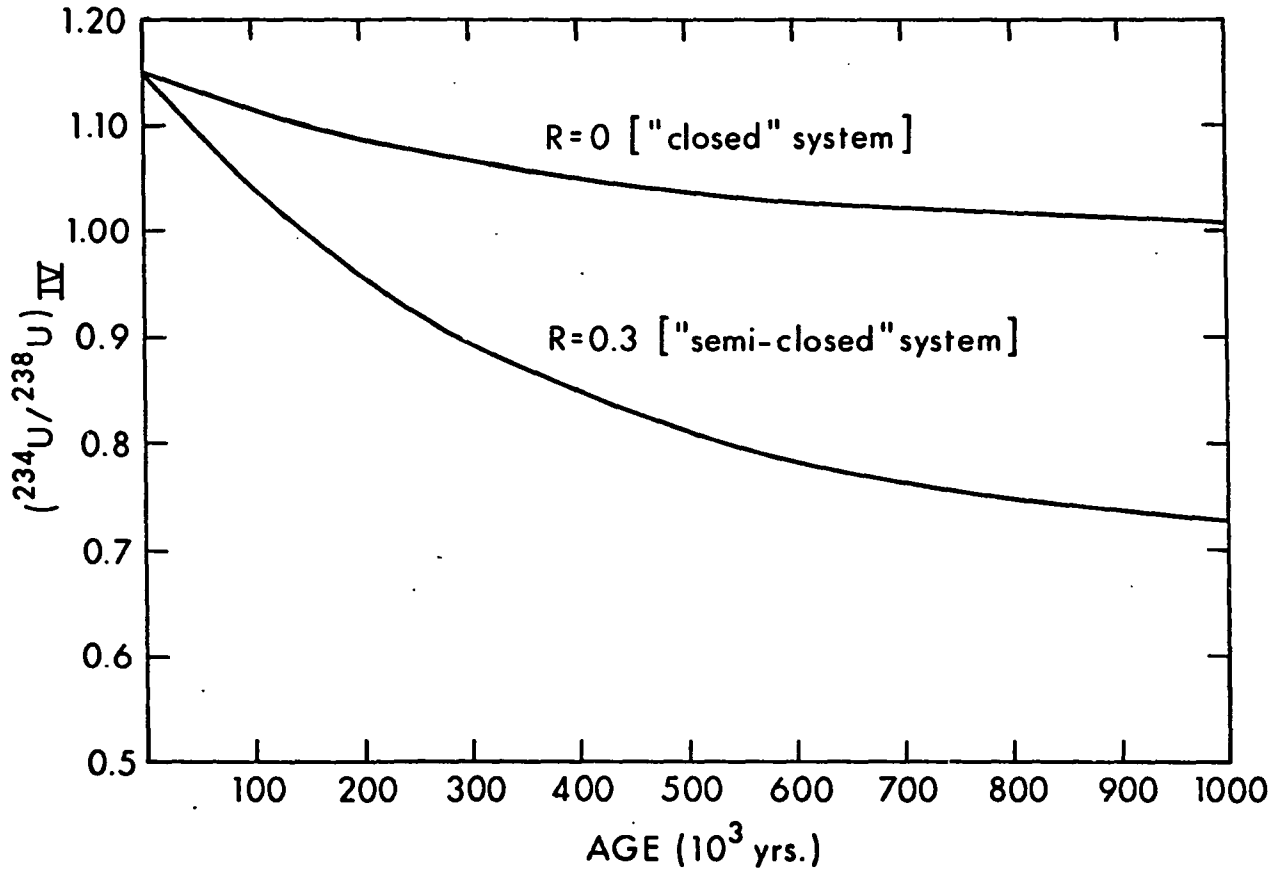
1.20
1.10
1.00
0.9
0.8
0.7
0.6
0.5
$(^{234}U/^{238}U)_{IV}$
R=0 ["closed" system]
R=0.3 ["semi-closed" system]
100
200
300
400
500
600
700
800
900
1000
AGE (10^3 yrs.)

are shown in Table 5. In Figure 10, a histogram of all $(^{234}U/^{238}U)_{total}$ activity ratio determinations in the South America phosphorites compares them with determinations from other areas. Ages based on the decay of ^{234}U toward secular equilibrium with the parent ^{238}U are reported both for a closed system calculation and the 'value' type system of Kolodny (1969a). The closed-system determinations were based on total uranium, whereas the "semi-closed" determinations were based on the $^{234}U/^{238}U$ activity ratios for tetravalent uranium. For very young samples, there were no significant differences between the ages obtained by the two methods, for older samples, the ages for a 'semi-closed' system were significantly younger than those for a closed system. In either case, as shown by the large errors quoted for age determinations in Table 5, the method is not a very sensitive indicator of absolute ages. This is inherent in the method, since the $^{234}U/^{238}U$ activity ratio cannot be measured to better than about 1 per cent, which when converted to absolute years may represent a time span of several thousand years.

Since at this time there is no way to determine the initial amount of ^{230}Th in phosphorite samples, absolute ages cannot be calculated by using the $^{230}Th/^{234}U$ activity ratios. However, if we assume that all the ^{230}Th measured in these samples is a daughter product of the parent ^{234}U within the phosphorite, we can calculate maximum ages. Since thorium is detectable in all samples, it is likely that some initial ^{230}Th was also incorporated into the phosphorite; in effect, lowering the ^{230}Th ages reported here. The

Table 5. Isotopic Data and Ages for Sea-Floor Phosphorites. Concentrations Are in Parts per Million (ppm); Ratios Are Activity Ratios. All Errors Listed Are Based on Counting Statistics

Sample	Uranium (ppm)	Thorium (ppm)	$(\frac{^{234}U}{^{238}U})$	$(\frac{^{230}Th}{^{234}U})$	Age (x 10^3 years) ^{234}U	^{234}U (IV)[1]	^{230}Th
			Peru - Chile				
PD-12-05							
light	168	2.4	1.15 ± 0.01	0.021 ± 0.001	Recent	Recent	≤2
dark	65	1.1	1.14 ± 0.01	0.040 ± 0.002	25 ± 25	--	≤5
fish bone	101	nd[2]	1.15 ± 0.01	0.020 ± 0.001	Recent	--	≤2
PD-15-13							
light	27	2.4	1.17 ± 0.03	0.050 ± 0.002	Recent	--	≤6
dark	102	3.2	1.15 ± 0.01	0.060 ± 0.003	Recent	15 ± 20	≤7
fish bone	101	0.4	1.14 ± 0.01	0.010 ± 0.001	25 ± 25	--	≤1
PD-15-17							
light	182	5.5	1.15 ± 0.01	0.029 ± 0.001	Recent	Recent	≤3
PD-18-30							
dark	72	2.3	1.14 ± 0.01	0.040 ± 0.002	25 ± 25	Recent	≤5
PD-19-30	51	3.7	1.11 ± 0.01	0.35 ± 0.02	110 ± 35	50 ± 20	≤46
PD-19-33	100	3.0	1.14 ± 0.01	0.080 ± 0.004	25 ± 25	Recent	≤9
PD-19-37	172	9.0	1.12 ± 0.01	0.40 ± 0.02	80 ± 30	35 ± 20	≤55
PD-21-24	102	3.1	1.12 ± 0.01	0.35 ± 0.02	80 ± 30	50 ± 20	≤46
PD-21-25	98	3.5	1.06 ± 0.01	0.71 ± 0.03	330 ± 65	>150	≤130
KK-71-161							
bulk	106	5.9	1.09 ± 0.01	0.40 ± 0.02	180 ± 45	--	≤55
surface	103	6.7	1.09 ± 0.01	0.46 ± 0.02	180 ± 45	70 ± 10	≤66
core	10	6.1	1.10 ± 0.01	0.62 ± 0.03	140 ± 40	--	≤102
KK-71-96	118	5.7	1.08 ± 0.01	0.53 ± 0.03	225 ± 45	--	≤81
A-183	96	5.7	1.11 ± 0.01	0.35 ± 0.02	110 ± 35	--	≤46
0544	16	2.2	1.00 ± 0.03	0.74 ± 0.03	>800	--	≤140
0546	67	4.7	1.06 ± 0.02	0.63 ± 0.03	330 ±140	--	≤105
0553	77	2.0	1.16 ± 0.01	0.020 ± 0.001	Recent	--	≤2
Sechura[3]	70	3.6	0.99 ± 0.01	1.02 ± 0.05	>800	--	>200
			Sea off California				
14415	122	2.4	0.98 ± 0.01	1.12 ± 0.06	>800	>150	>200
11876	41	1.1	0.99 ± 0.02	0.88 ± 0.04	>800	--	>200
			Chatham Rise				
X-45	241	1.1	0.99 ± 0.01	0.01 ± 0.05	>800	>150	>200
X-188	124	1.3	1.00 ± 0.01	1.01 ± 0.05	>800	--	>200
			Other Areas				
Blake Plateau	50	4.6	1.00 ± 0.01	0.99 ± 0.05	>800	--	>200
Necker Bank	23	8.2	0.99 ± 0.01	1.23 ± 0.06	>800	--	>200

[1] Ages based on $(\frac{^{234}U}{^{238}U})_{IV}$ values reported in Table 6; see text for discussion.

[2] nd = not detected.

[3] On-land sample, Sechura Desert, Northern Peru.

Figure 10. Histogram of $(^{234}U/^{238}U)_{total}$ activity ratios determined in phosphorites from the continental margins of Peru and Chile. Results reported by Kolodny and Kaplan (1970) shown for comparison.

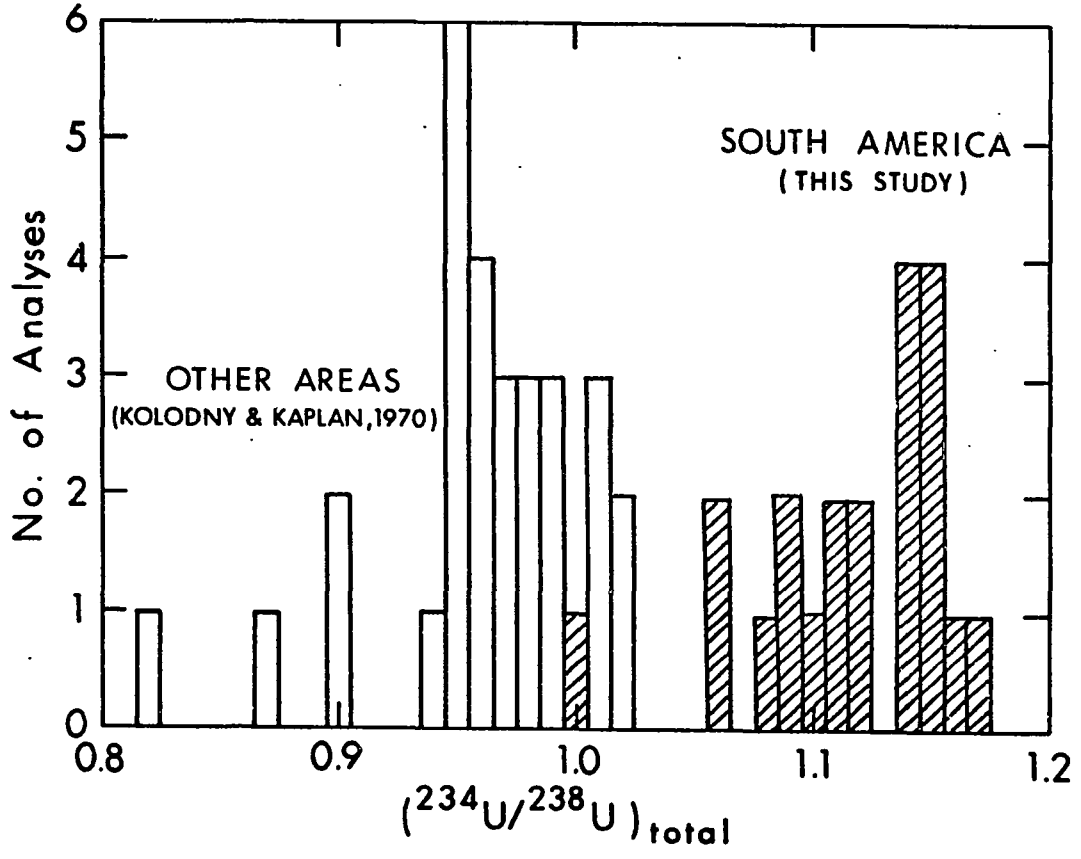
SOUTH AMERICA
(THIS STUDY)
OTHER AREAS
(KOLODNY & KAPLAN,1970)
No. of Analyses
0
1
2
3
4
5
6
0.8
0.9
1.0
1.1
1.2
$(^{234}U/^{238}U)_{total}$

maximum thorium ages reported in Table 5 were calculated assuming a closed system, so if a portion of the ^{234}U atoms were initially mobilized, the $^{230}Th/^{234}U$ activity ratios reported here are really too large, and a correction to lower the calculated ages is necessary. Since the two main assumptions in calculating thorium ages are both likely to be unreliable, with the effect of moving age determinations toward older ages, it would seem appropriate to regard such values as upper-limit ages.

Upon inspection of the data, it is evident that the ^{234}U ages based on the 'semi-closed' system are in good agreement with the maximum ^{230}Th ages, but those calculated on the basis of a closed system are invariably higher than the 'maximum' thorium ages. This discrepancy must be due to 'leakage' of some ^{234}U atoms out of the apatite structure, resulting in lowered $^{234}U/^{238}U$ activity ratios. This reasoning supports the results of Kolodny (1969a), and therefore his 'value-type' decay scheme is favored here. If the ^{230}Th ages do represent maximum ages, as they should, there is no way to reconcile some of the significantly higher closed system ^{234}U ages. In every case, ages based on the 'semi-closed' decay scheme of Kolodny agree within experimental error with the reported maximum thorium ages.

It is also possible that a relatively large and recent addition of sea-water uranium to the phosphorites could produce spuriously high $^{234}U/^{238}U$ values and low $^{230}Th/^{234}U$ values, resulting in deceptively young radiometric ages. It is considered unlikely here, however, for two main reasons: (1) there is no correlation in the data between uranium concentration and age; and (2) isotopic data in phosphorites

which have been shown to be old (such as those from off California and the Chatham Rise analyzed) do not show any evidence of secondary addition of uranium. As mentioned previously, it appears that any mobility of uranium in the marine apatite system involves a loss of uranium to sea water. Leaching of uranium from the phosphate rocks should not affect the $^{234}U/^{238}U$ activity ratios since there is no reason why weathering processes should leach one isotope in preference to another when the relative masses of the isotopes are similar. Rather, it is the simultaneous oxidation and disintegration of a $^{238}U(IV)$ atom to a $^{234}U(VI)$ atom which influences the net activity ratio. Correction for this factor has been made in the 'semi-closed' system ages reported in Table 5.

Because of the known ^{234}U migration in the apatite-sea water system, only ^{234}U ages which have been corrected for 'leakage' and maximum ^{230}Th ages are used in the geologic interpretation presented here. The corrected ^{234}U ages range from greater than 150,000 years before present to Holocene; and the ^{230}Th ages range from less than or equal to 140,000 years ago to Holocene. The 'best' age for each of the fifteen phosphorites sampled off South America was computed by taking the mean of the $^{234}U(IV)$ ages and the maximum ^{230}Th ages. ^{230}Th ages were used for samples which have no $^{234}U(IV)$ data. These ages are plotted in a histogram (Fig. 11). Upon inspection of the histogram, it is evident that the data are not distributed randomly but rather occur at intervals. Over 90 per cent of the Peru-Chile samples dated fell into one of four age groups: 0 to 10; 40 to 50; 100 to 105 and 130 to 140 thousand years before present.

Figure 11. Histogram of radiometric ages determined for phosphorites from the Peru-Chile area.

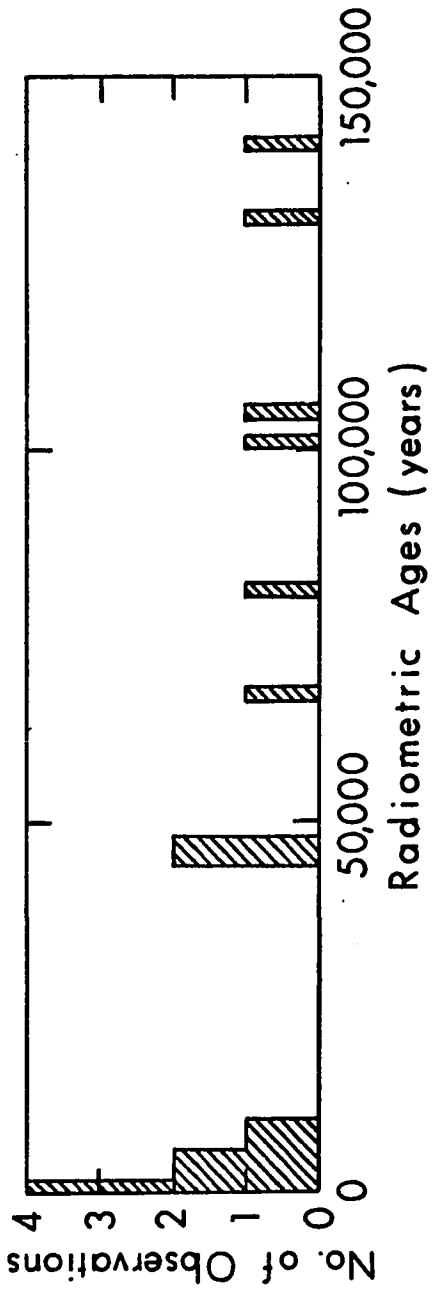
No. of Observations
0
1
2
3
4
0
50,000
100,000
150,000
Radiometric Ages (years)

Plotted in Figure 12 are all 15 radiometric dates determined for the Peru-Chile samples, together with a reconstruction of Veeh and Chappell's (1970) eustatic sea-level fluctuation curve. The curve was based on field observations and radiometric dates (radiocarbon and ^{230}Th) of uplifted coral reef terraces on New Guinea. All the ages of phosphorites appear to coincide with high eustatic stands of the sea. This relationship is most evident during the last 50,000 years. Samples (10) with radiometric ages within that range fall in two high stands of the sea which occurred during that interval. The remaining five samples have radiometric ages which may correlate with sea level fluctuations, but their number is too small for the correlation to be statistically sound.

If this correlation between phosphorite formation and high eustatic stands of the sea is valid, there should be some type of genetic relationship between the environmental conditions during interglacials and the production of apatite. Concentration of phosphatic material by sea level changes has been discussed by other authors (Baturin, 1971; Cook, 1967), and the association of the greensand-phosphate facies with a transgressive sea is well known (Goldman, 1922). Phosphorite deposits formed in this way are primarily the result of physical processes which accompany the sea-level change. Reworking of the phosphatic material and winnowing of the fines are the most important processes which tend to concentrate phosphatic sediments.

Figure 12. Correlation of radiometric ages of phosphorites from the Peru-Chile area of the South American continental margin with eustatic sea level changes over the last 150,000 years. The arrows represent radiometric ages determined in this study. Sea level curve redrawn from Veeh and Chappell (1970).

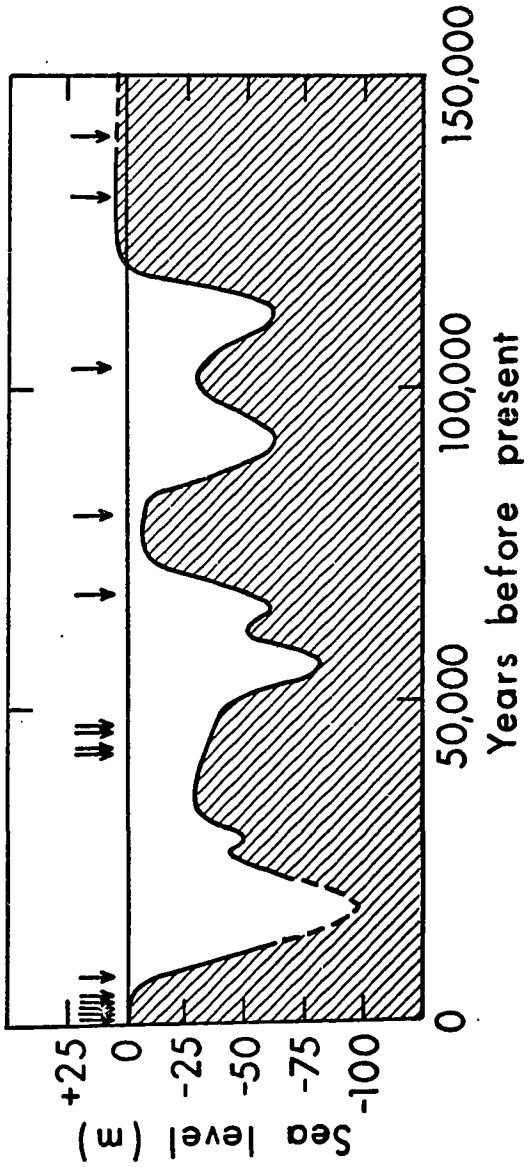
Sea level (m)
+25
0
-25
-50
-75
-100
0
50,000
100,000
150,000
Years before present

Since the radiometric ages measured here reflect the time of precipitation of the constituent apatite, it is unlikely that the sea-level correlation noted here is a result of reworking processes. It seems more plausible that physical and/or chemical factor(s) which directly relate to the precipitation of marine apatite were operating during those high stands of the sea. One factor which may vary closely with eustatic sea-level changes, and may influence apatite solubility in ocean water, is temperature. A possible correlation between periods of warmer-than-average ocean water temperatures and phosphorite formation was suggested by Kolodny (1969a). He noted that many phosphate deposits of the world are of Miocene age, a period of supposedly warm seas. Emiliani's (1970) generalized isotopic paleotemperature curve is reproduced in Figure 13, together with the phosphorite ages. Although the generalized curve shown is based on data from Atlantic deep-sea cores, the curve representing past conditions in the equatorial regions of the Pacific would probably be similar. Van Donk (1973) has shown, for example, that agreement of oxygen isotope fluctuations between cores taken from the equatorial regions of both the Atlantic and the Pacific is remarkably good. Cycles of estimated temperature in three cores from the tropical southeast Pacific, studied by Luz (1973), also were found to be in phase with cycles in Atlantic cores for the last 200,000 years. According to Dansgaard and Tauber (1969), at least 70 per cent of the oxygen isotopic fractionation observed over the last 400,000 years was due to isotopic changes in sea water rather

Figure 13. Correlation of radiometric ages of phosphorites from Peru-Chile area of the South American continental margin with changes in average surface-water temperatures over the last 150,000 years. The generalized isotopic paleotemperature curve was redrawn from Emiliani (1970).

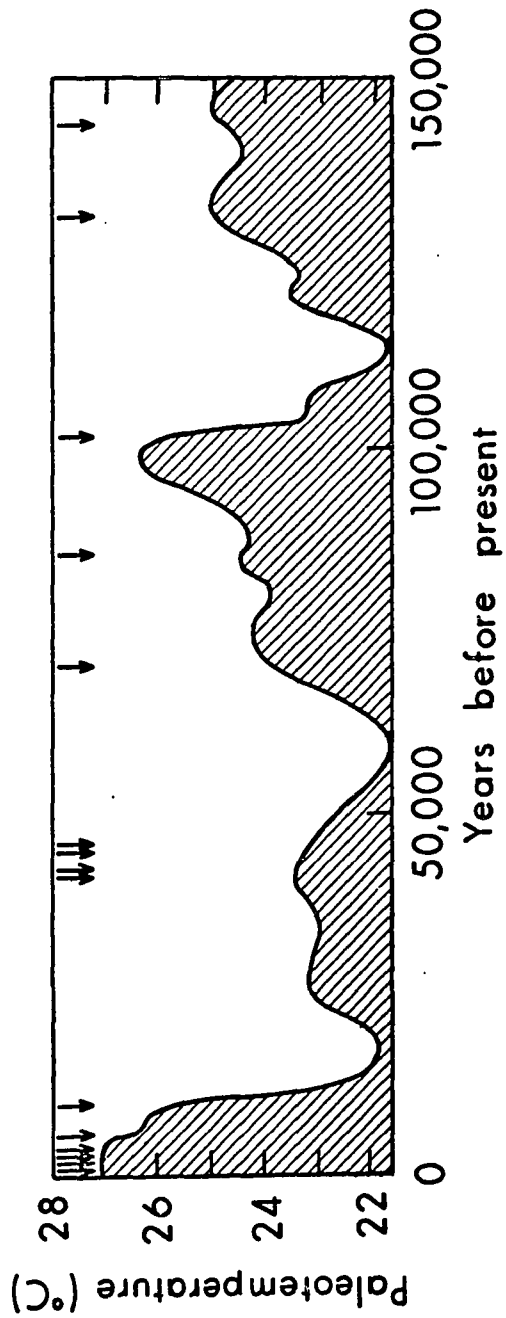
Paleotemperature (°C)
28
26
24
22
0
50,000
100,000
150,000
Years before present

than to changes in the ocean surface temperatures. If this is the case, then the magnitude of Emiliani's paleotemperature curve would necessarily diminish, but the general pattern would remain essentially the same. At least one paleo-climatic study (Dinkelman, 1973) of sediment cores from this general area has provided data which are in agreement with the apatite-temperature association suggested here. Dinkelman's results are based on radiolarian assemblages found in cores taken from the Panama Basin in the eastern equatorial Pacific. His data indicate a warm period in this area from approximately 50,000 to 40,000 years before present. Of the fifteen localities along the Peru-Chile coast from which phosphorite samples were dated, four provided samples within this age range.

In general, the paleotemperature curve suggests that phosphate deposition was favored by periods of warm seas. This relationship must be viewed with caution, however, since in an area of upwelling, vertical and horizontal advection will markedly alter the distribution of physical and chemical properties (Smith, 1968). Since past hydrographic conditions off the coasts of Peru and Chile cannot be determined with certainty, only estimates can be made concerning the paleo-oceanographic conditions which prevailed in those areas. If upwelling were operating off the west coast of South America during past interglacials, it would not be unreasonable to suspect that the thermal gradients in the coastal waters were quite low, as today. The intensity of upwelling during past periods off those coasts is not known, but Gardner (1973) has shown that off the west coast of

Africa upwelling was intensified during glacial stages. With continued additional upwelling of cold intermediate water to the surface layer, it is likely that any change in the surface water temperature would be subdued in the bottom waters on the continental shelf. The largest absolute temperature changes as given in Emiliani's (1970) paleotemperature curve are on the order of 5°C. This would translate to a magnitude of only a few degrees or less where cold waters are upwelling to the surface.

Because of these limitations, it is only hypothesized here that temperature fluctuations on the continental shelf off the west coast of South America during the Pleistocene were favorable to the precipitation of apatite. Kramer (1964) showed that apatite of a fixed composition will become less soluble in sea water with a rise in temperature. A rise in sea water temperature could also result in a loss of dissolved CO_2, with a consequent rise in pH, a situation which would also lower the solubility of apatite (Gulbrandsen, 1969). It is quite conceivable that other environmental changes which accompany high eustatic changes in sea-level may have influenced the deposition of thses phosphate deposits. Changes in organic productivity, intensity of upwelling, current patterns, and continental runoff probably had a significant influence on the sedimentary environment on the continental shelf. Unfortunately, it is difficult to assess the influence of these variables with regard to the production of sedimentary apatite because the magnitude (and in many cases the direction) of these changes are unknown. Since the

radiometric evidence indicates contemporary formation of phosphorite off the west coast of South America, a study of the present depositional conditions (rather than past environments) in this area would prove more valuable in formulating a satisfactory model for the genesis of marine phosphorites.

OXIDATION STATE STUDIES

Theory

Uranium is abundant in marine phosphate deposits. It has been suggested that the uranium is present in phosphorites as: (1) finely-dispersed grains of uranium oxide (Serebryakova and Razumnaya, 1962); (2) associated with organic matter; (3) incorporated into or absorbed upon detrital or authigenic mineral phases; or (4) contained within the constituent apatite. Most authors (Altschuler et al., 1958; Kolodny, 1969a) favor the latter interpretation as the most reasonable one. The fission-track results presented earlier support the contention that the uranium of phosphorites is mainly associated with the apatite.

Uranium occurs in both tetravalent and hexavalent states in phosphorites (Altschuler et al., 1958). U(IV) may substitute directly for Ca^{2+} in the apatite structure because of the similarity in their ionic radii. U(VI) in the apatite structure, however, is not so easily explained. Ames (1960) suggested that hexavalent uranium as the uranyl ion, UO_2^{2+}, substitutes for two calcium ions. His conclusions were based upon the experimental uptake of uranyl ions from an alkaline solution during the replacement of calcite by

carbonate apatite. McConnell (1973) suggested that hexavalent uranium occurs as UO_4^{2-} groups substituting similarly to AlO_4^{5-}, which is known to occur in significant amounts in some apatites (Fisher and McConnell, 1969). Kolodny (1969a) assumed that both U(IV) and U(VI) are structurally bound to the apatite lattice.

The relative amounts of uranium in each oxidation state are quite variable in phosphorites, ranging from 3 to 91 per cent tetravalent uranium, according to the results of Altschuler et al., (1958). These authors suggested that uranium initially is fixed in marine apatite predominantly as U(IV) and subsequently is oxidized by weathering to U(VI). Kolodny (1969a) reported a range of tetravalent uranium between 38 and 86 per cent of the total in samples with measurable U(IV). Samples from the Blake Plateau and from a Pacific seamount analyzed by Kolodny contained no measurable U(IV), probably because of the highly oxidizing conditions in those areas. Results of oxidation-state determinations can be grouped by regions. For example, phosphorites from the Chatham Rise area, display significantly higher U(IV) percentages than do samples from the sea off California (Kolodny, 1969a).

Results and Discussion

Uranium oxidation-state determinations are reported here for most of the phosphorites discussed in the previous section. The $^{234}U/^{238}U$ activity ratios are also reported for U (total), U(IV) and U(VI). The U(VI) values reported are calculated from the equation given by

Kolodny (1969a):

$$A = P_{(IV)} \cdot A_{(IV)} + P_{(VI)} \cdot A_{(VI)}$$

where A represents the appropriate activity and P is the weight fraction of the respective valance states. The concentrations, isotopic compositions, percentage of U(IV), and fractionation factors (f) for all samples analyzed are listed in Table 6. The fractionation factor indicates the degree of isotopic fractionation between the two oxidation states (Kolodny, 1969a).

The content of tetravalent uranium in samples from off South America ranged from 40 to 71 per cent of the total uranium. This range is nearly the same as that 38 to 79 per cent U(IV) reported by Kolodny for phosphate samples from the sea off California. The Chatham Rise phosphorites contained the highest proportion of U(IV), averaging close to 80 per cent U(IV). Figure 14 illustrates some regional differences when the per cent U(IV) values are plotted against total uranium. Kolodny's (1969a) results are plotted here for the Chatham Rise and the sea off California samples, and the approximate boundaries are delineated. Determinations in our laboratory of samples from the sea off California and the Chatham Rise agreed well with Kolodny's results. Most of the samples from South America fall into the same range as the California borderland samples. None of the samples from South America gave values which would place them within the range delineated by samples from the Chatham Rise area. This apparent segregation may be a reflection of

Table 6. Concentrations and Activity Ratios of Total, Tetravalent and Hexavalent Uranium in Sea-Floor Phosphorites. Concentrations in Parts per Million (ppm); Errors Shown Calculated from Counting Statistics

Sample	U Total (ppm)	U(IV) (ppm)	$(\frac{^{234}U}{^{238}U})_{Total}$	$(\frac{^{234}U}{^{238}U})_{IV}$	%U(IV)	$(\frac{^{234}U}{^{238}U})_{VI}$ [1]	f [2]
			South America				
PD-12-05 light	168 ± 3	67 ± 2	1.15 ± 0.01	1.14 ± 0.03	40	1.16	1.0
PD-15-13 dark	81 ± 1	46.5± 0.6	1.14 ± 0.01	1.13 ± 0.02	57	1.15	1.0
PD-15-17 light	219 ± 4	88 ± 2	1.15 ± 0.01	1.14 ± 0.03	40	1.16	1.0
PD-18-30 light	53 ± 1	33 ± 2	1.16 ± 0.02	1.19 ± 0.04	62	1.11	0.9
PD-19-30	50.1± 0.6	24.9± 0.5	1.11 ± 0.01	1.09 ± 0.02	50	1.13	1.0
PD-19-33	103 ± 1	55 ± 1	1.13 ± 0.01	1.15 ± 0.02	53	1.11	1.0
PD-19-37	156 ± 2	84 ± 2	1.12 ± 0.01	1.11 ± 0.02	54	1.13	1.0
PD-21-24	76 ± 1	54 ± 2	1.10 ± 0.02	1.09 ± 0.02	71	1.12	1.0
PD-21-25	85 ± 3	51 ± 1	1.04 ± 0.03	0.84 ± 0.03	60	1.34	1.6
KK-71-161	110 ± 2	74.5± 0.7	1.10 ± 0.02	1.07 ± 0.01	68	1.16	1.1
			Sea off California				
14415	97.5± 0.9	58.0± 0.8	1.00 ± 0.01	0.76 ± 0.01	59	1.34	1.8
Mean of 15 Samples, Kolodny (1969)	72	42	0.97	0.71	58	1.36	1.9
			Chatham Rise				
X-45	212 ± 2	189 ± 2	0.99 ± 0.01	0.79 ± 0.01	89	2.61	3.3
Mean of 7 Samples, Kolodny (1969)	231	181	0.99	0.72	78	2.06	2.9
			Straits of Florida				
GS-4A	158 ± 4	~2	0.99 ± 0.02	--	~1	--	--
GS-39X	187 ± 2	160 ± 4	0.98 ± 0.01	0.73 ± 0.02	85	2.40	3.3
GS-41NN	135 ± 1	~1	1.00 ± 0.01	--	~1	--	--
GS-716B	31.6± 0.5	~2	0.97 ± 0.01	--	~6	--	--
GS-11P	355 ± 5	194 ± 4	0.98 ± 0.01	0.84 ± 0.02	55	1.15	1.4
GS-25G	12.6± 0.5	~0.3	0.99 ± 0.02	--	~2	--	--

[1] Calculated by method given in Kolodny (1969).

[2] $f = \frac{(^{234}U/^{238}U)_{(VI)}}{(^{234}U/^{238}U)_{(IV)}}$ = fractionation index of uranium isotopes between two oxidation states.

Figure 14. Total uranium versus per cent tetravalent uranium for marine phosphate rock samples from the Chatham Rise and the Sea off California (Kolodny and Kaplan, 1970) and from the Peru-Chile continental margin (this study). Closed boxes represent samples from Peru and Chile; closed circles represent California borderland samples; and open circles represent samples from the Chatham Rise. Special symbols denote Chatham Rise and California borderland samples determined in our laboratory.

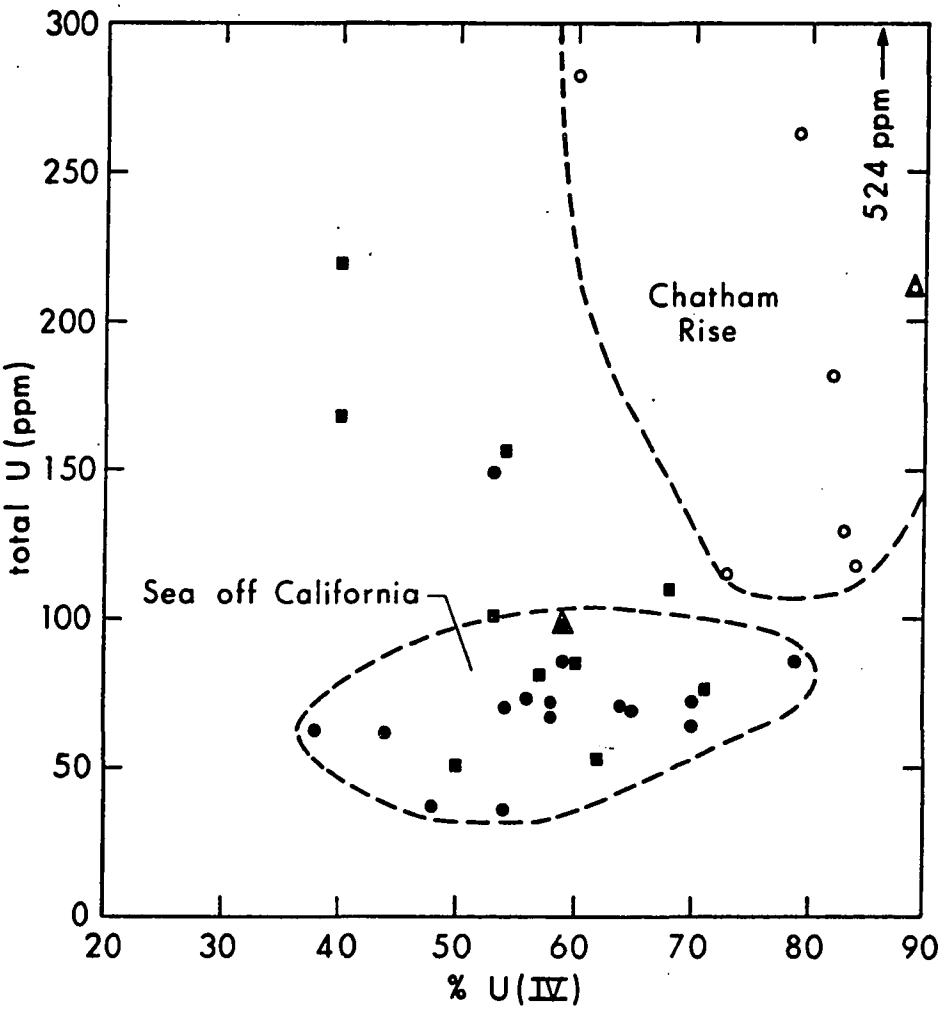
300
250
200
150
100
50
0
total U (ppm)
20
30
40
50
60
70
80
90
% U(IV)
524 ppm
Chatham
Rise
Sea off California

different modes of uranium fixation in the phosphorites. The Chatham Rise samples are phosphatized limestones (Norris, 1964; Summerhayes, 1967), whereas the phosphate rocks from the sea off California are described as pelletal or bedded phosphorites (Emery, 1960). It was suggested by Ames (1960) that certain cations may enter the apatite lattice more easily during the replacement of calcite by apatite. The possibility that some primary genetic aspect is responsible for the distribution of uranium oxidation states can be supported by the observation that the mode of formation of the South American phosphorites is similar to that of phosphorites from the sea off California.

Altschuler et al. (1958) contend that uranium is mostly incorporated into the apatite as U(IV) and that subsequent oxidation is responsible for the U(VI) content of phosphorites. The data presented here do not support their contention. If all of the uranium which entered the apatite structure initially was U(IV), it would not be unreasonable to expect the older samples would contain relatively less U(IV), because they would have had more time for oxidation to U(VI). This should be especially true in samples from the same area, since they would have been subjected to similar environmental conditions. However, just the opposite appears to be the case. The Chatham Rise phosphorites are of Miocene age (Norris, 1964). The California borderland deposits are Miocene with possible renewed Quaternary deposition (Emery, 1960). The phosphate rocks from the Peru-Chile area, on the other hand, have been dated here as late

Pleistocene to Holocene. There is little difference, however, between the relative amounts of U(IV) in samples from the sea off California and the younger Peru-Chile deposits. If only the samples from South America are considered, there is still no apparent relationship between age and the amount of oxidized (hexavalent) uranium. A more likely interpretation is that uranium is initially incorporated into the apatite lattice in both oxidation states. It may be that the redox potential of the environment determines which oxidation state will be the more abundant.

Another interesting aspect of the data concerns the fractionation of uranium isotopes between the two oxidation states. Kolodny (1969a) showed that a strong isotopic fractionation exists between tetravalent and hexavalent uranium in phosphate nodules. That fractionation, designated by the "f"factor in Table 6, is not significant in most of the younger Peru-Chile phosphorites, in agreement with Kolodny's model of uranium in marine apatite in which he suggested an 'escape' of ^{234}U atoms from the tetravalent to the hexavalent state. The 'escape' occurs when ^{234}U atoms are displaced into sites where they are more likely to be oxidized than is the ^{238}U parent. Since this 'displacement' of ^{234}U atoms occurs during radioactive decay, it is obvious that the isotopic fractionation is related to age; i.e., more radioactive disintegrations will allow more ^{234}U atoms to become oxidized. It is reassuring to note that the fractionation factors determined in our laboratory for samples from the sea off California and the Chatham Rise agree well with Kolodny's average values for these areas.

Phosphate samples from the Straits of Florida also were analyzed during this study for their uranium content and isotopic composition of total and tetravalent uranium. Because the Straits of Florida represent a highly oxygenated environment in contrast to the reducing environment off Peru-Chile, a significant difference in the distribution of uranium oxidation states between these two areas was anticipated. Samples analyzed included four from the surface of the Pourtales Terrace. This area is composed mostly of a Miocene hardground with a partial covering of Quaternary carbonate sand and gravel (Gorsline and Milligan, 1963; Gomberg, 1973). Two samples from the seaward-facing escarpment of the terrace also were analyzed. These samples probably consist of pre-Miocene material. Analysis showed insignificant amounts of U(IV) in samples from the surface of the terrace but larger amounts in the samples from the escarpment. This may be due to a change in depositional environment from pre-Miocene reducing conditions to the highly oxidizing conditions which characterize the Straits of Florida today. Discussion of these results with regard to the geologic history of the Pourtales Terrace will be presented elsewhere (Burnett and Gomberg, in preparation).

The study of the Pourtales Terrace phosphorites illustrates that information on the valence of uranium in marine apatite may be useful for studies of past environments in some cases. Kolodny (1969a) did show, however, that the relative amount of U(IV) was lower (although still significant) in the oxidized, light-colored outer sections than in the darker interior portions of two phosphorite

nodules from off California. If uranium oxidation-state results are interpreted with some degree of caution, they could be useful for paleo-environmental reconstructions; or more specifically, they could be used to verify whether a particular facies was reducing or oxidizing.

SUMMARY

The distribution of uranium within sea-floor phosphorites from off the west coast of South America has been studied by fission-track techniques. Results indicate that the uranium is primarily associated with the collophane (micro-crystalline apatite) fraction of the phosphorites. Uranium-series disequilibrium methods, therefore, should provide reliable ages for apatite precipitation if the uranium incorporation is syngenetic with the apatite formation.

Radiometric ages based on the natural disequilibrium of uranium isotopes in sea water indicate that marine phosphorites are currently forming along the continental margins of Peru and Chile. The absolute ages determined here from fifteen samples range from late Pleistocene to Holocene. The pattern of uranium-series ages suggests that phosphate deposition was episodic rather than continuous over the last 150,000 years, and the ages coincide well with periods of high eustatic sea-level stands. Since apatite solubility is known to decrease with an increase of temperature, it would appear that past fluctuations of sea-water temperature influenced the precipitation of apatite in the oceans.

The fractionation of uranium isotopes between oxidation states in the relatively young phosphorites from South America has been shown to be low compared with that in older deposits. This supports the contention of Kolodny, who suggested that the major mechanism by which $^{234}U/^{238}U$ is being fractionated is displacement of ^{234}U atoms into sites where they are more 'oxidizable than is the ^{238}U parent atom. The relative amount of U(IV) contained in phosphate deposits is not only related to age but also appears to be a function of how reducing the environment was during deposition and how much, if any, uranium had been oxidized since having been incorporated into the apatite structure. Determinations of oxidation state from phosphorite samples from the Pourtales Terrace, Straits of Florida, suggest that these data may indicate the oxidizing conditions of a past environment.

The conclusions reached here, on the basis of the uranium-series disequilibrium results, bear on several important aspects of the genesis of sea-floor phosphorites. After the mineralogical and chemical data are presented in the next section, an attempt will be made to synthesize these results into a working hypothesis for the origin of phosphate deposits off Peru and Chile.

PART III: GEOCHEMICAL STUDIES AND MODEL OF PHOSPHORITE GENESIS

INTRODUCTION

Although the literature on phosphorites is quite extensive, our present knowledge concerning the origin of these deposits is still incomplete. Several theories have been put forth over the years in an attempt to explain the mode of formation of marine phosphate deposits. The first marine phosphorite nodules dredged from the sea floor on the Agulhas Bank during the Challenger Expedition were explained by Murray and Renard (1891) as the result of a catastrophic destruction of life. Blackwelder (1916) suggested that the phosphatic material precipitates directly out of sea water depleted in dissolved oxygen. A relationship between phosphatic deposits and climatic variations was proposed by Pardee (1917), who explained the formation of the Permian Phosphoria Formation of the Western United States as a result of the cool conditions associated with the Permian glaciation. Mansfield (1940) attempted to correlate periods of phosphate deposition within the geologic record to periods of widespread vulcanism. His idea was that an addition of F to the oceans as HF from volcanoes would lower the solubility of apatite and chemical precipitation of this mineral would result.

Most modern theories of phosphorite formation are modeled after Kazakov's (1937) model of direct inorganic precipitation of marine apatite. The main premise of this theory is that the ascent of phosphate-rich waters in regions of upwelling involves a decrease in partial pressure of CO_2 with a consequent rise in the pH. This results in supersaturation of sea water with respect to carbonate fluorapatite, and direct inorganic precipitation then results.

Dietz et al. (1942) and Emery (1960) favored this type of interpretation after investigating phosphate rocks from the sea floor off California.

D'Anglejan (1967), in a study of the marine phosphorites off Baja California, concluded that the main source of phosphate was the dissolution of marine organisms. The physical and chemical factors which favor precipitation of marine apatite were reviewed by Gulbrandsen (1969). A review by Tooms et al. (1969) contains a comprehensive summary of past and current ideas related to the genesis of marine phosphorites. These authors suggested that carbonate apatite forms within the interstitial waters of sediments where phosphate is more concentrated than in the bottom waters.

Studies have shown that phosphorites may also form by replacement of previously existing materials, usually carbonates. Phosphate-bearing solutions washed down from guano deposits may replace underlying limestone (Hutchinson, 1950). Phosphatized foraminiferal limestones from the tops of Pacific seamounts were described by Hamilton (1956), and from the Straits of Florida by Gorsline and Milligan (1963). The phosphatization of fecal pellets has been proposed by Bushinsky (1964, 1966) as a mechanism which may form a pelletal phosphorite. D'Anglejan (1968) recognized an increase in the amount of apatite in the lower sections of sediment cores recovered on the California borderland. He attributed this increase to a replacement of foraminiferal shells by carbonate fluorapatite.

Carbonate skeletons and fecal pellets are not the only materials capable of being phosphatized. For example, Goldberg and Parker (1960) report the occurrence of phosphatized wood dredged from a depth of 410 m in the Gulf of Tehuantepec. Even calcic plagioclase phenocrysts of volcanic rocks in association with seamount phosphorites have been phosphatized (Lisitzin, personal communication).

Because of the strong evidence supporting the formation of marine phosphorites by replacement mechanisms, several investigators have expressed the opinion that replacement may be the only way phosphate rock deposits are formed. Pevear (1966, 1967), for example, exclusively favored a replacement-type mechanism producing phosphorite deposits. It has recently been shown experimentally by Martens and Harriss (1970) that the presence of Mg^{2+} ions in solutions resembling sea water inhibits the precipitation of apatite. In view of their results, these authors find it difficult to believe that apatite is formed in either an estuarine or an oceanic environment by direct precipitation. They suggest that apatite replacement of calcite is the principal phosphate buffering mechanism in today's oceans.

In this investigation, marine phosphate rocks from the sea floor off the western coasts of Peru and Chile have been analyzed for their bulk chemical and mineral composition. The objective was to characterize these deposits geochemically and to compare them with phosphorites described from other areas of the world. To my knowledge, no prior chemical or mineralogical results have been reported for the phosphate deposits of the South American continental margin.

A series of gravity cores taken along a profile at approximately 12° S. latitude on the Peru shelf resulted in the recovery of several undisturbed cores of organic-rich muds and some phosphate rock. These sediments have been studied to elucidate the genetic relationship between the phosphorites and the associated sediment. Without some examination of these sediments, for example, it would not be possible to state explicitly whether or not the phosphate rocks are the product of a replacement mechanism within the sediments. Whatever the mode of origin of these deposits, it seems most unlikely that they formed without some type of interaction with the associated sediment.

In addition to the bulk mineral and chemical analyses, electron microprobe studies have been performed on many of the phosphate rocks. Because the mineral constituents of phosphorites typically are inhomogeneous, this type of analysis is desirable. Microprobe analyses were made of selected 'spots' within the rock specimens and electron-beam scanning techniques were employed to show elemental distributions within small areas. Such studies are valuable for assessing the relationships between the skeletal and detrital components and the phosphatic matrix of the deposits.

Because of the extremely small grain-size of the apatite of phosphorites (individual crystals are usually on the order of a micron or less), an ordinary petrographic microscope is inadequate to study small-scale structure or texture. For this reason, a scanning electron microscope (SEM) was employed for examination of the micro-structure and apatite growth fabrics within the phosphate rocks.

METHODS

X-ray Mineralogy

A semi-quantitative X-ray mineralogy technique developed for the shore-based analysis of samples collected by the Deep Sea Drilling Project (DSDP) has been employed for this study. Both the theoretical and practical aspects of the method have been discussed by Rex and Murray (1970) and Fan and Rex (1972). The method determines a concentration factor for each mineral analyzed. This factor is the mass absorption coefficient ratio of that mineral to quartz for the optical slit system used. The factor is determined experimentally by analyzing standards prepared from pure mineral phases mixed with an equivalent weight of high purity quartz (St. Peter sandstone). The intensities of the various X-ray peaks representative of the constituent minerals are multiplied by their respective concentration factors. The products are then divided by the sum of all the factor-intensity pairs for the weight percentage of each mineral phase in that sample. Concentration factors for the seven most common minerals in the samples were determined in our laboratory. None of the concentration factors which I have determined differs significantly from those reported by Fan and Rex (1972), and it was possible to use the computerized data-reduction scheme developed for the DSDP, modified so that all peaks were identified manually and the baseline was drawn by hand.

Sample powders used for mineralogical analysis were taken from the same splits used for chemical analysis, except in a few cases

where not enough sample was available; it was necessary then to grind new powder from the original samples. Dry sample powders were ground for two hours in an agate pulverizer and then pressed into 'spec-caps' for analysis. Uniform grinding times and pressures ensured that effects due to variable grain size and surface features would be minimal.

Samples were run on a Norelco diffractometer with Ni-filtered Cu radiation and an operating potential of 40 KV with a 20 MA current. Goniometer scans from 2^{o} to at least 60^{o} 2θ were run at 1^{o} per minute. Diffractograms were studied visually to identify as many mineral phases as possible. All identifications reported here are based on the appearance of at least two, and in most cases at least three, characteristic peaks of minerals as reported in the ASTM powder diffraction file. After all identifications were made, a baseline was constructed by manually drawing lines tangent to the lowest background traces in the diffractogram. Peak heights were used as a measure of the intensity of each mineral present within the sample. The intensities were then punched onto cards for data analysis using the 'Minlog' program developed at the X-ray mineralogy laboratory of DSDP.

The computer program subtracted intensities due to the presence of interfering peaks and then computed the relative weight percentage of each mineral. This process effectively normalized the weight-percentages to 100 per cent, and therefore the amount of non-crystalline substances, moisture, organic matter, and undetected minerals cannot be accounted for by this procedure.

According to results published by the staff of the DSDP X-ray mineralogy laboratory, the analytical precision of this method depends both on abundances and on the degree of preferred orientation encounted. Rex and Murray (1970) report standard deviations ranging from 20 per cent of the amount present at 1 per cent abundance, to 10 per cent at 50 per cent abundance. These authors report that the relative abundances of minerals determined in this manner appear to be excellent.

Bulk Chemical Analysis

X-ray emission techniques were employed to determine the bulk chemical composition of the phosphate rocks. The method of analysis, similar to that described by Norrish and Hutton (1969) and Andermann (1961), involves fusing the dried and powdered sample into glass beads using a constant proportion of lithium tetraborate as a flux. The glass is then pulverized to a fine powder and pressed into 'spec-caps' for analysis. The manufacture of the borate glass has the advantages of insuring homogeneity within the sample, eliminating particle-size effects, and reducing 'matrix' effects by the addition of a common dilutant. Phosphate rock powders were mixed in a 1:3 ratio with lithium tetraborate and were fused at 1000^{o}C for 15 minutes in platinum crucibles. The loss on ignition (L.O.I.) values were determined separately by igniting the sample powders without the borate flux.

Unfortunately, no phosphate rock samples that had been chemically analyzed previously were available as standards. Therefore,

synthetic standards were manufactured from chemical reagents. Reagents were carefully mixed and fused into a set of five borate glass standards which covered the anticipated range of compositions of the phosphate rock samples.

Analyses were performed using an Applied Research Laboratories Quantometer VXQ 72000. An array of fixed monochromators, each optimized for the detection of one characteristic wave length, allows the simultaneous determination of up to twelve elements. A rhodium tube powered by a 3-KW generator was used as an X-ray source; it was operated at 50 KV and 40 MA for these analyses. The entire analytical system, including the X-ray tube and the fixed monochromators, operates in a vacuum for highest efficiency. Intensities are stored on capacitors until a reference channel capacitor has accumulated a predetermined voltage. All the channels are then printed out on a teletype, and the cycle is begun again. The samples reported here were analyzed for approximately thirty seconds.

Intensities were converted to weight percentages by calibration with the synthetic beads of known composition. Linear regression equations were computed on a Wang 720C computing calculator. The regression analysis of the concentration and intensity data for Si, Al, Fe, Ca, K, S, and P produced correlation coefficients equal to or greater than 0.99. Mg and Na produced coefficients of 0.98 and 0.96, respectively.

Five replicate samples of U.S.G.S. rock standard BCR-1, analyzed in the same way on the same instrument, provided an estimate of the analytical precision (G. Gribble, personal communication). Coefficients of variation for CaO and Fe_2O_3 (total iron) were less than 1 per cent; less than 2 per cent for SiO_2, Al_2O_3 and K_2O; 2.46 per cent for MgO; 4.46 per cent for P_2O_5, and 5.49 per cent Na_2O. The coefficient of variation for P_2O_5 in BCR-1 is deceptively high because of the low phosphorus content (0.35 per cent P_2O_5); a much higher precision is anticipated in the phosphate-rich samples analyzed here.

Because a fluorine monochromator was not available for this study, electron microprobe techniques were used for F analyses on the same glass beads. The method was essentially the same as just described, i.e., intensities were measured in both the artifically prepared standards and the phosphate rock samples. Other elements determined in this fashion by microprobe techniques agreed well with results by X-ray emission methods.

Electron Probe Microanalysis

A Materials Analysis Company MAC-5-SA3 microprobe interfaced to a Digital Equipment Corporation PDP-8L computer was employed for the microanalysis studies. The computer interface allowed on-line data reduction of all elemental determinations while the beam was still focused on the spot. This allowed the operator to evaluate the data before moving on to the next spot. The analysis technique used was essentially that of Bence and Albee (1968), using the inter-element

correction factors of Albee and Ray (1970). Pure mineral phases were used as standards for all elements. A more complete discussion of this instrument and the data reduction scheme may be found in Chodos and Albee (1972).

Samples selected for microanalysis were prepared as polished thin sections which could be examined optically before microprobe work was begun. Photomicrographs were taken of several areas within each section, to be used as reference 'maps' during microanalysis. The photomicrographs were annotated at points of interest, and then the electron beam was focused on the corresponding spot on the thin section. At an operating potential of 15 KV with a spot size greater than 10μ, no destruction of the sample by the electron beam was detected.

The data reduction program also provided data on the 1σ relative standard deviation based on counting statistics. Since σ varies inversely with abundance, the major oxides are usually determined with the highest precision. In most of the analyses reported here, SiO_2, CaO, and P_2O_5 have relative standard deviations less than 1 per cent; Al_2O_3, MgO and SO_3 less than 2 per cent; FeO (total iron) and K_2O less than 3 per cent; F less than 4 per cent; and Na_2O about 5 per cent. It should also be pointed out that in most cases, results reported which are lower than 0.1 per cent do not have any significance (A. Chodos, personal communication). The accuracy of this method has been reported as about 2 or 3 per cent for oxides constituting more than 5 per cent by weight of the sample (Gancarz et al., 1971).

Scanning Electron Microscopy

Micro-examinations were performed with a Cambridge S4-10 Stereoscan Scanning Electron Microscope (SEM) equipped with a Nuclear Diodes EDAX non-dispersive X-ray analyzer. Impact-fractured sections of selected phosphate rock samples were mounted on standard SEM sample plugs. Because of the extremely fine grain-size and highly irregular surface textures of these samples, it was difficult to prevent charging of the sample surface during analysis. Charging was due mainly to inadequate conductive coating or improper grounding. By trial and error, I found that a vacuum-evaporated, gold-palladium coating followed by a thin coat of evaporated carbon gave the best results.

Most SEM observations were performed at an operating potential of 20 KV in order to maintain a high degree of resolution. Very few X-ray analyses were attempted because of strong interference from the metals used to coat the samples on the principal X-ray emission lines of all the elements of interest. The crystals identified as apatite, however, were confirmed as such in a few specimens coated solely with carbon.

MINERALOGICAL AND GEOCHEMICAL INVESTIGATIONS

Microscopic Observations

All of the phosphate rock samples used in this study were optically examined using standard thin section techniques. Few of the nodules possessed any definite internal structure. Bedding was observed on a microscopic scale in only a few cases. Phosphatic

pellets or ovules were abundant in some samples, but entirely absent in others. Petrographically, these deposits would be classified as 'bedded' phosphorites, according to the terminology used by Pettijohn (1957). In general, these samples could also be described as phosphatic siltstones and/or sandstones, according to the predominant grain size of the constituent detrital minerals.

The main mineral component recognized optically in these deposits was a cryptocrystalline variety of apatite termed collophane. This material is optically isotropic except in a few cases where anisotropic varieties were observed surrounding mineral grains. Microprobe and X-ray diffraction procedures have confirmed that this material is a fluorine-rich variety of apatite, probably francolite (carbonate fluorapatite with greater than 1 per cent F (McConnell, 1958)). Other mineral phases identified optically included quartz, feldspar (both plagioclase and orthoclase), glauconite, dolomite, opaques, and calcite in the form of foraminiferal shells. Skeletal remains of opaline silica and phosphatic fish bones were also observed. The presence of carbonaceous material was inferred from the coloring of the matrix material, ranging from very light tan to dark brown or black. The phosphatic ovules were occasionally zoned into lighter and darker colors, presumably as a consequence of varying amounts of included organic matter.

Photomicrographs of a few typical thin sections are shown in Figure 15. The areas in the first two photographs are quite similar in that they are composed of large amounts of angular to subangular

Figure 15. (a) Photomicrograph in plane light of phosphate-rich area in a thin section of sample KK-71-161.

(b) As above. Angular and subangular quartz and other mineral grains enclosed in a dark, collophane matrix in sample PD-15-13 (dark).

(c) As above. A large phosphate clast (dark area) enclosed in a light collophane matrix in sample PD-21-24.

(d) As above. Rock fragments, clasts, and other allogenic components contained within a phosphate-rich matrix in sample PD-21-24.

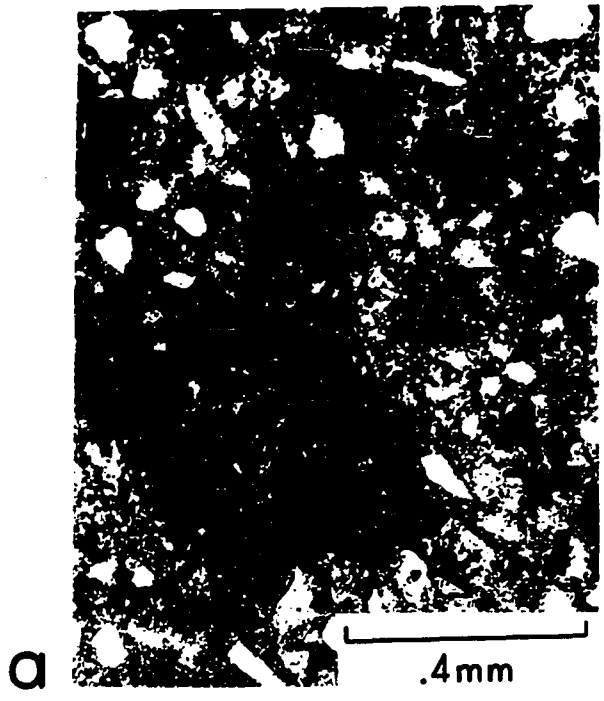

a

b

c

d

quartz grains and other minerals 'floating' in a dark colloplane matrix. Figure 15c shows dark, collophane-rich clasts surrounded by lighter-colored phosphatic material. Phosphorite clasts, as well as some acidic rock fragments, can also be seen in 15d, photographed from the same section. The presence of these clasts indicates at least one prior generation of phosphate deposits. It should be pointed out, however, that evidence of reworking was minimal, in the majority of samples examined, and it was entirely lacking in samples that were radiometrically dated as of Holocene age.

A few microfossils were observed in these sections. Figure 16a shows an included foraminiferal shell in sample PD-19-37. The shell, completely surrounded by a light-colored collophane matrix, has retained its original calcitic composition. A view under crossed nicols is shown in Figure 16b. A completely phosphatized foraminiferal test from the same section is shown in Figure 16c. It may be that the phosphatizing process was operating before induration of the phosphate rock, resulting in a collection of both phosphatized and unphosphatized microfossils.

The phosphatic pellets observed were for the most part internally structureless, i.e., having no apparent concentric layering. For this reason the term ovule (Williams et al., 1954) may be used. Quartz, feldspar, and glauconite grains were the most common phases which served as centers for ovule development. Typical ovoid grains are illustrated in Figure 17. Figure 17b, taken under crossed nicols, display some anisotropic features within the

Figure 16. (a) Photomicrograph taken in plane light of a thin section of sample PD-19-37. The foram shell has remained completely unphosphatized, even though it is completely surrounded by phosphatic material.

(b) Same area as in (a) taken under crossed nicols.

(c) As above. A completely phosphatized foram contained within the same thin section as (a).

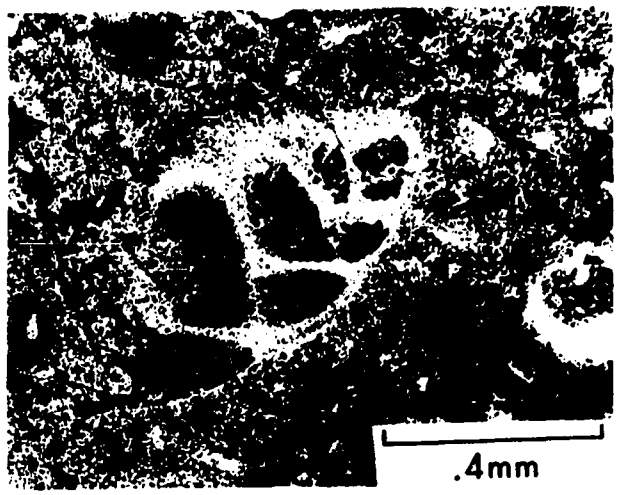
a
.4mm

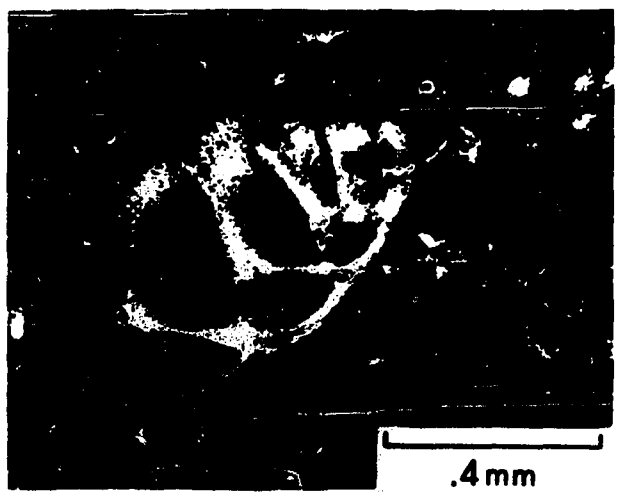
b
.4mm

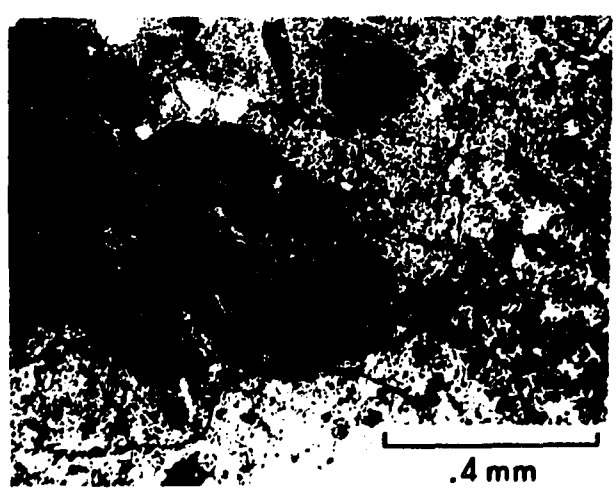
c
.4 mm

Figure 17. (a) Photomicrograph taken in plane light of a phosphate 'ovule' in a thin section of sample PD-21-24. The large grain in the center is feldspar.

(b) Same area as in (a) taken under crossed nicols. Both isotropic and anisotropic materials visible within the ovule structure.

(c) As above. A phosphate 'halo' shown developed around a glauconite grain in sample PD-19-37.

(d) As above. Phosphatic material is shown surrounding a detrital quartz grain in sample PD-21-24.

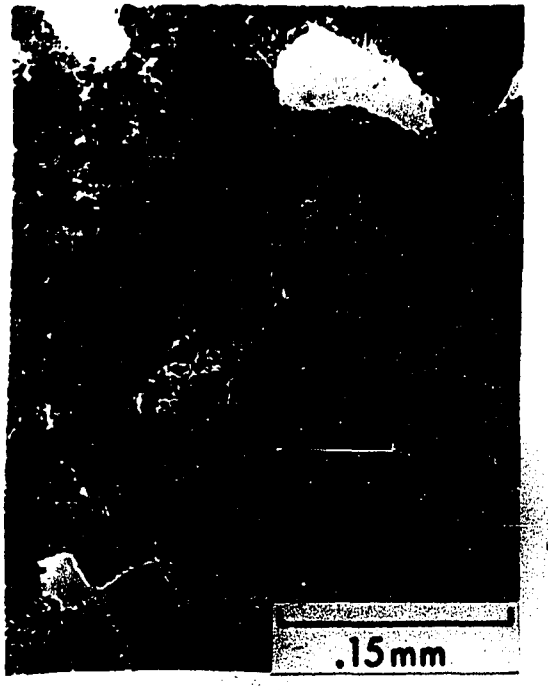

a

b

c

d

phosphate material surrounding the feldspar grain. This may be an expression of increased grain size of the phosphate minerals or simply a result of the inclusion of admixed clay minerals associated with the feldspar. Rooney and Kerr (1967) described phosphate pellets from North Carolina which commonly have an outer light-colored rim of anisotropic phosphate.

Mineralogy and Bulk Chemical Composition of the Phosphate Rocks

Results of the bulk chemical analyses and the semi-quantitative X-ray diffraction mineralogical analyses are presented in Table 7. Sixteen rock samples from the South American shelf and six samples from other areas were chemically analyzed. Eleven samples from South America and three samples from other areas were analyzed by X-ray diffraction techniques. A typical X-ray diffractogram for one of the phosphate rock samples is shown in Figure 18.

Ten mineral phases were identified by X-ray techniques within the phosphate rocks. Typically, five or six mineral phases were observed within any one sample. Apatite was the major phase, with varying amounts of detrital quartz, mica, kaolinite, feldspars, and tremolite. Small quantities of calcite, dolomite, and pyrite were also identified, but it is uncertain whether these minerals are authigenic or allogenic. The phase reported as 'mica' consists primarily of glauconite. This has been confirmed optically and by microprobe techniques.

Examination of the chemical data reveals that all the rock samples from the South American continental margin are characterized

Table 7. Chemical Compositions, Elemental Ratios and Approximate Mineralogical Compositions of Phosphate Rocks from the Sea Floor off South America and Other Areas. All Compositions Are Given in Weight Percent

	PD-12-05		PD-15-13		PD-15-17		PD-18-30	
	light	dark	light	dark	light	dark	light	dark
SiO_2	18.86	12.41	44.48	30.37	25.77	21.21	33.89	23.59
Al_2O_3	4.82	3.27	9.08	5.76	4.43	4.80	9.82	6.15
Fe_2O_3[1]	1.39	1.26	2.09	1.53	6.05	3.27	2.68	2.84
MgO	1.09	1.02	0.68	0.86	1.05	1.36	1.34	1.24
CaO	36.32	41.45	21.37	31.17	29.00	33.94	25.09	32.97
Na_2O	0.85	0.80	1.00	0.90	0.88	0.83	0.98	0.86
K_2O	1.11	0.85	2.01	1.48	1.11	1.22	2.11	1.56
P_2O_5	24.54	28.82	12.76	18.96	19.03	22.14	16.02	22.30
S	0.04	0.12	0.27	0.16	0.32	0.14	0.06	0.01
F	2.36	2.63	1.35	1.95	2.09	2.36	1.62	2.22
L.O.I.[2]	10.24	7.80	4.73	7.52	11.73	11.06	6.12	8.60
Total	101.62	100.43	99.82	100.66	101.46	102.33	99.73	102.34
Less O	0.99	1.11	0.57	0.82	0.88	0.99	0.68	0.93
TOTAL	100.63	99.32	99.25	99.84	100.58	101.34	99.05	101.41
CaO/P_2O_5	1.48	1.44	1.67	1.64	1.52	1.53	1.57	1.48
F/P_2O_5	0.096	0.091	0.106	0.103	0.110	0.106	0.101	0.099
Mica	17	--[3]	--	3	--	0	--	0
Kaolinite	4	--	--	2	--	2	--	0
Quartz	13	--	--	16	--	13	--	10
Potassium feldspar	0	--	--	15	--	0	--	0
Plagioclase	12	--	--	19	--	11	--	23
Tremolite	0	--	--	0	--	0	--	0
Calcite	0	--	--	0	--	0	--	0
Dolomite	0	--	--	0	--	0	--	4
Apatite	54	--	--	43	--	67	--	63
Pyrite	0	--	--	2	--	7	--	0

[1]Total iron reported as Fe_2O.

[2]Loss on ignition @ 1000°C.

[3]Minus sign = not looked for; nd = not detected.

	PD-19-30	PD-19-33	PD-19-37	PD-21-25	A-183	KK-71-161	0546	0553
SiO_2	17.99	12.68	16.67	13.31	10.17	41.40	22.62	27.89
Al_2O_3	5.07	3.10	3.74	3.39	1.99	8.20	5.11	6.75
Fe_2O_3	2.69	1.75	6.34	2.39	1.42	3.68	1.69	1.71
MgO	0.85	1.11	1.23	0.74	0.88	4.87	1.48	1.13
CaO	36.02	40.01	33.79	40.51	42.35	19.10	34.60	30.34
Na_2O	0.86	0.76	0.75	0.90	0.70	0.75	0.77	0.91
K_2O	1.27	0.76	1.78	0.81	0.78	1.65	1.12	1.47
P_2O_5	25.06	28.71	22.43	27.67	29.00	5.95	21.96	19.80
S	0.39	0.12	0.09	0.23	0.09	0.05	0.15	0.15
F	2.25	2.57	2.24	2.49	2.61	0.59	2.46	2.18
L.O.I.	7.43	9.27	10.21	8.69	10.28	15.60	9.77	8.20
Total	99.88	100.84	99.27	101.13	100.27	101.84	101.73	100.53
Less O	0.95	1.08	0.94	1.05	1.10	0.25	1.03	0.92
TOTAL	98.93	99.76	98.33	100.08	99.17	101.59	100.70	99.61
CaO/P_2O_5	1.44	1.39	1.51	1.46	1.46	3.21	1.57	1.53
F/P_2O_5	0.090	0.089	0.100	0.090	0.090	0.099	0.112	0.110
Mica	0	0	12	0	0	4	--	12
Kaolinite	0	0	3	0	0	0	--	4
Quartz	5	4	4	8	7	25	--	24
Potassium feldspar	10	0	0	8	0	10	--	0
Plagioclase	14	15	12	20	12	25	--	23
Tremolite	0	3	0	0	0	0	--	0
Calcite	0	0	0	0	0	0	--	0
Dolomite	0	2	0	0	0	28	--	2
Apatite	67	76	66	61	81	8	--	33
Pyrite	4	0	3	3	0	0	--	2

	Sea off California		Chatham Rise		Blake Plateau	Necker Bank
	14415	14002	X-45	X-79		
SiO_2	8.17	9.70	0.45	1.55	0.20	nd
Al_2O_3	1.06	1.71	nd	nd	0.51	nd
Fe_2O_3	1.00	0.99	1.48	2.18	2.80	1.14
MgO	0.64	0.78	0.50	0.49	1.02	1.83
CaO	44.78	44.18	53.31	51.25	51.33	50.73
Na_2O	0.80	0.87	0.57	0.53	0.58	0.46
K_2O	0.64	0.56	0.54	0.73	0.45	0.15
P_2O_5	30.61	30.65	19.51	20.43	25.80	14.62
S	0.34	0.36	0.30	0.40	0.61	0.30
F	2.95	3.98	2.28	2.65	3.25	1.38
L.O.I.	9.34	--	21.72	20.02	15.20	30.10
Total	100.33	--	100.66	100.23	101.74	100.71
Less O	1.24	--	0.96	1.11	1.37	0.58
TOTAL	99.08	--	99.70	99.12	100.37	100.13
CaO/P_2O_5	1.46	1.44	2.73	2.51	1.99	3.47
F/P_2O_5	0.096	0.130	0.117	0.130	0.126	0.094
Mica	0	--	0	--	--	--
Kaolinite	3	--	0	--	--	--
Quartz	5	--	0	--	--	--
Potassium feldspar	18	--	0	--	--	--
Plagioclase	0	--	0	--	--	--
Tremolite	0	--	0	--	--	--
Calcite	0	--	46	--	26	--
Dolomite	0	--	0	--	--	--
Apatite	72	--	54	--	72	--
Pyrite	2	--	0	--	2	--

Figure 18. Typical X-ray diffractogram of one of the phosphate rock samples (sample PD-15-13 dark).

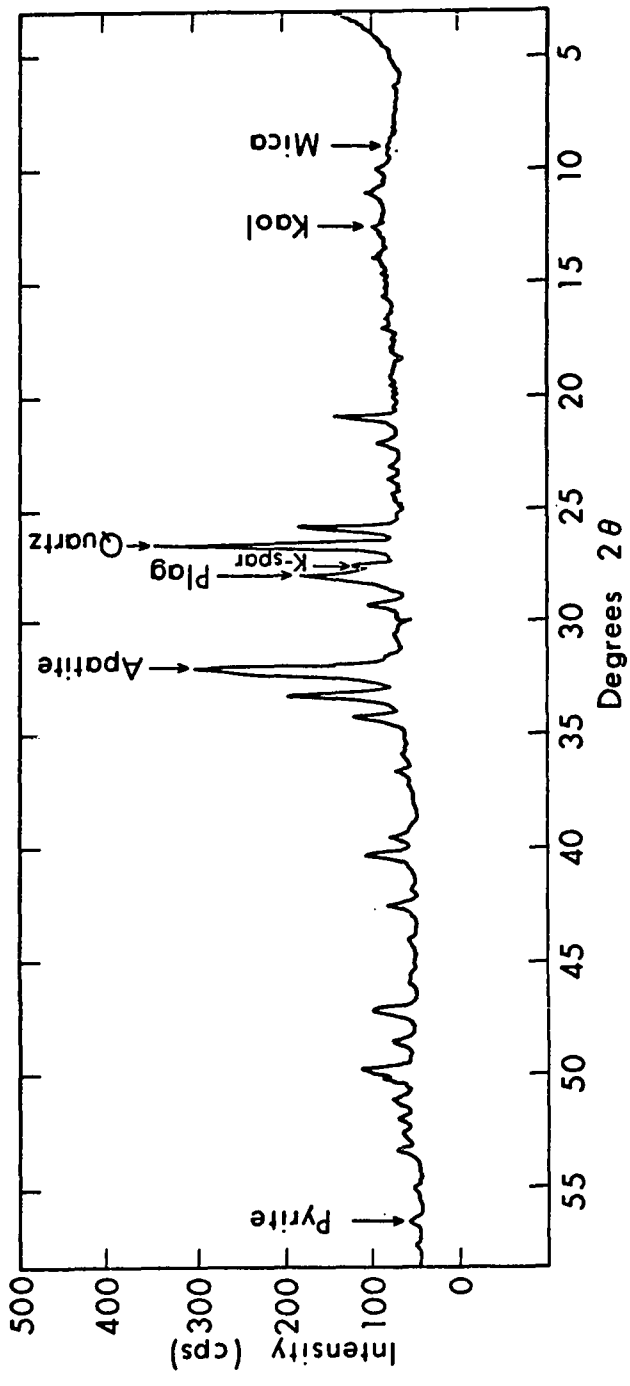
Intensity (cps)
500
400
300
200
100
0
55
50
45
40
35
30
25
20
15
10
5
Degrees 2θ
Pyrite
Apatite
Quartz
K-spar
Plag
Kaol
Mica

by high P_2O_5 values. Although the phosphorus content of sample KK-71-161 would be considered high with respect to the average crustal abundance, it is not of the same magnitude as that of the other phosphate rocks, and will not be considered in the following discussion. The data suggest that the bulk composition of phosphorites from this area is primarily controlled by the degree of sorting or segregation of the authigenic components (essentially apatite) from the allogenic constituents. Chemically, the phosphate rocks may be described in terms of three major components: SiO_2, CaO, and P_2O_5. The CaO/P_2O_5 ratio varies only within narrow limits and its mean value (1.50) is only slightly higher than that expected for a pure carbonate apatite phase. Since calcite is present in only negligible amounts, any CaO not associated with apatite is probably contained in the detrital phases, such as plagioclase. Since no other phosphate mineral was identified, it is assumed that all the P_2O_5 is contained within the apatite. Silica, which varies considerably from sample to sample, is related primarily to the content of allogenic silicate minerals, although there is also a significant contribution of SiO_2 from skeletal opaline material.

To illustrate how bulk chemical composition may be influenced by compositional changes within minerals, Figure 19 shows the content of P_2O_5 plotted against the weight percentage of apatite. The line representing the locus of all points for a theoretically pure apatite ($Ca_5(PO_4)_3F$) is given for comparison. The scatter shown in this plot may be attributed to two sources: (1) inaccuracy of the

Figure 19. Weight per cent P_2O_5 versus weight per cent apatite. The line representing an ideal composition for a non-carbonate fluorapatite is shown for comparison.

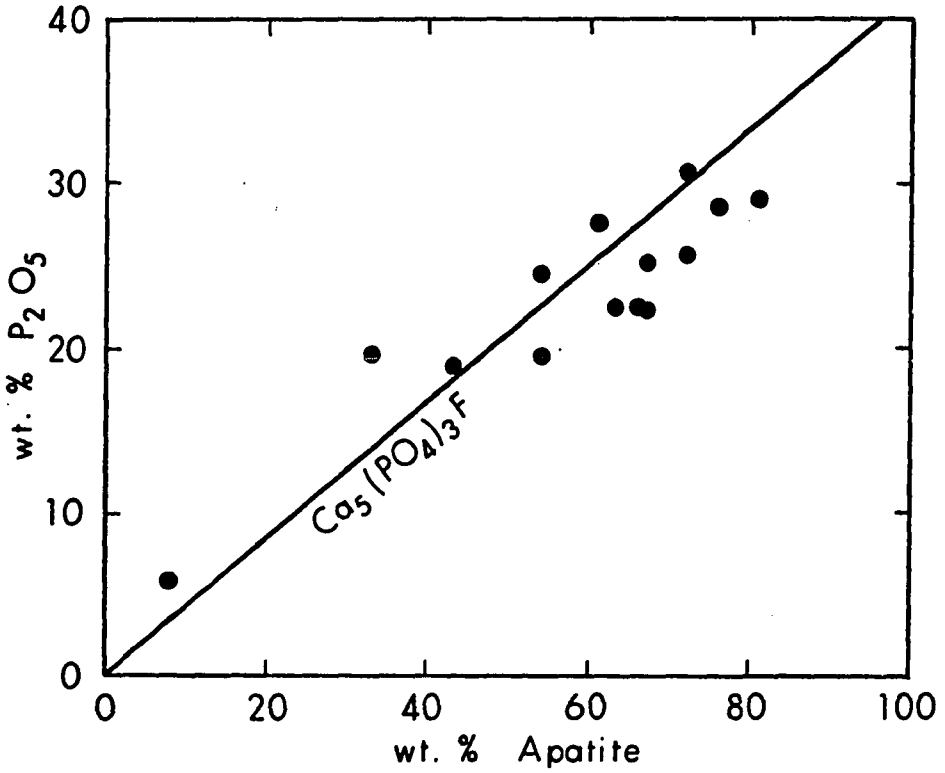
40
30
20
10
0
wt. % P_2O_5
$Ca_5(PO_4)_3F$
0
20
40
60
80
100
wt. % Apatite

mineralogical determinations, and (2) varying substitution by CO_3^{2-} within the apatite lattice. Substitution of PO_4^{3-} by CO_3^{2-} would result in variable P_2O_5 values corresponding to any fixed amount of apatite. Unfortunately, the data do not permit a quantitative evaluation of this mechanism.

The F/P_2O_5 ratios in the phosphorite samples from South America are fairly consistent, varying less than 20 per cent. Most samples have F/P_2O_5 ratios greater than the ideal ratio of 0.089 for a non-carbonate fluorapatite. The 'excess' F is probably incorporated into the apatite lattice to balance the excess positive charge created by substitution of CO_3^{2-} for PO_4^{3-} (Gulbrandsen et al., 1966). Rooney and Kerr (1967) and Parker (1971) have observed this relationship in sedimentary phosphate deposits.

Gulbrandsen (1966) showed that for phosphatic rocks of the Phosphoria Formation, Na and S are covariant, with an atomic ratio of approximately 1:1. He suggests that this is due to a 'coupled' substitution of Na^+ and SO_4^{2-} for Ca^{2+} and PO_4^{3-}. A similar relationship was noted by Parker (1971) in phosphates from the Agulhas Bank. This covariance was not noted for the South American samples, however, probably because both of these elements are distributed among several phases. Sulfur occurs in pyrite and apatite; and sodium, which also may be included in the apatite, is present in some of the detrital mineral phases, especially the alkali feldspars.

Most other chemical constituents in the phosphate rocks are associated primarily with the allogenic components. MgO may be

contributed from glauconite and dolomite and by some substitution of Mg^{2+} for Ca^{2+} in the apatite structure. Although some samples contained no detectable Mg-bearing phase, chemical analysis showed significant quantities of MgO. Both Al_2O_3 and K_2O were present in significant amounts in all samples analyzed. The Al_2O_3/K_2O ratio is fairly consistent (about 4), indicating that these elements are probably contained within the same phase. The micas and alkali feldspars are the most likely sites for these elements.

The average chemical composition of the Peru-Chile phosphorites, together with averages for phosphate rocks from other areas, is reported in Table 8. Mineralogically, the Peru-Chile phosphate deposits more closely resemble the bedded phosphorites of the California borderland and the Phosphoria Formation, as compared with the phosphatized limestones of the Agulhas Bank. This relationship is evidenced in the average CaO/P_2O_5 ratios. The highest ratio was found in the Agulhas Bank deposits because of the high CaO contribution from biogenic calcite.

Mineralogy of the Associated Sediment

The results of the X-ray mineralogy analyses for sediments in association with the phosphate deposits are presented in Table 9. It should be emphasized that these data do not represent absolute mineral weight percentages, because of the large non-crystalline fraction of these sediments. The solid components of the organic-rich diatomaceous oozes in this area consist primarily of amorphous opaline silica. Since all results are normalized to 100 per cent,

Table 8. Average Chemical Composition of Phosphate Rocks from the Sea Floor off South America Compared to Reported Averages from Other Areas

	Peru-Chile[1]	Agulhas Bank[2]	California[3]	Phosphoria[4]
SiO_2	22.13	12.84	--[5]	11.9
Al_2O_3	5.15	1.85	1.47	1.7
Fe_2O_3[6]	2.85	8.24	--	1.1
MgO	1.07	1.35	--	0.3
CaO	33.93	37.29	44.91	44.0
Na_2O	0.85	0.67	--	0.6
K_2O	1.30	1.29	--	0.5
P_2O_5	22.61	16.18	28.15	30.5
S	0.16	0.40	--	0.7
F	2.22	2.10	3.08	3.1
L.O.I.	8.78	18.15	--	6.5[7]
Total	101.05	100.36	--	100.9
Less O	0.93	0.88	--	1.3
TOTAL	100.12	99.47	--	99.6
CaO/P_2O_5	1.50	2.30	1.59	1.44
F/P_2O_5	0.098	0.130	0.109	0.100

[1] This study, average of 15 analyses.

[2] Parker (1971), average of 21 analyses.

[3] Dietz et al. (1942), average of 6 analyses.

[4] Gulbrandsen (1966), average of 60 analyses.

[5] Not determined.

[6] Total iron reported as Fe_2O_3.

[7] Total of H_2O, CO_2, and organic matter.

Table 9. Results of X-ray Mineralogy Studies of Sediments Associated with Marine Phosphorites from off the Coast of Peru. All Data Represent Approximate Weight Percentages of the Crystalline Fraction of the Sediment Normalized to 100%

Depth (cm)	Calc.	Dolo.	Arag.[1]	Quar.	Plag.	K-Feld.	Kaol.	Mica	Chlo.[1]	Pyri.	Apat.	Trem.	Sepi.[1]	Augi.
						KK-71-GC-01								
Top	3	0	0	25	21	19	9	23	0	0	0	0	0	0
20	0	0	0	31	37	0	0	20	8	0	4	0	0	0
44	0	2	0	21	36	0	0	17	4	3	4	4	9	0
60	0	0	0	26	28	0	0	20	4	3	5	2	10	2
						KK-71-GC-02								
Top	41	3	0	13	18	0	0	14	5	2	4	0	0	0
12	45	3	0	15	14	0	0	12	2	2	0	7	0	0
24	35	6	0	12	16	0	3	18	0	2	8	0	0	0
						KK-71-GC-03								
4	18	<1	0	18	24	8	4	11	4	2	8	2	0	0
11	8	2	9	24	16	0	0	18	7	4	8	4	0	0
20	0	1	11	23	22	0	3	20	6	4	6	2	0	5
40	9	0	0	29	28	0	6	20	2	0	8	0	0	0
60	0	0	0	38	28	0	9	20	2	5	0	2	0	4
						KK-71-GC-06								
Top	3	0	0	22	24	14	3	23	2	4	0	5	0	0
18	1	<1	0	26	19	15	5	25	1	5	0	3	0	0
34	4	1	0	24	20	18	8	24	1	0	0	0	0	0
44	0	<1	0	25	25	18	6	23	<1	0	0	2	0	0
80	0	0	0	31	30	0	8	27	2	0	0	2	0	1
						KK-71-RC-03								
Top	26	0	0	20	13	9	7	19	0	6	0	0	0	0
10	38	0	0	20	10	11	6	15	0	0	0	0	0	0
20	29	<1	0	21	0	13	<1	15	0	0	7	0	15	0
40	43	<1	0	18	9	7	3	13	0	0	0	0	6	0
60	31	0	0	18	12	15	5	19	0	0	0	0	0	0
80	41	0	0	19	12	12	4	12	0	0	0	0	0	0
						KK-71-FFC-163								
Top	7	1	0	11	28	21	0	23	2	3	4	0	0	0

[1]Arag. = aragonite, Chlo. = chlorite, Sepi. = sepiolite, Augi. = augite.
All other minerals as in Table 7.

the results for the crystalline components are all too high. The relative concentrations, however, are considered meaningful and may be used for interpretative purposes.

All of the mineral phases detected in the phosphate rocks were also found in the associated sediment. Calcite, aragonite, chlorite, sepiolite, and augite were also found. Calcite is an important constituent in core samples GC-02 and RC-03, both of which contain appreciable numbers of foraminiferal tests. Chlorite was found in all core samples except RC-03. Sepiolite, augite, and aragonite were detected in only a few cases and are considered minor phases. The minerals observed most commonly include quartz, plagioclase, alkali feldspar, and kaolinite. All of these phases appear to be of detrital origin. Glauconite, reported here as 'mica', was also detected in all the sediments. A significant portion of the glauconite probably formed within the sediments, although some reworking is evident. This was indicated by the occurrence of glauconite aggregates or greensands (especially prevalent in sediment core FFC-163). Apatite was found in all the sediment cores investigated except GC-06 and RC-03 (except from 20-cm depth). Dolomite was often present but usually in minor amounts.

In the cores that contained detectable amounts of apatite, the content of dolomite and chlorite was distinctly higher than in the apatite-free sediments. It may be significant that the only core (RC-03) with virtually no detectable chlorite and with extremely low amounts of dolomite also contained no apatite. The content of

pyrite also was lower in those sediments not containing apatite. The relative and absolute quantities of the other minerals present, although variable, did not appear to show any sympathetic relationship to apatite. The possible genetic relationships displayed by the covariance of some of these minerals will be discussed in a subsequent section.

The occurrence of small (a few millimeters in diameter) pellets found in somewhat discrete layers was noted in cores GC-01, -02, and -03. Many of these pellets were found to be soft and friable, although some were well indurated. Similar pellets have been described from the organic-rich diatomaceous oozes found on the continental shelf of southwest Africa (Baturin, 1969, 1971; Veeh et al., in press). A few of these small pellets were hand-picked from the cores and prepared for X-ray mineralogical analysis. The minerals identified and their approximate weight percentages are given in Table 10. Quartz and apatite are the only phases which occur in every sample. The enrichment of apatite, with respect to the sediments analyzed, is quite striking. Apatite constituted up to 86 per cent of the crystalline fraction.

MICROANALYSIS

Electron Microprobe Studies

To evaluate the chemical composition of the main phosphate-bearing phase, apatite, the phosphate rock samples were analyzed using microprobe techniques. It was hoped that careful analysis of selected areas within the rock specimens would eliminate at least

Table 10. Approximate Mineral Compositions of Semi-consolidated and Indurated Pellets Separated from Organic-rich Sediment. All Values Are in Weight Percent of the Crystalline Fraction

Depth (cm)	Calc.	Dolo.	Quar.	Plag.	K-feld.	Apat.	Augi.
			KK-71-GC-01				
Top	7	0	30	22	0	28	13
30	0	0	32	0	0	68	0
			KK-71-GC-02				
Top	9	0	6	12	17	56	0
22	0	74	5	0	0	21	0
			KK-71-GC-03				
Top	21	0	31	11	0	37	0
43	38	0	11	9	0	42	0
70	7	0	7	0	0	86	0

some of the 'diluting' effect of allogenic components. Thus, a composition more representative of the material forming authigenically on the sea floor would be obtained.

Besides allowing a complete elemental analysis of a selected 'spot,' such as on a polished thin section, microprobe techniques make possible the 'mapping' of elemental distributions by employing electron-beam scan techniques. Two sets of elemental displays are presented in Figures 20 and 21. The relative concentration of each element is shown by the density of white dots within the field of the photograph. The scan photographs displayed in Figure 20 show grains of quartz, alkali feldspar, and plagioclase enclosed within a calcium- and phosphorus-rich matrix. Note that calcium has a wider distribution than phosphorus. This is attributed to a combination of two effects: (1) calcium is also contained in some of the allogenic phases, i.e., plagioclase; and (2) small rhombs of dolomite were observed optically in the matrix of this sample. No scan of magnesium distribution was attempted, unfortunately.

The elemental distribution of Ca, P, Na, F, Si, and Al of a plagioclase grain surrounded by phosphate material is shown in Figure 21. The feldspar grain appears to have been a good surface for apatite growth. Note that the Ca and P contents are significantly higher within the area immediately surrounding the feldspar grain than farther into the phosphatic matrix. It could be that this phosphate 'halo' represents an initial stage in the formation of

Figure 20. Electron beam scan photographs of a portion of sample KK-71-161.

(a) Silicon

(b) Aluminum

(c) Potassium

(d) Sodium

(e) Calcium

(f) Phosphorus

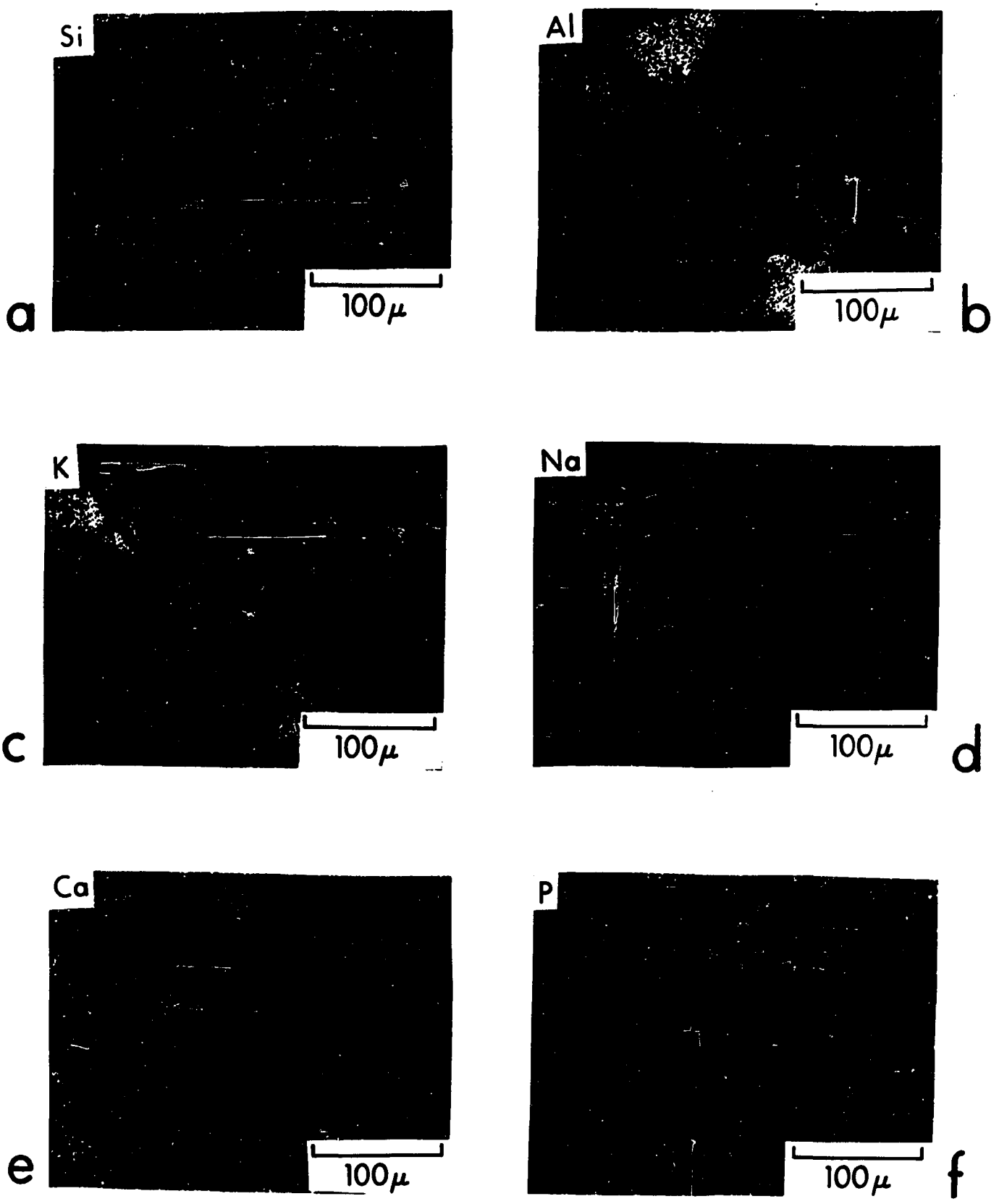
Si
100μ
a
Al
100μ
b
K
100μ
c
Na
100μ
d
Ca
100μ
e
P
100μ
f

Figure 21. Electron beam scan photographs of a portion of sample PD-21-24.

(a) Calcium

(b) Phosphorus

(c) Sodium

(d) Fluorine

(e) Silicon

(f) Aluminum

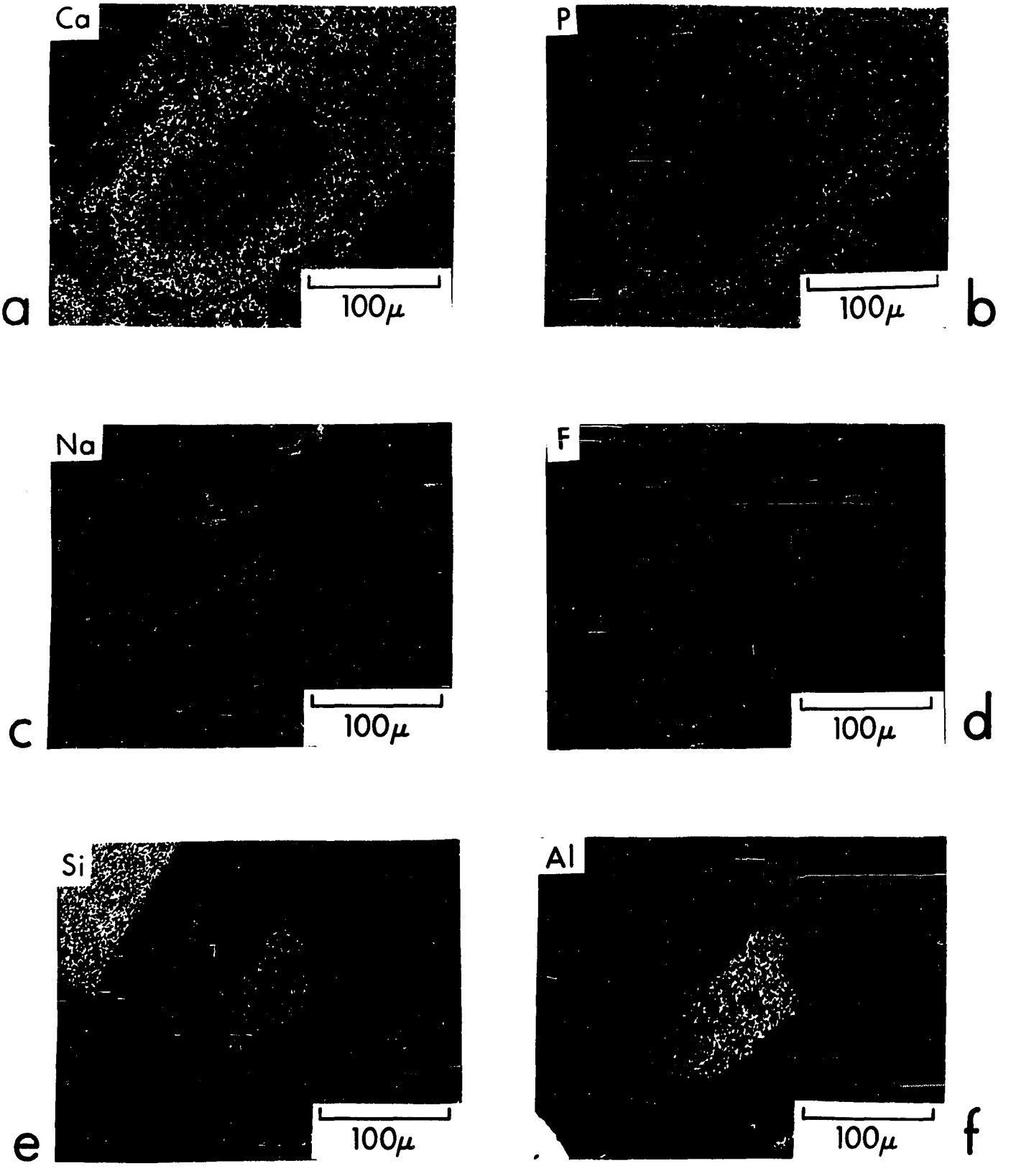
Ca
100μ
a
P
100μ
b
Na
100μ
c
F
100μ
d
Si
100μ
e
Al
100μ
f

structured phosphate 'pellets' which are so commonly observed in bedded phosphorite deposits (Dietz et al., 1942; Rooney and Kerr, 1967).

Two or more spot analyses of the phosphate-rich matrix (optically identified as collophane) were performed in ten of the samples from the Peru-Chile area. The averaged analyses for each specimen are reported in Table 11. The spot size used for these analyses varied from about 10 to 30 microns in diameter although most analyses were performed with a 15-micron spot. Although smaller diameters would have been preferred, the electron beam appeared to damage the specimen when smaller spot sizes were used.

When the data of Table 11 are examined, several important differences may be noted between these results and the bulk chemical analyses reported earlier (see Tables 7 and 8). The contents of Si, Al, and Fe are lower than those reported for the bulk composition, a result which was anticipated since these elements are principally contained within the allogenic components, which the 'spot' analysis excludes. For the same reason, it is not surprising that CaO, P_2O_5, and F, the main components of apatite, are enriched in the matrix material in relation to the whole rock. The Na and Mg content, however, is about the same in the collophane matrix as in the bulk material. This may mean that an important portion of these elements is contained within the apatite phase. Both Na and Mg are known to be able to substitute for Ca in the apatite structure (Cruft et al., 1965; McConnell, 1973). The elemental ratios CaO/P_2O_5 and F/P_2O_5

Table 11. Average Microprobe Analyses of Phosphatic-rich Material (Collophane) Contained Within Ten Polished Thin Sections of Phosphate Rocks from the Sea Floor off Peru and Chile. All Analyses Are in Weight Percent

	PD-12-05 light (3)[1]	PD-13-15 dark (2)	PD-15-17 light (2)	PD-18-30 dark (3)	PD-19-30 (4)	PD-19-33 (3)	PD-19-37 (3)	PD-21-24 (2)	PD-21-25 (9)	KK-71-161 (2)
SiO_2	3.53	7.16	7.06	6.18	6.84	3.17	16.03	4.51	2.86	15.07
Al_2O_3	1.44	1.23	1.62	1.73	3.01	0.83	3.82	0.68	1.05	4.69
FeO[2]	0.44	0.80	1.30	2.24	0.82	0.77	1.10	1.22	0.71	2.99
MgO	0.94	1.03	1.73	1.45	0.89	1.33	1.04	1.07	1.10	1.40
CaO	39.05	43.38	42.09	44.26	44.65	44.63	38.85	46.41	46.46	35.41
Na_2O	1.01	1.02	0.83	0.93	1.20	0.79	1.11	0.78	1.27	1.03
P_2O_5	26.10	29.83	27.64	29.76	30.23	27.65	25.74	29.28	30.45	23.82
F	2.56	3.08	2.75	3.05	2.81	2.64	2.57	3.14	3.36	2.41
Cl	0.83	0.17	0.39	0.20	0.48	0.15	0.10	0.11	0.26	0.31
Y_2O_3	0.02	<0.01	0.01	0.01	0.03	0.02	0.01	<0.01	0.02	0.02
La_2O_3	<0.01	0.32	0.03	0.01	0.08	0.01	<0.01	<0.01	0.02	0.02
Ce_2O_3	<0.01	<0.01	0.11	0.06	0.27	0.06	0.10	0.10	0.03	0.01
Nd_2O_3	<0.01	0.23	<0.01	0.04	0.02	0.03	0.11	0.01	0.03	0.07
TOTAL	74.95	88.27	85.57	89.92	91.33	82.08	90.59	87.33	87.62	87.25
CaO/P_2O_5	1.50	1.45	1.52	1.49	1.48	1.61	1.51	1.58	1.52	1.49
F/P_2O_5	0.098	0.103	0.099	0.102	0.093	0.095	0.100	0.107	0.110	0.103

[1]Number of spots analyzed.

[2]Total iron reported as FeO.

calculated for the matrix material are about the same as those reported earlier for the bulk analyses. The ratios are consistent with those reported for pure carbonate fluorapatites (Deer, et al., 1966; Gulbrandsen, 1969).

Yttrium and the rare earth elements (REE) lanthanum, cerium, and neodymium were also determined by microprobe techniques. Their contents were generally too low to be determined precisely. As a consequence, any interpretations involving the REE distribution within these samples would be highly suspect. Further study of the REE content of phosphorites using more sensitive neutron activation techniques is planned.

Chemical analyses of some of the other phases present within these samples was also considered desirable. Of special interest were those minerals which may have formed authigenically within the surrounding sediment or minerals which displayed some type of diagenetic alteration. Microprobe analyses of selected mineral grains from two samples are presented in Tables 12 and 13. The 'spot' numbers in these tables correspond to the annotations on the photomicrographs of the analyzed areas (Figures 22 and 23). A different microprobe program was used to analyze the silicate phases than the phosphorite since the matrices are different and required different inter-elemental corrections (A. Chodos, personal communication). All the mineral analyses reported here were analyzed first by the 'phosphate' program (indicated by a cross on the photomicrographs) and then repeated at a later date by the 'silicate' program

Table 12. Microprobe Analyses of Selected Spots of a Polished Thin Section of PD-19-37. All Analyses Are in Weight Percent; Spot Numbers Coincide with Annotations on Figure 22

Spot Number:	1 'matrix'	2 glauconite	3 'halo'	4 glauconite	5 'matrix'
SiO_2	29.25	14.84	7.65	49.52	14.56
Al_2O_3	7.81	3.13	2.65	3.83	2.66
FeO[1]	0.67	60.85	2.78	28.37	1.33
MgO	0.51	2.14	1.41	3.24	1.27
CaO	28.65	0.24	43.27	0.17	41.31
Na_2O	1.57	0.56	0.99	0.31	0.95
K_2O	-- [2]	1.75	--	7.70	--
P_2O_5	19.75	1.65	27.58	0.20	28.01
F	1.73	<0.01	3.18	0.02	2.67
Cl	0.10	0.32	0.14	0.19	0.09
Y_2O_3	<0.01	<0.01	0.02	0.03	0.01
La_2O_3	<0.01	<0.01	<0.01	<0.01	<0.01
Ce_2O_3	0.08	<0.01	0.08	<0.01	0.06
Nd_2O_3	0.14	0.09	<0.01	0.02	0.19
TOTAL	90.28	85.61	89.77	93.62	93.12

[1]Total iron reported as FeO.

[2]K_2O not analyzed for using 'phosphate' program; 'silicate' program used to analyze silicate phases.

Figure 22. Photomicrographs of a polished thin section of sample PD-19-37 showing 'spots' analyzed by electron microprobe techniques. Spot numbers correspond to the locations of the analyses presented in Table 12. Spot number '1' (not shown) is located in the fine-grained matrix.

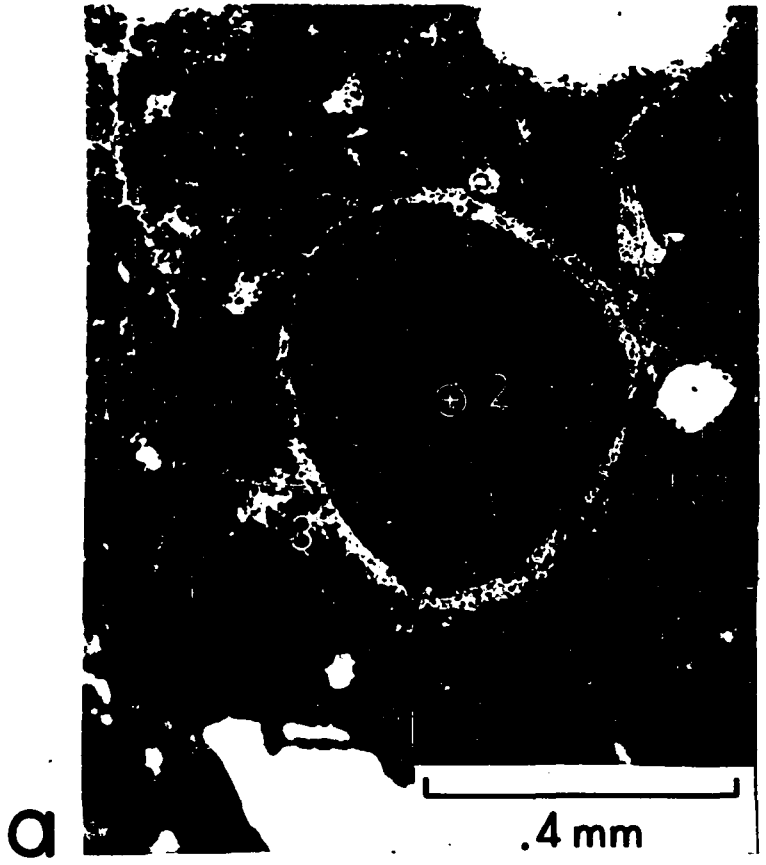

a

b

Table 13. Microprobe Analyses of Selected Spots of a Polished Thin Section of PD-21-24. All Analyses Are in Weight Percent; Spot Numbers Coincide with Annotations on Figure 23

Spot Number:	1 glauconite	2 plagioclase	3 'matrix'	4 glauconite	5 'halo'
SiO_2	50.61	55.96	5.65	49.97	6.60
Al_2O_3	6.52	28.15	0.81	6.79	1.69
FeO[1]	25.12	0.88	1.19	27.12	2.66
MgO	3.59	0.10	1.01	3.17	1.26
CaO	0.79	10.70	46.33	0.24	40.02
Na_2O	0.34	5.19	0.91	0.53	1.13
K_2O	8.10	0.38	-- [2]	7.48	--
P_2O_5	0.56	--	30.38	0.22	26.48
F	0.07	--	3.53	0.02	2.32
Cl	0.59	--	0.13	0.22	0.36
Y_2O_3	0.01	--	0.01	0.01	0.01
La_2O_3	0.01	--	0.01	0.01	0.01
Ce_2O_3	0.06	--	0.03	0.02	0.11
Nd_2O_3	0.01	--	0.01	0.13	0.12
TOTAL	96.38	101.36	90.00	95.93	82.77

[1]Total iron reported as FeO.

[2]Not determined.

Figure 23. Photomicrographs of a polished thin section of sample PD-21-24 showing 'spots' analyzed by electron microprobe techniques. Spot numbers correspond to the locations of the analyses presented in Table 13.

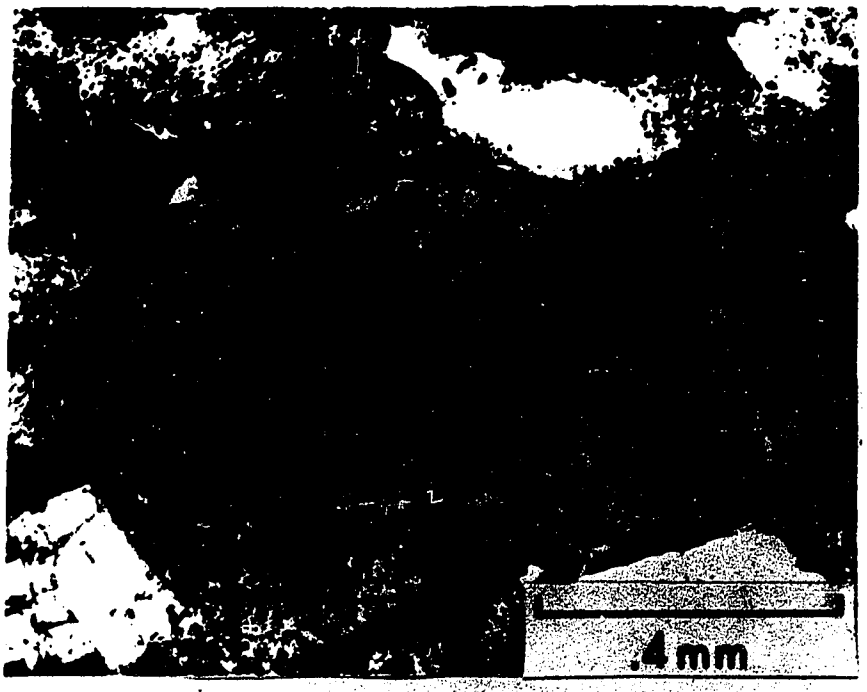

a

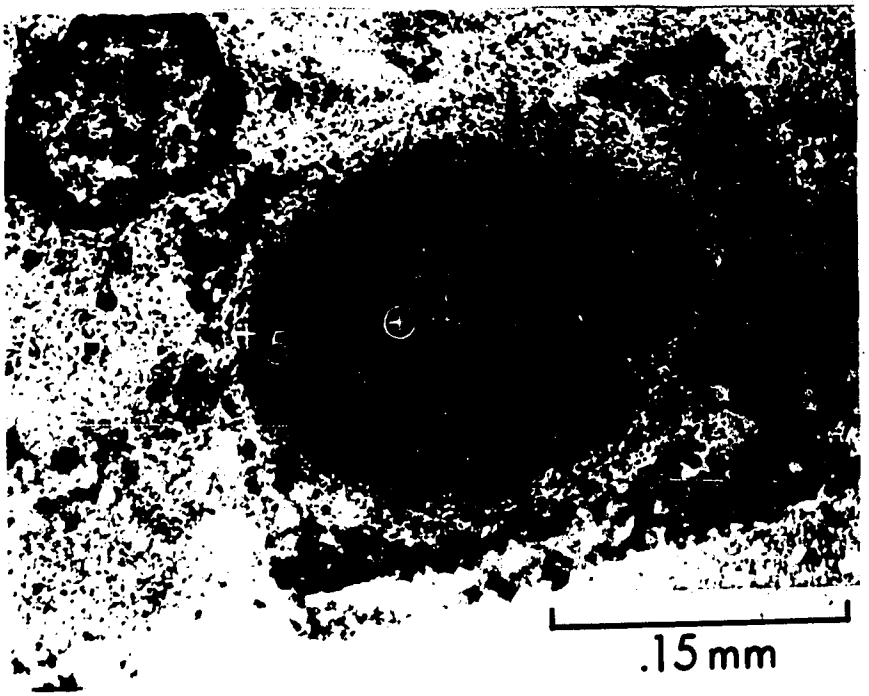

b

(indicated by a circle). The two analyses were quite close and did not show any systematic differences. Failure to return to exactly the same 'spot' probably accounts for most of the observed variance. Except for P and REE, the analyses reported in Tables 12 and 13 for the silicate phases were determined using the 'silicate' program.

Glauconite grains, which are quite common in some of the phosphate rocks, vary from pale green, translucent varieties to those completely opaque to transmitted light. Presumably, this difference in appearance is the result of some type of surface coating. Grains showing intermediate degrees of opaqueness are very common. These grains typically show coloration at the outer surfaces and along the fractures within the minerals. Baturin et al. (1970) have reported that the glauconite occurring within phosphate rocks from the shelf of southwest Africa was typically pyritized. Initially, this was thought to be a satisfactory explanation for the opaque materials observed here, especially since pyrite was detected by X-ray diffraction techniques. However, sulfur proved to be very low in this opaque material. It now seems more likely that the opaque material represents a hydrated iron oxide or 'limonite' phase. Table 12 presents the analysis of a completely opaque grain. The other three glauconite analyses reported are more representative of typical glauconite grains. The feldspar grain analyzed (Table 13) is a calcium-rich plagioclase, with a composition equivalent to labradorite. This grain (spot 2 in Table 13 and Figure 23) is the same mineral contained in the electron beam scan photographs of Figure 21.

Scanning Electron Microscopy

Examination of sedimentary phosphate rocks with an ordinary petrographic microscope does not allow study of individual apatite crystals because of their extremely fine-grained texture. However, the micron-sized crystals of sedimentary apatite are well within the range of a modern scanning electron microscope (SEM). Examination of several phosphate rock specimens by SEM techniques resulted in much valuable information regarding the fabric, crystal size, and crystal habit of the sedimentary apatite. Rooney and Kerr (1967) published two transmission electron photomicrographs of fractured phosphate pellets from Miocene rocks in the coastal plain of North Carolina. They reported that apatite crystals ranged in size from 0.2 to 1 micron. The basal sections of the crystals in their photographs are hexagonal. The apatite crystals shown here in the electron micrographs (Figures 24 and 25) are somewhat variable in size but generally are on the order of 1 micron in length. Most of the crystals are prismatic, many being doubly terminated. Basal sections are hexagonal.

Apatite was seen on several different types of surfaces during the course of the SEM observations. Apatite crystals in association with mineral grains and biogenic components are shown in Figure 24. Opaline silica, especially diatom frustules, was the most frequently observed type of surface on which apatite was found. Figure 25 illustrates the close association between opaline silica and apatite. It is not known whether this association represents surfaces of

Figure 24. Scanning electron micrographs of freshly fractured surfaces of phosphate rocks.

(a) sample PD-12-05

(b) sample PD-19-37

(c) sample PD-19-30

(d) sample PD-15-13

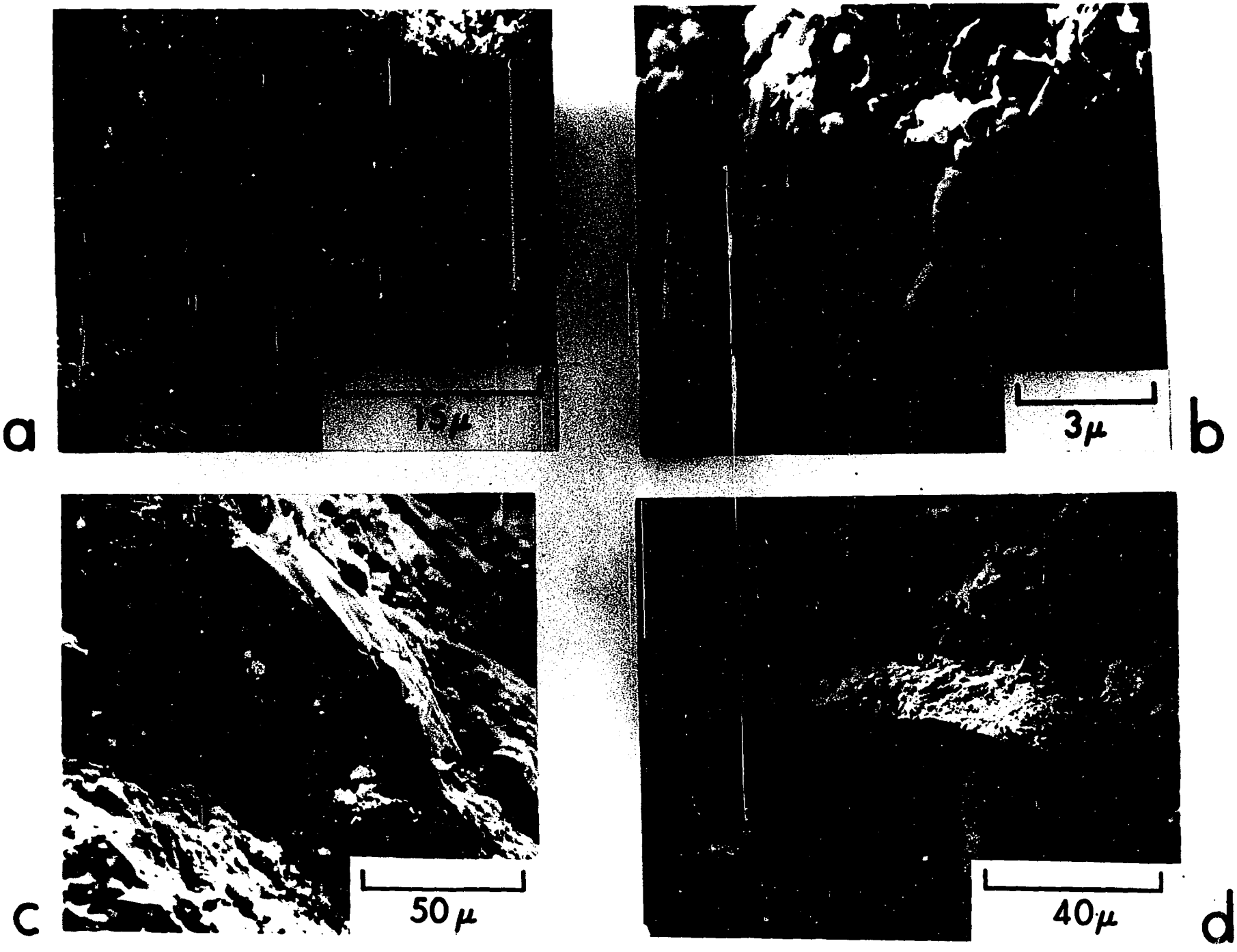
a
15μ
3μ
b
c
50μ
40μ
d

Figure 25. (a) Scanning electron micrograph of a freshly fractured surface of sample PD-12-05.

(b) As above. Apatite shown growing on the surface of a diatom frustule.

(c) As above, higher magnification than shown in (b).

(d) As above, still higher magnification.

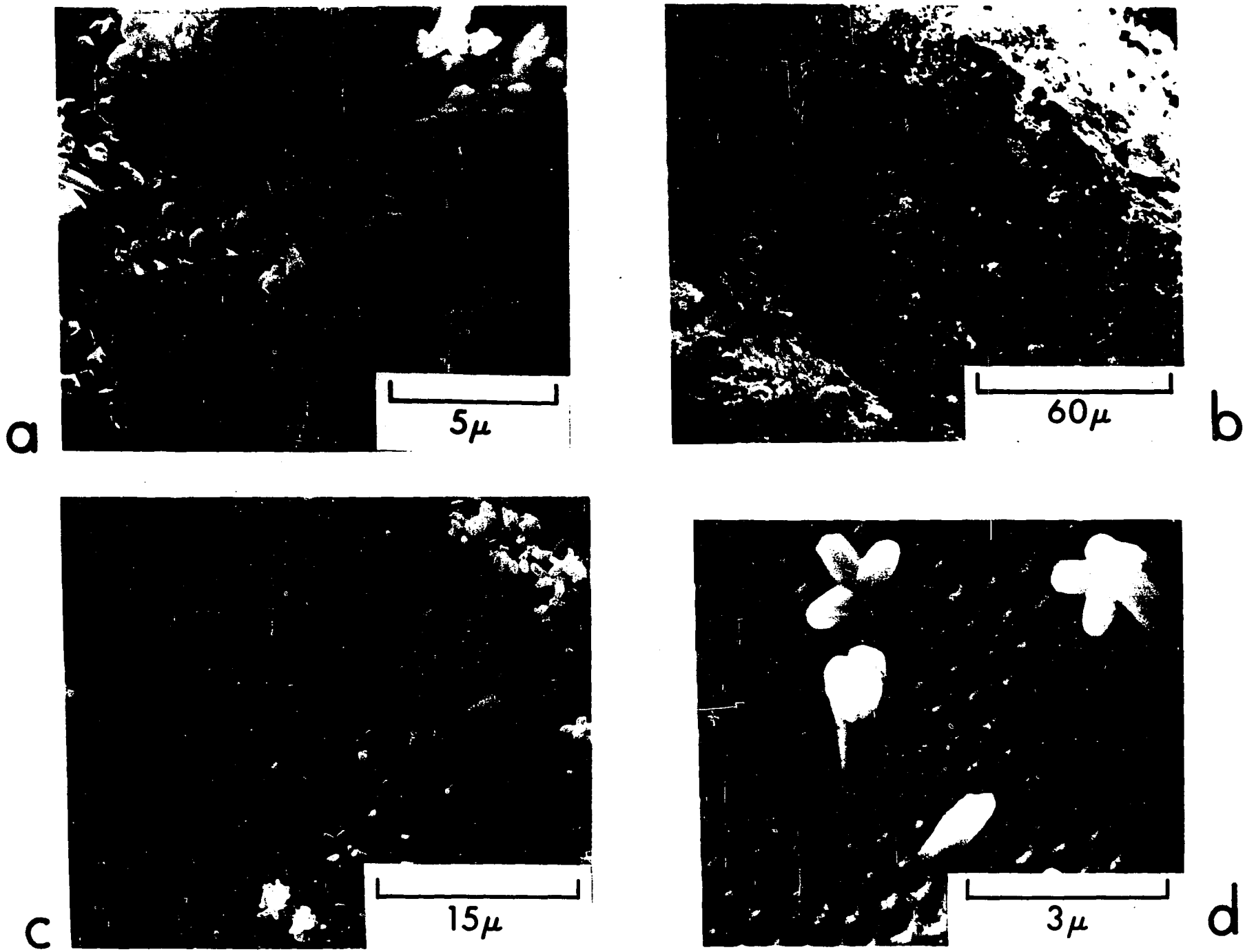
a
5μ
60μ
b
c
15μ
3μ
d

nucleation for growth of apatite or is simply a function of the relative abundance of the two components, both being major components in these deposits. It is conceivable that small fragments of calcite served as 'seeds' for epitaxial growth of apatite.

It is clear that the phosphate rock deposits described here were formed authigenically. For example, the external morphology of many of the nodules rules out transportation as a significant factor. The lumpiness and friability of the small phosphate pellets found within the cores of diatomaceous ooze also suggest an authigenic origin. These lines of evidence, however, do not confirm how the apatite was formed, i.e., by replacement of previously existent materials (such as calcium carbonate) or by direct inorganic precipitation. It was hoped that the SEM studies would help elucidate this problem.

Electron micrographs showed that apatite commonly occurs in clusters and 'rosettes.' Apatite appears to have grown within the pores and other openings of the biological material. These observations favor the deduction that apatite formed by direct precipitation. The euhedral crystal forms and the growth of apatite on the surfaces of minerals support formation by precipitation rather than by replacement. In addition, the elemental ratios reported earlier are very close to those expected for pure apatite. These ratios imply that there are no 'unreplaced residuals' which might have been present if apatite had formed by replacement of calcite.

Although some phosphate replacement may have occurred within these deposits, most of the apatite seems to have been precipitated directly from pore solutions. Besides the evidence cited above, there is also a conspicuous lack of features which would normally suggest formation by replacement. Among the criteria usually given as evidence of replacement (Pettijohn, 1957), pseudomorphism, embayed contacts, and automorphic crystals transecting earlier structures are either completely lacking or very subordinant in the samples studied. Pseudomorphism of microfossils, such as may be seen in the Agulhas Bank deposits (Parker, 1971), can be considered conclusive evidence of replacement. Although some examples of pseudomorphism were observed (see Figure 16), they were scarce and not of any significance.

The close association between authigenic crystals of apatite and allogenic components such as siliceous skeletal debris and detrital mineral grains is instructive for two reasons. First, the SEM photos clearly illustrate the cause of a problem discussed in the previous section dealing with electron probe microanalysis. That is, an electron beam 15 microns in diameter used for microanalysis 'averages' many individual grains, and analyzes several components at the same time. For example, if one of the areas in Figure 25 were analyzed using a 15-micron 'spot,' the analysis would show a contribution to the silica content from the biogenic materials. Second, the common occurrence of apatite growing on the surfaces and in the openings of the allogenic constituents implies that these

surfaces may represent sites of nucleation for the chemically precipitated apatite. Direct inorganic precipitation of apatite within the anaerobic sediments is demonstrated in Figure 26, two SEM photographs of a soft, friable pellet hand-picked from one of the sediment cores. Authigenic apatite is a major component of these pellets. The significance of apatite formation within the sediments of this area in relation to the formation of phosphate rock deposits will be discussed in the following section.

ORIGIN OF MARINE PHOSPHATE DEPOSITS

Introduction

To relate the data presented here to genesis of sea-floor phosphorite deposits, it is necessary to show how certain conditions or circumstances favor the precipitation of marine apatite within the sediments of the Peru-Chile shelf. To explain phosphorite formation by direct inorganic precipitation from sea water would require unique set of circumstances. For example, although the bulk of ocean water is apparently near equilibrium or saturated with respect to carbonate fluorapatite (Kramer, 1964; Roberson, 1966; Pytkowicz and Kester, 1967), skeletal phosphatic materials are known to be dissolving in deep ocean water (Arrhenius, 1963). Skopintsev (1972) showed however that when the apparent dissociation constants of phosphoric acid for sea water (calculated by Kester and Pytkowicz, 1967) are used with a correction for the complexing of phosphate ion, one finds that ocean water is undersaturated with respect to

Figure 26. (a) Scanning electron micrograph of authigenic apatite growing within a core of diatomaceous ooze from the Peru shelf. The sample shown is a small pellet hand-picked from a depth of 22 cm from core sample KK-71-GC-02.

(b) As above, higher magnification than (a).

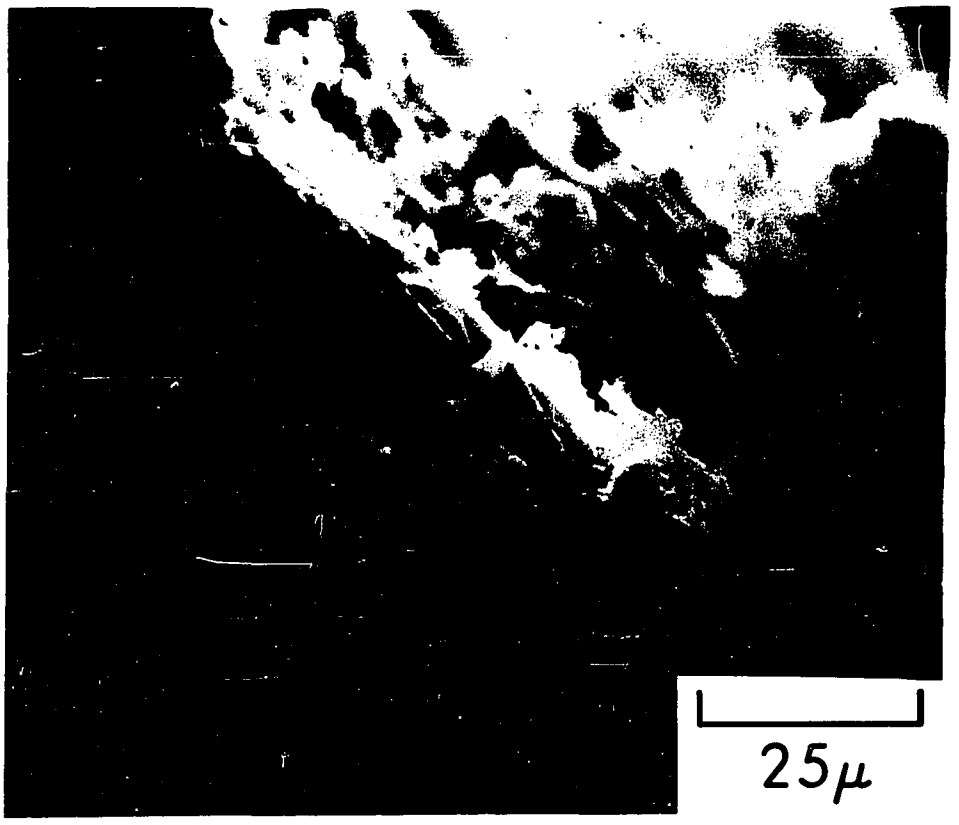

a

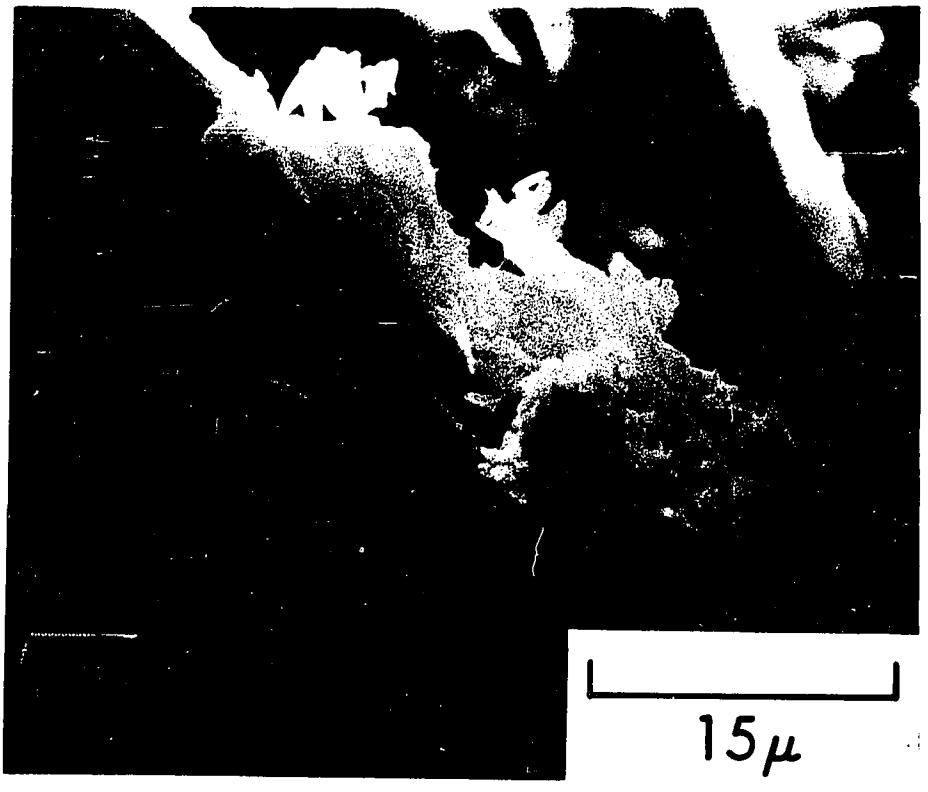

b

calcium phosphate, the degree of saturation being about 30 per cent. The relationship between solubility and apatite composition has not been adequately studied, so it is not possible to make a definitive statement regarding ion substitution and solubility. If Skopintsev's data are applicable to a carbonate fluorapatite composition, then it is not surprising that apatite precipitation is restricted to special environments.

If Kazakov's (1937) suggestion that apatite precipitates inorganically from sea water is accepted as an explanation for the formation of phosphate deposits, yet another problem arises: the conditions necessary for apatite precipitation which he proposed are essentially the same conditions which would favor calcium carbonate precipitation (Gulbrandsen, 1969). The ascension of cold CO_2-enriched waters into a warmer, shallow area, with subsequent loss of CO_2 and rise in pH, would favor both calcium carbonate and apatite precipitation. If apatite is precipitating out of the pore waters of reducing sediments in this area, then there should be an explanation for the apparent absence of authigenic calcium carbonate formation. Berner et al. (1970) have shown that pore waters of anoxic sediments may become supersaturated with respect to $CaCO_3$ without precipitation because of the inhibiting effect of dissolved organic matter. The presence of high organic content in these sediments may be significant as an inhibiting agent for calcium carbonate deposition.

Phosphorites have been shown to be currently forming on the Peru-Chile continental margin (see previous section), and hence

parameter measurements in this area would be indicative of the environment of present day phosphate deposition. But since it now appears that large-scale phosphate deposition is no longer occurring in many areas of the sea floor where large older deposits are found (Kolodny, 1969b), analysis of environmental data from those areas with the same purpose in mind would seem unwarranted. It would be of interest, however, to compare environmental data from those areas with data under which phosphate deposits are currently forming. Unfortunately, a thorough investigation of the chemical and physical characteristics of the water column and detailed interstitial water studies in areas of current phosphorite formation (such as off South America) have not yet been conducted. A model of phosphorite genesis, based on evidence in this report, is presented here as a working hypothesis awaiting verification or modification by more detailed studies.

Characteristics of Depositional Environment

An interesting relationship is evident between the depth distribution of Holocene phosphate rock samples recovered off the west coast of South America and the dissolved oxygen content of the overlying water. Figure 27 shows the depth distribution of dissolved oxygen and temperature from ten hydrographic stations off South America. As seen, there are two depth zones where recently-formed phosphorite occurs, one at approximately 100 meters and the other around 400 meters. These two depth zones roughly coincide with the upper

Figure 27. Depth distribution of dissolved oxygen and temperature from ten hydrographic stations off South America between 10°S and 22°S. All hydrographic stations were located immediately adjacent to areas where phosphorite samples were dredged. Depth distribution of Holocene phosphorite rocks in this area is indicated by open circles. These data (supplied by A. Soutar) were collected during the SOTOW Expedition of Scripps Institution of Oceanography in May 1972.

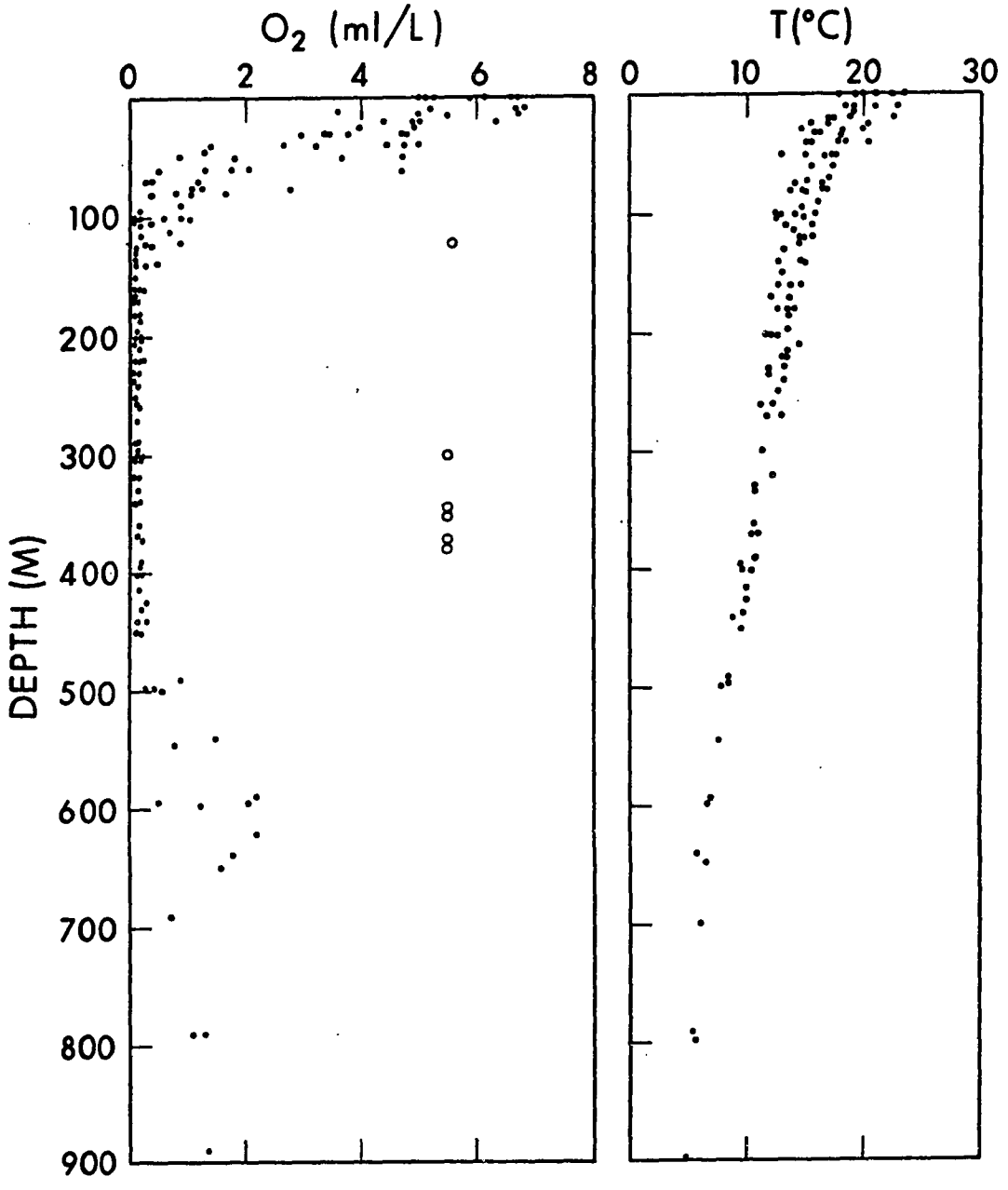
O2 (ml/L)
0
2
4
6
8
T(°C)
0
10
20
30
DEPTH (M)
100
200
300
400
500
600
700
800
900

and lower boundaries of the intersection of the oxygen minimum with the continental margin. Wherever youthful phosphorite was encountered, the bottom waters were deficient in dissolved oxygen; values as low as 0.07 ml/l O_2 were recorded. It is likely that the pronounced oxygen minimum is a consequence of the high organic productivity off these coasts.

Why conditions should be more favorable for phosphorite formation near the upper and lower boundaries of the oxygen minimum layer is unclear, although it could be related to a sharp rise in the pH at these boundaries. It is known that pH distribution in the oceans closely follows the dissolved oxygen distribution (Park, 1966). It has been established that the solubility of apatite decreases with an increase in pH (Roberson, 1966; Pytkowicz and Kester, 1967). Therefore apatite may tend to precipitate more readily at the boundaries of the oxygen minimum layer where there is likely to be a sharp increase in the pH of the bottom waters. This type of mechanism suggests, however, that apatite is precipitating directly from sea water. It may be more realistic to consider precipitation from interstitial waters. How the dissolved oxygen content of the overlying waters affects the chemistry of pore waters within the diatomaceous oozes of this area is uncertain at this time. Results from the Santa Barbara Basin, however, imply a close relationship between pore water chemistry and the oxidizing conditions of the overlying water (Sholkovitz, 1973). Sholkovitz showed that inter-

stitial water compositions are extremely sensitive to slight changes in the oxygen content of the sea water under which deposition occurs. The phosphate content, for example, was several times higher where the dissolved oxygen was lowest. The bottom water from the Santa Barbara Basin contained 0.1 ml/l dissolved oxygen, a value quite similar to the values measured off South America.

Pore waters squeezed from anoxic sediments from various areas have several characteristics in common. The phosphate content of these waters is often several orders of magnitude higher than that of the overlying sea water or waters squeezed from sediments deposited under more oxidizing conditions. Bray et al. (1973), for example, showed that phosphate concentrations in pore waters from Chesapeake Bay sediments average 1000 times those for the bay water. The orthophosphate in this case was found to be in equilibrium with vivianite, as was supported by the presence of this mineral in the bay sediments. Berner (in press) reports high phosphate contents in pore waters from several anoxic environments, including a value of 1000 ppm PO_4^{3-} in the top few centimeters of a highly polluted sediment in New Haven harbor. Brooks et al. (1968), after noting a calcium depletion with depth in high phosphate pore waters from the Santa Barbara Basin, suggested that in situ precipitation of apatite partially controls the calcium distribution in the interstitial waters. Sholkovitz (1973), however, showed that authigenic calcium phosphate formation may not be necessary to explain Ca^{2+} depletions in the anoxic pore waters from the Santa Barbara Basin. His model

successfully predicted both the interstitial water concentration of PO_4^{3-} by mechanisms of authigenic precipitation of calcite, and the decomposition of organic material by reduction of SO_4^{2-}. This model also predicted the alkalinity and NH_4^+ contents of the pore waters.

The interstitial water composition for a core sampled on the Peru shelf is shown graphically in Figure 28. The data from this core were kindly provided by Dr. Edward Sholkovitz, University of Edinburgh. Distribution of the components is not unlike patterns noted elsewhere for anoxic sediments. The decrease in the SO_4^{2-} content is likely related to the production of authigenic pyrite, found in the sediments from this area. The rise in alkalinity is probably related to decomposition of organic materials. Electrical neutrality is probably maintained by counterbalancing the changes in Ca^{2+} and Mg^{2+} (which usually show depletion in anoxic pore waters), NH_4^+ production, and change in SO_4^{2-} content with a coincident rise in HCO_3^-, i.e., $\Delta Ca^{2+} + \Delta Mg^{2+} + NH_4^+ - \Delta SO_4^{2-} = \Delta HCO_3^-$ (Sayles et al., in press). Unfortunately, Ca^{2+} and Mg^{2+} data for the core were not available to test this simple model. The core's phosphate distribution is particularly interesting. If the equilibrium value for total dissolved phosphate in ocean water is approximately 0.2 micromoles per liter (shown by the arrow in Figure 28) as suggested by Roberson (1966), then the PO_4^{3-} content in the pore waters is well over two orders of magnitude above the saturation value. The PO_4^{3-} curve with depth shows a definite maximum at about 15 cm, implying that precipitation of a phosphate phase begins at that level. This type

Figure 28. Interstitial water concentrations of phosphate, sulfate, and silica, and alkalinity as a function of depth for core 271 (Peru shelf). Arrow represents solubility of apatite as determined by Roberson (1966). Position: 11° 56.0' S, 77° 40.7' W; Depth: 185 m. Data provided by E. Sholkovitz.

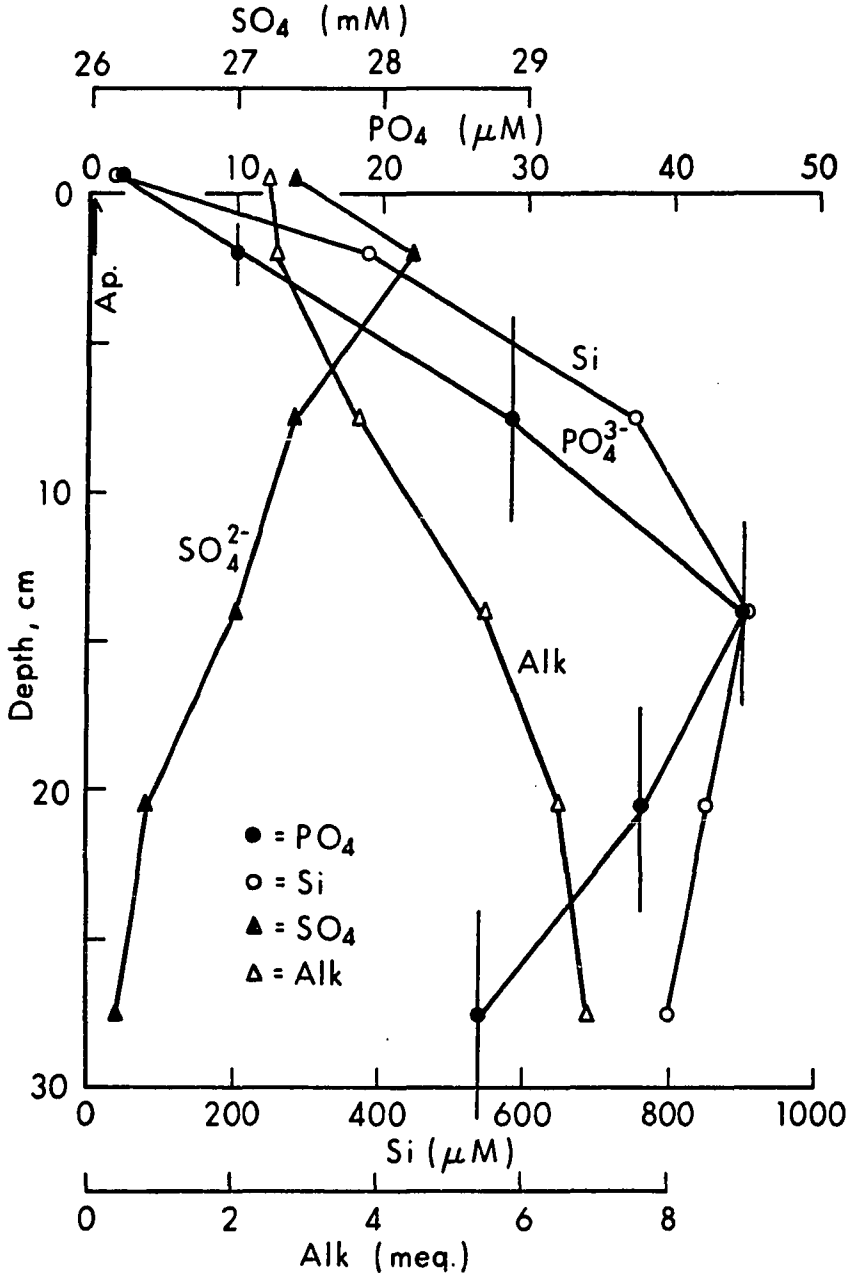
SO4 (mM)
26
27
28
29
PO4 (μM)
0
10
20
30
40
50
0
Ap.
Si
PO4 3-
10
SO4 2-
Depth, cm
Alk
20
● = PO4
○ = Si
▲ = SO4
△ = Alk
30
0
200
400
600
800
1000
Si (μM)
0
2
4
6
8
Alk (meq.)

of curve is not usually encountered for PO_4^{3-} in pore waters of anoxic sediments. More typically, the values move steadily up to some apparent equilibrium value, remaining more or less at that value in the deeper levels of the core. The curves for Long Island Sound and the Santa Barbara Basin presented by Berner (in press) show that type of PO_4^{3-} distribution.

As seen, the distribution curve for dissolved silica is similar to the PO_4^{3-} curve. One is tempted to propose a relationship between the control mechanisms for silica and phosphate in the core because of the close similarity in their distributions. The data of Hurd (1973) for Central Pacific radiolarian oozes suggest that at some level in the sediment, authigenic mineral formation on the surfaces of the opaline skeletal materials effectively 'armors' the test and reduces the release rate of dissolved silica. It may be that in a shallow water situation, such as on the Peru shelf, apatite forming on the surfaces of the skeletal material of diatoms may eventually form an impermeable layer and prevent any further solution. Although verification of this mechanism must await future research, the SEM photographs of authigenic apatite growing on the surface of a diatom frustule (Figure 25) do seem to support this contention.

Authigenic apatite has also been reported (Ristvet, 1973) occurring in the Holocene anoxic lagoonal sediments of Kaneohe Bay, Hawaii. Direct inorganic precipitation of apatite out of natural waters, other than pore waters, is not well documented, although often proposed. Richards et al. (1965) suggested that the inorganic

precipitation of some calcium phosphate minerals may help control the PO_4^{3-} distribution in Lake Nitinat, an anoxic fjord of Vancouver Island, British Columbia. Murphy (1973) reports that the production of apatite is evident in Onondaga Lake, New York, but he fails to say how it was recognized and what criteria were used to establish its authigenic character. Ever since Kazakov (1937) proposed a reasonable scheme for phosphorite formation by direct inorganic precipitation out of nutrient-rich bottom waters, his mechanism has been applied by many investigators to explain the formation of phosphorite deposits (except those obviously formed by replacement). After the various prerequisites necessary for apatite precipitation have been considered, it will be shown that a more realistic model would require apatite to precipitate from pore waters rather than the overlying ocean water.

Conditions Favorable for Apatite Precipitation

The physical and chemical conditions which are most effective in controlling apatite precipitation out of aqueous solutions will be reviewed before a model for the formation of inorganically precipitated phosphorites is proposed. Most of the factors to be considered are 'limiting conditions,' i.e., there may be threshold values below which apatite precipitation is not possible. In general, it appears that there are at least five characteristics of natural aqueous solutions that would favor the inorganic precipitation of apatite:

1) High dissolved inorganic phosphate content;

2) High Ca/Mg ratio;

3) High pH;

4) High temperature; and

5) Suitable nucleation sites.

Phosphate may be supplied to anoxic pore waters from decomposition of phosphorus-containing organic materials and from reduction of hydrous ferric oxides which bind phosphate to their surfaces under oxidizing conditions (Stumm and Leckie, 1970). The contribution from decaying organic materials is almost certainly the more significant. Diatoms are known to contain large quantities of phosphorus (R. M. Garrels, personal communication) and should therefore provide the pore waters of diatomaceous oozes with a high content of dissolved phosphate. If large quantities of apatite are to be generated from the pore waters of the organic-rich oozes, the PO_4^{3-} content of the interstitial fluids must be continually replenished while apatite is being precipitated. A region such as the Peru continental shelf with extremely high organic productivity should ensure that a constant supply of organic phosphorus is delivered to the sediment.

It has been shown experimentally (Bachra et al., 1965; Martens and Harriss, 1970) that Mg^{2+} ions inhibit the precipitation of apatite, probably because Mg^{2+} competes with Ca^{2+} for sites in the apatite structure. In view of these results, and since Mg^{2+} is so abundant in sea water, it is difficult to explain how apatite could possibly form in the ocean. According to the work of Martens and

Harriss (1970), there is probably some threshold value for the Ca/Mg ratio above which crystalline apatite may precipitate. This ratio remains almost invariant in normal sea water, even in nearshore areas. Pore water compositions, however, are known to vary greatly from sea water values (see review of DSDP data by Broecker, in press). It seems plausible therefore, that diagenetic reactions occurring in anoxic sediments could raise the Ca/Mg ratio to the point where apatite could precipitate. Many reactions believed to occur under anaerobic conditions would have this effect. Drever (1971), for example, suggested that Mg^{2+} may replace Fe^{3+} in clays under anoxic conditions. The Fe^{3+} is then reduced and combines with sulfides. Interfering Mg^{2+} ions may also be removed by ion exchange, substitution of Mg^{2+} for Ca^{2+} carbonates (dolomitization), and the authigenic formation of Mg-rich silicates, such as sepiolite, palygorskite, nontronite, or chlorite. It is possible that a combination of these reactions controls the Mg^{2+} concentration in anoxic pore waters. A correlation between the presence of Mg-rich phases and the occurrence of apatite in the sediments from the Peru shelf was pointed out earlier. The amount of dolomite encountered within these sediments was admittedly quite low, but much dolomite is necessary to affect the Ca/Mg ratio significantly in the pore waters.

Roberson (1966) and Pytkowicz and Kester (1967) have shown that the solubility of apatite in sea water is greatly affected by pH variations. At higher pH values, apatite is less soluble. Berner (1969) showed in a series of laboratory experiments that a rise in

pH may be expected during the decomposition of organic matter (fish and clams) because of the formation of NH_4^+ and other nitrogenous bases from the breakdown of proteins and other biochemical compounds. Since apatite solubility is so sensitive to variations in pH, it is tempting to consider pH as a major factor in apatite precipitation. The variation of pH in anoxic sediments during early diagenesis is affected by other variables, however, such as release of CO_2 into the pores during oxidation of organic materials. The fact that an increase in pH also favors $CaCO_3$ precipitation, as pointed out by Gulbrandsen (1969), must also be considered. Since dissolved carbonate species in sea water are several orders of magnitude higher than phosphate species, a coprecipitation of apatite and calcite would surely result in the apatite being completely overwhelmed by the calcium carbonate. In order for large quantities of apatite to form with only negligible amounts of calcite present, it is probably more important that the dissolved PO_4^{3-} content be raised to the point where the Ca^{2+} concentration in the pore waters is being controlled by the apatite rather than by carbonate equilibria.

It appears from the thermodynamic solubility product constants for carbonate fluorapatite calculated at two different temperatures by Kramer (1964) that apatite is less soluble at higher temperatures. It is conceivable that, for a given system which is close to equilibrium with respect to apatite, temperature variation of only a few degrees could determine whether apatite will precipitate. As noted in a previous section of this report (Part II) there appears

to be a relationship between periods of phosphorite deposition and periods of warm average sea-water temperatures. This relationship, if confirmed, may prove to be a valuable avenue of research in the field of paleo-oceanography.

A factor which has not received much discussion in the literature (at least with regard to phosphorite formation) is the availability of suitable nucleation sites for apatite growth. From evidence presented in the literature, it appears that calcite provides the best surface for apatite nucleation. Stumm and Morgan (1970) showed experimentally that calcite acts as a well-matched surface for the nucleation of apatite. Presumably, the apatite forms epitaxially on the calcite. Stumm and Leckie (1971) demonstrated that the precipitation of apatite is greatly accelerated by calcite, the surface of which acts as a nucleating agent for crystallization. Berner (in press) has verified this by showing that pore waters from high carbonate (> 95 per cent $CaCO_3$), fine-grained sediments are in equilibrium with apatite at all depths. In the absence of calcite, PO_4^{3-} contents of a solution may reach values greatly in excess of equilibrium. However, from the petrographic and SEM results presented earlier, it would appear that other surfaces may serve as nucleation sites in the absence of carbonate. Siliceous skeletal materials, feldspar crystals, and fish-bone apatite, appear to be favored sites of initiation of authigenic apatite growth when calcite is not present.

Model of Phosphorite Genesis

In view of the data presented in this report, I submit the following model as representing the most likely combination of events which would generate the extensive phosphate rock deposits found on the sea floor off the coasts of Peru and Chile.

During periods of high average sea-water temperatures, inorganic precipitation of apatite occurs within the anoxic pore waters of the diatomaceous oozes on the continental shelf. High PO_4^{3-} contents in the pore waters initiates apatite precipitation, especially where the sediments are deposited in oxygen-deficient waters. The high biological productivity of the region which provides a large input of organic phosphorus to the sediment, ensures a constant supply of phosphate to the pore waters. Interfering Mg^{2+} ions are removed from solution by diagenetic reactions (see below) involving both the solid and fluid phase of the sediment. Replacement reactions involving carbonates or silicates may be responsible for the increase of the Ca/Mg ratio. Apatite precipitation initially occurs on nucleation sites such as the surfaces of siliceous skeletal debris. After precipitation begins, it may be self-perpetuating as long as there is sufficient phosphate, since the early-formed crystals of apatite offer large surface areas for continued growth.

General types of reactions which are likely to occur in the pore waters within these sediments during diagenesis are summarized

below:

$$(1)\quad SO_4^{2-} + \text{'organic matter'} \rightleftharpoons H_2S + HCO_3^- + HPO_4^{2-} + NH_4^+ + CH_4$$

and

$$(2)\quad 2\ Fe^{3+}\ \text{Clay} + 3\ Mg^{2+} + 4\ S \rightleftharpoons 3\ Mg^{2+}\ \text{Clay} + 2\ \underset{\text{(pyrite)}}{Fe\ S_2}$$

and/or

$$(3)\quad \underset{\text{(calcite)}}{2\ CaCO_3} + Mg^{2+} \rightleftharpoons \underset{\text{(dolomite)}}{CaMg(CO_3)_2} + Ca^{2+}$$

and/or

$$(4)\quad \underset{\text{(kaolinite)}}{Al_2Si_2O_5\ (OH)_4} + 5\ Mg^{2+} + 10\ HCO_3^- + H_4SiO_4 \rightleftharpoons Mg_5Al_2Si_3O_{10}\ (OH)_8 + 10\ CO_2 + 5\ H_2O$$

and

$$(5)\quad 5\ Ca^{2+} + 3\ HPO_4^{2-} + F^- \rightleftharpoons \underset{\text{(apatite)}}{Ca_5(PO_4)_3\ F} + 3\ H^+ .$$

No attempt is made in the above generalized reactions to describe the complete stoichiometry of the reactants and products. The 'organic matter' in reaction (1) is the decomposable material which supplies the dissolved phosphate to the pore waters. The material

would probably have a C:N:P ratio on the order of 106:16:1, the value for living planktonic species (Richards, 1965). Reactions (2), (3), and (4) are the mechanisms proposed for removal of interfering Mg^{2+} ions. Although there is little evidence to support a reaction such as (4) in modern shallow water marine sediments, reactions such as (2) and (3) seem quite reasonable. Reaction (2) has been shown by Drever (1971) to be a major control of Mg^{2+} ions in the oceans. Reaction (5), involving the precipitation of apatite, is simplified for a general composition.

If the bulk of the apatite is forming in the anoxic pore waters of the organic-rich sediments of this area, how is the incipiently produced apatite changed into indurated phosphate rocks? Baturin (1971) suggested that small phosphatic concretions formed authigenically within the diatomaceous oozes on the shelf of southwest Africa are concentrated into phosphate-rich deposits as a result of sea-level dynamics. He suggested that during the periods of low sea level, the fine-grained fraction of the sediments is eroded away, concentrating the phosphorite initially into coarse-grained sediments and ultimately into nodular deposits. This mechanism is adopted here with the added consideration of the tectonic movements on the continental margin. Since the west coast of South America is tectonically active, it seems reasonable to suppose that cycles of erosion and sedimentation are often influenced by tectonic events. A portion of the shelf which is uplifted, for example, could be cut off from its source of detrital sedimentation and the phosphate-

bearing sediment may be winnowed, concentrating the phosphorite. If these types of mechanisms are responsible for generating the indurated phosphatic deposits, the time scale of apatite precipitation-physical concentration-lithification must be quite short, i.e., on the order of a few thousand years, at least for the deposits from the Peru shelf. Several nodules from this area were dated radiometrically as less than a few thousand years old.

SUMMARY

Geochemical and mineralogical studies of phosphate rock samples from the continental margins of Peru and Chile show that a fluorine-rich variety of apatite, most likely francolite, is the major phosphate component. The chemical and mineralogical compositions reflect varying degrees of dilution of this phosphatic material by other authigenic minerals and various allogenic components. Microanalysis showed that the phosphate rocks have a complex composition even within very small areas. Examination by the scanning electron microscope revealed that apatite appears to favor certain types of surfaces for nucleation. For example, apatite seems to grow actively on siliceous skeletal materials such as diatom frustules. Authigenic apatite was also observed in small pellets separated from cores of diatomaceous ooze associated with the phosphate deposits.

After considering the characteristics of the depositional environment and the various factors and controls of apatite

precipitation, the following model for the genesis of these deposits is proposed. The data indicate that apatite is chemically precipitated out of the anoxic pore waters of an area. I propose that apatite is forming exclusively within the sediments and not in the overlying waters because: (1) the phosphate content within the pore waters may be more concentrated than in the overlying bottom waters by as much as several orders of magnitude; (2) there is no reasonable mechanism to raise the Ca/Mg ratio in sea water to the point where apatite may precipitate, but diagenetic reactions could significantly deplete anoxic pore waters of Mg^{2+} to that point; and (3) surfaces for apatite nucleation are more readily available within the sediments. The concentration of the initially precipitated apatite into indurated phosphate rocks is probably brought about by physical processes such as winnowing and reworking. These processes could be in response to changes in the sedimentary environment such as those which may be brought about by tectonic disturbances.

This model of phosphorite genesis was developed specifically to satisfy the observations reported for the phosphate rock deposits of the Peru-Chile continental margin. The model should, however, be applicable to similar deposits elsewhere, such as those on the continental shelf of southwest Africa. It would also seem likely that the origin of ancient 'bedded' phosphorites now located on land was similar.

LIST OF REFERENCES

Albee, A. L. and L. Ray, 1970. Correction factors for electron probe micro-analysis of silicates, oxides, carbonates, phosphates and sulfates. Anal. Chem., v. 42, p. 1408.

Altschuler, Z. S., R. S. Clarke, and E. Y. Young, 1958. Geochemistry of uranium in apatite and phosphorite. U. S. Geol. Surv. Prof. Paper 314-D, 90 pp.

Ames, L. L., 1960. Some cation substitutions during the formation of phosphorite from calcite. Econ. Geol., v. 55, p. 354-362.

Andermann, G., 1961. Improvements in the x-ray emission analysis of cement raw mix. Anal. Chem., v. 33, p. 1689-1698.

Arrhenius, G., 1963. Pelagic sediments. In The Sea, M. N. Hill, editor. John Wiley & Sons, Inc., New York, p. 655-727.

Arrhenius, G., M. N. Bramlette, and E. Picciotto, 1958. Localization of radioactive and stable heavy nuclides in ocean sediments. Nature, v. 180, p. 85-86.

Bachra, B. N., O. R. Travtz, and S. L. Simon, 1965. Precipitation of calcium carbonates and phosphates-III; The effect of magnesium and fluoride ions on the spontaneous precipitation of calcium carbonates and phosphates. Arch. Oral Biol., v. 10, p. 731-738.

Barnes, J. W., E. J. Lang, and H. A. Potratz, 1956. Ratio of ionium to thorium in coral limestone. Science, v. 124, p. 175-176.

Baturin, G. N., 1969. Authigenic phosphate concretions in Recent sediments of the Southwest African Shelf. Dokl. Earth Sci. Sect. English Transl., v. 189, p. 227-230.

_____, 1971. Formation of phosphate sediments and water dynamics. Oceanology, v. 11, p. 372-376.

Baturin, G. N., A. V. Kochenov, and V. P. Petelin, 1970. Phosphorite formation on the shelf of southwest Africa. Lithol. Min. Resources, p. 266-276.

Baturin, G. N., K. I. Merkulova, and P. I. Chalov, 1972. Radiometric evidence for recent formation of phosphatic nodules in marine shelf sediments. Mar. Geol., v. 13, p. 37-41.

Bence, A. E. and A. L. Albee, 1968. Empirical correction factors for the electron microanalysis of silicates and oxides. J. Geol., v. 76, p. 382.

Bender, M. L., T. L. Ku, and W. S. Broecker, 1966. Manganese nodules, their evolution. Science, v. 151, p. 325-328.

Bender, M. L., T. L. Ku, and W. S. Broecker, 1970. Accumulation rates of manganese in pelagic sediments and nodules. Earth Planet. Sci. Lett., v. 8, p. 143.

Berner, R. A., 1969. Chemical changes affecting dissolved calcium during the bacterial decomposition of fish and clams in sea water. Mar. Geol., v. 7, p. 253-274.

_____, in press. Kinetic models for the early diagenesis of nitrogen, sulfur, phosphorus, and silicon in anoxic marine sediments. In The Sea, E. Goldberg, editor, Sillen Memorial Volume, V. 5.

Berner, R. A., M. R. Scott, and C. Thomlinson, 1970. Carbonate alkalinity in the pore waters of anoxic marine sediments. Limnol. Oceanog., v. 15, p. 544-549.

Blackwelder, E., 1916. The geologic role of phosphorus. Amer. J. Sci., 4th ser., v. 42, p. 285-298.

Blanchard, R. L., 1963. Uranium decay series disequilibrium in age determination of marine calcium carbonates. Ph.D. dissertation, Washington University.

Bray, J. T., O. P. Bricker, B. N. Troup, 1973. Phosphate in interstitial waters of anoxic sediments: oxidation effects during sampling procedure. Science, v. 180, p. 1362-1364.

Broecker, W. S., 1963. A preliminary evaluation of uranium series inequilibrium as a tool for absolute age measurement on marine carbonates. J. Geophys. Res., v. 68, p. 2817-2834.

_____, in press. Interstitial water studies, Leg 15 - introduction and summary. In Heezen, B. C., MacGregor, I. G., et al., Initial Reports of the Deep Sea Drilling Project, V. 20,

Broecker, W. S. and D. L. Thurber, 1965. Uranium series dating of corals and oolites from Bahaman and Florida Key limestones. Science, v. 149, p. 55-60.

Broecker, W. S., D. L. Thurber, J. Goddard, T. H. Ku, R. K. Matthews, and K. F. Mesolella, 1968. Milankovitch hypothesis supported by precise dating of coral reefs and deep-sea sediments. Science, v. 159, p. 297-300.

Brongersma-Sanders, M., 1957. Mass Mortality in the Sea. In Hegpeth, J. W., editor, Treatise on Marine Ecology and Paleoecology, V. 1, Ecol: Geol. Soc. Amer. Mem. 67,

Brooks, R. R., B. J. Presley, and I. R. Kaplan, 1968. Trace elements in the interstitial waters of marine sediments. Geochim. Cosmochim. Acta, v. 32, p. 397-414.

Burnett, W. C. and D. N. Gomberg, in preparation. Uranium in phosphate deposits from the Pourtales Terrace, Straits of Florida; possible indication of environmental change.

Burnett, W. C., H. H. Veeh, and A. Soutar, 1973. Geochemistry and radiometric ages of sea-floor phosphorites from the continental margin of Peru and Chile (abs.). Geol. Soc. Amer. Abstr. with Programs, v. 5, p. 18-19.

Bushinsky, G. I., 1964. On shallow water origin of phosphorite sediments. In: L. M. J. U. Van Straaten (editor), Deltaic and Shallow Marine Deposits. Elsevier, Amsterdam, pp. 62-69.

_____, 1966. The origin of marine phosphorites. Lithol. Miner. Deposits, pp. 292-311.

Chodos, A. A., and A. L. Albee, 1972. Automated microprobe analysis and applications to analysis of exotic lunar phases. Proc. 6th Int. Conf. X-ray Optics and Microanalysis, p. 779-784.

Clarke, R. S. and A. S. Altschuler, 1958. Determination of the oxidation state of uranium in apatite and phosphorite deposits. Goechim. Cosmochim. Acta, v. 13, p. 127-142.

Cook, Peter J., 1967. Winnowing--an important process in the concentration of the stairway sandstone (Ordovician) phosphorites of Central Australia. J. Sed. Petrol., v. 37, p. 818-828.

Cruft, E. F., C. O. Ingamells, and J. Muysson, 1965. Chemical analysis and the stoichiometry of apatite. Geochim. Cosmochim. Acta, v. 29, p. 581-597.

D'Anglejan, B. F., 1967. Origin of marine phosphorites off Baja California, Mexico. Mar. Geol., v. 5, p. 15-44.

_____, 1968. Phosphate diagenesis of carbonate sediments as a mode of in situ formation of marine phosphorites: observations in a core from the Eastern Pacific. Canadian J. Earth Sci., v. 5, p. 81-87.

Dansgaard, W. and H. Tauber, 1969. Glacier oxygen-18 content and Pleistocene ocean temperatures. Science, v. 166, p. 499-502.

Deer, W. A., R. A. Howie, and J. Zussman, 1966. An Introduction to the Rock-forming Minerals. John Wiley & Sons, Inc. New York.

Dietz, R. S., K. O. Emery, and F. P. Shepard, 1942. Phosphorite deposits on the sea floor off Southern California. Bull. Geol. Soc. Amer., v. 53, p. 815-848.

Dinkelman, M. G., 1973. Late Quaternary radiolarian paleo-oceanography of the Panama Basin, Eastern Equatorial Pacific (abs.). Geol. Soc. Amer. Abstrs. with Programs, v. 5, p. 598-599.

Dooley, J. R., H. C. Granger, and J. N. Rosholt, 1966. Uranium-234 fractionation in the sandstone-type uranium deposits of the Ambrosia Lake District, New Mexico. Econ. Geol., v. 61, p. 1362-1382.

Drever, J. I., 1971. Magnesium-iron replacement in clay minerals in anoxic marine sediments. Science, v. 172, p. 1334-1336.

Emery, K. O., 1960. The Sea Off Southern California. John Wiley & Sons, New York.

Emiliani, L., 1970. Pleistocene paleotemperatures. Science, v. 168, p. 822-824.

Fan, P. F. and R. W. Rex, 1972. X-ray mineralogy studies-Leg 14. Initial Reports of the Deep Sea Drilling Project, V. 14, p. 677-725.

Fisher, D. J. and D. McConnell, 1969. Aluminium-rich apatite. Science, v. 164, p. 551-553.

Fleming, E. H., A. Ghirso, and B. B. Cunningham, 1952. ^{234}U, ^{235}U, and ^{238}U alpha activities and half lives. Phys. Rev., v. 88, p. 642.

Friedlander, G. and J. W. Kennedy, 1957. Nuclear and Radiochemistry. John Wiley & Sons, Inc., New York.

Gancarz, A. J., A. L. Albee, A. A. Chodos, 1971. Petrologic and mineralogic investigation of some crystalline rocks returned by the Apollo 14 Mission. Earth Planet Sci. Lett., v. 12, p. 1-18.

Gardner, J. V., 1973. Eastern equatorial Atlantic: sea-surface temperature and circulation response to global climatic changes during the past 200,000 years (abs.). Geol. Soc. Amer. Abstrs. with Programs, v. 5, pp. 629.

Goldberg, E. D. and M. Koide, 1962. Geochronological studies of deep sea sediments by the ionium/thorium method. Geochim. Cosmochim. Acta, v. 26, p. 417-450.

Goldberg, E. D. and R. H. Parker, 1960. Phosphatized wood from the Pacific sea floor. Bull. Geol. Soc. Amer., v. 71, p. 631-632.

Goldman, M. I., 1922. Basal glauconite and phosphate beds. Science, v. 56, p. 171-173.

Gomberg, David, 1973. Drowning of the Floridan Platform margin and formation of a condensed sedimentary sequence (abs.). Geol. Soc. Amer. Absts. with Programs, v. 5, p. 640.

Gorsline, D. S. and D. B. Milligan, 1963. Phosphate deposits along the margin of Pourtales Terrace. Deep-Sea Res., v. 10, p. 259-262.

Gulbrandsen, R. A., 1966. Chemical composition of phosphorites of the Phosphoria Formation. Geochim. Cosmochim. Acta, v. 30, p. 769-778.

_____, 1969. Physical and chemical factors in the formation of marine apatite. Econ. Geol., v. 64, p. 365-382.

Gulbrandsen, R. A., J. R. Kramer, L. B. Beatty, R. E. Mays, 1966. Carbonate-bearing apatite from Faraday Township, Ontario, Canada. Amer. Mineral., v. 51, p. 819-824.

Hamilton, E. L., 1956. Sunken islands of the Mid-Pacific Mountains. Geol. Soc. Amer. Mem. 64, 97 pp.

Hurd, D. C., 1973. Interactions of biogenic opal, sediment and seawater in the Central Equatorial Pacific. Geochim. Cosmochim. Acta, v. 37, p. 2257-2282.

Hutchinson, G. E., 1950. The biogeochemistry of vertebrate excretion. Amer. Mus. Nat. Hist. Bull., v. 96, New York.

Kaufman, Aaron, 1971. U-series dating of Dead Sea Basin carbonates. Geochim. Cosmochim. Acta, v. 35, p. 1269-1281.

Kaufman, A. and W. S. Broecker, 1965. Comparison of ^{230}Th and ^{14}C ages for carbonate materials from Lakes Lahontan and Bonneville. J. Geophys. Res., v. 70, p. 4039-4054.

Kaufman, A., W. S. Broecker, T. L. Ku, and D. L. Thurber, 1971. The status of U-series methods of dating mollusks. Geochim. Cosmochim. Acta, v. 35, p. 1155-1184.

Kazakov, A. V., 1937. The phosphorite facies and the genesis of phosphorites. In Geological investigations of agricultural ores, U.S.S.R. Trans. Sci. Inst. Fertilizers Insectofungicides, No. 142, p. 93-113.

Kester, D. R. and R. M. Pytkowicz, 1967. Determination of the apparent dissociation constants of phosphoric acid in seawater. Limnol. Oceanog., v. 12, p. 243-252.

Kigoshi, K., 1971. Alpha-recoil thorium-234: dissolution into water and the uranium-234/uranium-238 disequilibrium in nature. Science, v. 173, p. 47-48.

Kleeman, J. D. and J. F. Lovering, 1967. Uranium distribution in rocks by fission-track registration in Lexan plastic. Science, v. 156, p. 512-513.

Koide, H. and E. D. Goldberg, 1965. Uranium-234/uranium-238 in sea water. In Progress in Oceanography, v. 3, Pergamon Press, p. 173-177.

Kolodny, Yehoshua, 1969a. Studies in geochemistry of uranium and phosphorites. Ph.D. Dissertation, U.C.L.A., 220 pp.

_____, 1969b. Are marine phosphorites forming today? Nature, v. 224, no. 5223, p. 1017-1019.

Kolodny, Y. and I. R. Kaplan, 1970. Uranium isotopes in sea floor phosphorites. Geochim. Cosmochim. Acta, v. 34, p. 3-24.

Kramer, J. R., 1964. Sea water: Saturation with apatites and carbonates. Science, v. 146, p. 637-638.

Ku, T. L., 1965. An evaluation of the $^{234}U/^{238}U$ method as a tool for dating pelagic sediments. J. Geophys. Res., v. 70, p. 3457-3474.

Ku, T. L. and W. S. Broecker, 1967. Uranium, thorium, and protactinium in a manganese nodule. Earth Planet. Sci. Lett., v. 2, p. 317-320.

Luz, B., 1973. Climatic fluctuations and shifting water mass boundaries in the East Pacific indicated by Late Pleistocene planktonic foraminifera (abs.). Geol. Soc. Amer. Absts. with Programs, v. 5, p. 722.

Mansfield, G. R., 1940. The role of fluorine in phosphate deposition. Am. Jour. Sci., v. 238, p. 863-879.

Martens, C. S. and R. C. Harriss, 1970. Inhibition of apatite precipitation in the marine environment by magnesium ions. Geochim. Cosmochim. Acta, v. 34, p. 621-625.

McConnell, D., 1958. The apatite-like mineral of sediments. Econ. Geol., v. 53, p. 110-111.

_____, 1973. Apatite. Springer-Verlag, New York.

McKelvey, V. E., 1967. Phosphate deposits. U. S. Geol. Surv. Bull. 1252-D, p. D1-D2.

Murphy, C. B., 1973. Effect of restricted use of phosphate-based detergents on Onondaga Lake. Science, v. 182, p. 379-381.

Murray, J. and A. F. Reynard, 1891. Scientific results, H. M. S. Challenger, deep-sea deposits, p. 391-400.

Norris, R. M., 1964. Sediments of Chatham Rise. New Zealand Oceanogr. Inst. Mem., No. 26, 39 pp.

Norrish, K. and J. T. Hutton, 1969. An accurate x-ray spectographic method for the analysis of a wide range of geological samples. Geochim. Cosmochim. Acta, v. 33, p. 431-455.

Osmond, J. K., J. R. Carpenter, and H. L. Windom, 1965. $^{230}Th/^{234}U$ age of Pleistocene corals and oolites of Florida. J. Geophys. Res., v. 70, p. 1843-1847.

Pardee, J. T., 1917. The Garrison and Phillipsburg phosphate fields, Montana. U. S. Geol. Surv. Bull. 640, p. 195-250.

Park, K., 1966. Deep-sea pH. Science, v. 154, p. 1540-1542.

Parker, R. J., 1971. The petrography and major element geochemistry of phosphorite nodule deposits on the Agulhas Bank, South Africa. S. Afr. Nat. Comm. Oceanog. Res. Mar. Geol. Prog. Bull., v. 2, 94 pp.

Parker, R. J. and W. G. Siesser, 1972. Petrology and origin of some phosphorites from the South African continental margin. J. Sed. Petrol., v. 42, p. 434-440.

Pasho, D. W., 1973. Character and origin of marine phosphorites. Univ. Southern Calif. Geol. 72-5, 188 pp.

Pettijohn, F. J., 1957. Sedimentary Rocks. Harper and Bros., New York.

Pevear, D. R., 1966. The estuarine formation of the United States Atlantic Coastal Plain phosphate. Econ. Geol., v. 61, no. 2, p. 251-255.

_____, 1967. Shallow water phosphorites. Econ. Geol., v. 62, p. 562-575.

Pytkowicz, R. M. and D. R. Kester, 1967. Relative calcium phosphate saturation in two regions of the North Pacific Ocean. Limnol. Oceanog., v. 12, p. 714-718.

Rex, R. W. and B. Murray, 1970. X-ray mineralogy. Appendix in: Initial Reports of the Deep Sea Drilling Project, V. 4, p. 748-753.

Richards, F. A., 1965. Anoxic basins and fjords. In Chemical Oceanography, J. P. Riley and G. Skirrow, editors, v. 1, p. 611-645, Academic Press.

Richards, F. A., J. D. Cline, W. W. Broenkow, and L. P. Atkinson, 1965. Some consequences of the decomposition of organic matter in Lake Nitinat, an anoxic fjord. Limnol. Oceanog., v. 10, (Suppl.), p. R185-R201.

Ristvet, B. L., 1973. Recent authigenic nontronite and montmorillonite-illite from Kaneohe Bay, Oahu, Hawaii (abs.). Geol. Soc. Amer. Absts. with Programs, v. 5, p. 781-782.

Roberson, C. E., 1966. Solubility implications of apatite in sea water. In Geological Survey Research 1966: U. S. Geol. Surv. Prof. Paper 550-D, p. 178-185.

Rooney, T. P. and P. F. Kerr, 1967. Mineralogic nature and origin of phosphorite, Beaufort County, North Carolina. Geol. Soc. Amer. Bull., v. 78, p. 731-748.

Sackett, W. M., 1958. Ionium-uranium ratios in marine deposited calcium carbonates and related materials. Ph.D. dissertation, Washington University, St. Louis, Mo.

Sayles, F. L., F. T. Manheim, and L. S. Waterman, in press. Interstitial water studies on small core samples: Leg 15. In Heezen, B. C., MacGregor, I. G., et al., Initial Reports of the Deep Sea Drilling Project, V. 20, Washington (U. S. Government Printing Office).

Serebryakova, M. B. and Y. G. Razumnaya, 1962. Form of occurrence of uranium in apatite. Dokl. Earth Sci. Sed., English Trans., v. 143, p. 153-156.

Sholkovitz, E., 1973. Interstitial water chemistry of the Santa Barbara Basin sediments. Geochim. Cosmochim. Acta, v. 37, p. 2043-2073.

Skopintsev, B. A., 1972. Saturation of deep black sea waters with calcium phosphate. Oceanology, v. 12, p. 672-677.

Smith, R. L., 1968. Upwelling. Oceanogr. Mar. Biol. Ann. Rev., v. 6, p. 11-46.

Stumm, W. and J. O. Leckie, 1970. Phosphate exchange with sediments; its role in the productivity of surface waters. Advances in Water Pollution Research, v. 2, Pergamon Press, New York.

Stumm, W. and J. J. Morgan, 1970. Aquatic Chemistry, An Introduction Emphasizing Chemical Equilibria in Natural Waters. Wiley-Interscience, New York.

Summerhayes, C. P., 1967. Marine environments of economic mineral deposition around New Zealand: A Review. New Zealand J. Marine Freshwater Res., v. 1, p. 267-282.

Swaine, D. J., 1962. The trace element content of fertilizers. Tech. Comm. 52, Farnham Royal, England: Commonwealth Agr. Bureaux, 306 pp.

Tatsumoto, M. and E. D. Goldberg, 1959. Some aspects of the marine geochemistry of uranium. Geochim. Cosmochim. Acta, v. 17, p. 201-208.

Thurber, D. L., 1962. Anomalous $^{234}U/^{238}U$ in nature. J. Geophys. Res., v. 67, p. 4518-4520.

Thurber, D. L., W. S. Broecker, R. L. Blanchard, and H. A. Potratz, 1965. Uranium series ages of Pacific atoll coral. Science, v. 149, p. 55-58.

Tooms, J. S., C. P. Summerhayes, and D. S. Cronan, 1969. Geochemistry of Marine Phosphate and Manganese deposits. Oceanog. Marine Biol. Ann. Rev., v. 7, p. 49-100.

Toribara, T. Y. and L. Koval, 1967. Isolation of thorium in biological samples. Talanta, v. 14, p. 403-407.

van Donk, Jan, 1973. A complete Pleistocene O^{18} record for the Atlantic Ocean (abs.). Geol. Soc. Amer. Absts. with Programs, v. 5, p. 847.

Veeh, H. H., 1966. $^{230}Th/^{238}U$ and $^{234}U/^{238}U$ ages of Pleistocene high sea level stands. J. Geophys. Res., v. 71, p. 3379-3386.

_____, 1968. $^{234}U/^{238}U$ in the East Pacific Sector of the Antarctic Ocean and in the Red Sea. Geochim. Cosmochim. Acta, v. 32, p. 117-119.

Veeh, H. H. and J. Chappell, 1970. Astronomical theory of climatic change: support from New Guinea. Science, v. 167, p. 862-865.

Veeh, H. H., W. C. Burnett, and A. Soutar, 1973. Contemporary phosphorite on the continental margin of Peru. Science, v. 181, p. 845-847.

Veeh, H. H., H. Polach, S. E. Calvert, and N. B. Price, in press. Uranium accumulation rates and fixation in organic-rich sediments and phosphorizes on the southwest African shelf.

Williams, H., F. J. Turner, and C. M. Gilbert, 1954. Petrography. W. H. Freeman & Co., San Francisco.